THE UNIVERSITY
of EDINBURGH

Machine Learning and Privacy Preserving Algorithms for Spatial and Temporal Sensing

Abhirup Ghosh

Doctor of Philosophy

Laboratory for Foundations of Computer Science
School of Informatics
University of Edinburgh

2019

Abstract

Sensing physical and social environments are ubiquitous in modern mobile phones, IoT devices, and infrastructure-based settings. Information engraved in such data, especially the time and location attributes have unprecedented potential to characterize individual and crowd behavior, natural and technological processes. However, it is challenging to extract abstract knowledge from the data due to its massive size, sequential structure, asynchronous operation, noisy characteristics, privacy concerns, and real time analysis requirements. Therefore, the primary goal of this thesis is to propose theoretically grounded and practically useful algorithms to learn from location and time stamps in sensor data. The proposed methods are inspired by tools from geometry, topology, and statistics. They leverage structures in the temporal and spatial data by probabilistically modeling noise, exploring topological structures embedded, and utilizing statistical structure to protect personal information and simultaneously learn aggregate information. Proposed algorithms are geared towards streaming and distributed operation for efficiency. The usefulness of the methods is argued using mathematical analysis and empirical experiments on real and artificial datasets.

Lay Summary

Modern personal devices continuously record the social and physical context of their users. Time and location stamps associated with these sensing data are often important for personalization and optimization across applications. However, it is challenging to learn high level abstract knowledge from the sensing data mainly due to huge dataset size, noisy environment, and realtime analysis requirement. Moreover, even anonymized data used with best of intentions can leak sensitive information about data contributors. So, in this thesis, we discuss novel mechanisms inspired by statistics and geometry to learn fundamental patterns inscribed in the data while protecting the privacy of the individual users. Following are the specific problems we address here.

Periodicity is fundamental and useful to characterize and forecast time series. For example, our footsteps, heart beats, traffic surges, etc., have regular repeating patterns. But, it is challenging to automatically detect the periodicity in real world signals due to dynamic period and phase and therefore popular frequency domain methods do not apply. Here, we propose an online algorithm that guesses several periods and iteratively refines them as it observes the signal.

Timings of important events are often sensitive. For example, we don't want an adversary to know the exact check-in times, but the aggregate information is required for service optimization. We propose techniques to introduce carefully chosen noise such as perturb the event timings or introduce spurious events so that no adversary can learn sensitive event timings with confidence, while aggregate inferences, like event density is preserved.

Location is another fundamental attribute in the sensing data. Mobility traces are important in many practical applications, for example, predicting future location. We propose a general framework to apply standard machine learning tools for location trajectories. The fundamental idea is that the way the objects move around the obstacles in the domain constitutes the most important characteristics of the mobility pattern.

Location is also sensitive, for example, check-in at a hospital. To protect location privacy, we develop algorithms to protect exact location stamps while ensuring that the aggregate inferences are useful. These mechanisms are well beyond simple anonymization and are inspired by the strongest form of privacy.

Acknowledgements

First and foremost, I want to thank Rik, my primary supervisor. Our numerous technical discussions have shaped all the works in this thesis and beyond. His guidance, continuous encouragement, and support have taught me perseverance and helped me to survive in the time of despair. His ability to make complex arguments simple, find the core concepts with ease, and connect myriad ideas had taught me essential skills of a researcher. I consider myself blessed to have the chance to work with him. I also thank Mahesh, my second supervisor, for showing me new directions regarding both specific research questions and setting broad research agenda. From all the academics in the NetSys, especially, Rik, Mahesh, and Paul, I learned the science and art of presentation.

I am fortunate to work with Christopher Lucas, Subramanian Ramamoorthy, and Jie Gao. They all have contributed significantly to this thesis. I thank Chris for his technical guidance in the work on periodicity, being my examiner in the annual reviews, and continuously helping me to shape my research and career. I thank Ram as his ideas helped us to structure our work on mobility analysis. I am thankful to Jie for her support in all the privacy related works in this thesis. Her vast experience, technical depth, and conceptual breadth essentially textured these works. I am grateful to Paul Patras and Thomas Heinis for taking the time to review my thesis and being the examiners in my defense.

I appreciate Jiaxin for our discussions regarding Chapter 3 and Chapter 5. I feel lucky to work with brilliant colleagues and kind friends, Yota, Maria, and Benedek. I specially thank Benedek for his contribution in the experiments regarding location prediction in Section 4.7. I thank Yota and Maria for numerous technical discussions and continuous support in every way possible. I am also thankful to Lauren for our discussions on privacy.

I am also grateful to have Rajkaran as a friend and a colleague. Our countless technical and non-technical discussions helped me in research and life. I thank Mah-Rukh for our discussions on network measurement. I also appreciate Manick, Priyank, Saumay, Aprit, Rakesh, Prasun, and Sumit for their support to continue life outside of research.

Last but not the least, without my family this thesis would not have been possible. They continuously guided me to be a better human being and inspired me to cross the hardest hurdles.

I first appreciate my parents; Without them, I would not have come this far in life. From the time I remember, they nurtured me to have all the qualities of life that they could think of. Their patience, blessings, continuous encouragement, and support had started weaving the very letters of this thesis long before I started writing it. Their continuous struggle reminds me that life is much bigger than a PhD and gave me the essential strength to overcome all the obstacles in the way to this book.

Finally, I thank my loving wife, Maitri, for walking the whole journey with me. A PhD is not a bed of roses neither it is full of nails. We walked the bloody roads of desperation as well as the time of euphoria together. She deserves equal credit for this thesis if not more. The hot meals that she prepared every single day, sleepless nights that she spent to make my writing perfect or my presentation flawless, responsibilities that she alone handled to run the family, vacations that she organized take a necessary break from stressful life, countless prayers that she made, sacrifices that she made with her life and career have all counted and finally resulted in this book.

Declaration

I declare that this thesis was composed by myself, that the work contained herein is my own except where explicitly stated otherwise in the text, and that this work has not been submitted for any other degree or professional qualification except as specified.

(*Abhirup Ghosh*)

To my loving family,

Table of Contents

Chapter 1

Introduction

Modern mobile phones and IoT devices are equipped with a rich collection of sensing modalities, for example, location, proximity, audio, temperature, humidity, etc. Infrastructures like cellular towers, transport services track users for service optimization. The recent popularity of the personal devices and sensing infrastructures are generating a huge amount of raw sensing data in terms of user activities, application usage, location, health, etc. In this thesis, we seek efficient and accurate methods to learn high level abstract patterns from such sensor data for applications across domains, such as smart cities, smart transport, traffic management, etc. Further, these sensing data contain sensitive personal attributes, so we also aim to sanitize the data to protect user privacy while preserving utility for aggregate learning.

Out of numerous applications of sensor data, the most interesting and useful ones are the context-aware applications (Schilit et al., 1994). They adapt according to the timings and locations of use, user's social situation, user activities, etc. Among other factors, location and time stamp are the most important and fundamental context indicators in the majority of the applications. Henceforth, in this thesis we consider multiple ubiquitous and fundamental problems to concerning these two attributes.

In general, sensors continuously sample the environment at regular or irregular intervals. Values between samples can be interpolated to approximate the continuous signal or sensors can extract discrete events without considering continuity. Events can be real valued or binary denoting occurrence of interest. For temporal streams, we consider discrete events without explicitly approximating continuity between events. Whereas, spatial data is considered in both the fla-

vors, with continuity (e.g., piece-wise linear GPS trajectories) and discrete events (e.g., check-in). All the chapters in this dissertation only consider location and time attributes in the data and do not deal with the content of the events.

The collected sensor data, traditionally, are sent to servers for analysis. However, the communication is costly and sharing personal data with an unknown server raises user privacy concerns. Fortunately for us, the sensors are tiny computers with computing, storage, and communication capabilities and this opens the opportunity to analyze the collected data in the sensors themselves. However, the processing algorithms often pose intensive resource requirements beyond the capacities of the battery operated sensors. Therefore, a viable middle-ground is to process the raw data partially in the sensors and share the extracted knowledge or features with the servers for further analysis and fusion. This architecture constitutes the main theme across all the chapters presented in this thesis.

1.1 Challenges in learning from sensor data

This section describes the primary challenges to learn from sensor data and the broad design choices for learning algorithms to overcome them.

Massive dataset size. Sensors generate huge datasets as they collect data continuously and there are multiple sensing modalities. Therefore, it is costly to store the raw data in the sensors or send them to servers; which makes the online methods necessary over batch processing techniques. For applications requiring aggregation over multiple sensors, in-device processing needs to be augmented with distributed computing techniques.

Noisy data. Noise is the unstructured part of the data which do not follow a particular pattern. Data from the real world are often noisy due to complex generation mechanisms and intrinsic characteristics of the sensors. For example, location trajectories have noisy GPS points due to inaccurate localization, personal and group preferences, road conditions, etc. Traditional learning systems pre-process the data to remove certain noise (e.g., using high pass filters), however, noise often constitute an essential part of the sensing data (e.g., changing periodicity in footsteps). Moreover, online processing constraint makes noise removal difficult. Therefore, the analysis algorithms in this regime need to be

robust to realistic noises.

Sequential structure. Due to continuous recording, sensor data often are sequential. Sequences are complex objects to process and well-studied standard machine learning methods for point cloud data do not apply to sequences. Therefore, simplifying assumptions (e.g., Markov assumption) and customized learning tools (e.g., Long short-term memory neural network) are developed. In this thesis, we explore the possibility of embedding the sequences in a nice geometric space so that all existing learning and mining tools apply for further analysis.

Asynchronous operation. In many applications, events are captured asynchronously, i.e., at real-valued timestamps. Blurring the event timing to fit synchronous rounds make data useless in time critical applications. Besides, deciding the interval for synchronous rounds is difficult. Whereas sensor data captured in synchronous rounds is studied across domains, asynchronous events are not well understood.

Time and space efficiency. Sensors have limited resource in terms of storage, computation, energy, and communication, therefore, to run analysis algorithms in the sensors the methods need to be time and space efficient. Moreover, the context evolves quickly, therefore it needs to be processed fast to have relevant results. A powerful resort to address this challenge is to have approximate processing and compromise accuracy for efficiency.

User privacy. User centric sensing data has unavoidable privacy concerns. For example, a traffic management system may want to track cars to predict and manage congestion, but the users of the cars shall have privacy concerns in sharing their routes. Therefore, an interesting research direction is to learn aggregate inference without sacrificing individual privacy (Dwork, 2006).

1.2 Key topics in learning from sensor data

This section describes interesting and fundamental research problems concerning time and location context in sensor data. There are three main avenues – data collection, learning from the collected data and preserving privacy of individual users. Each topic encompasses multiple problems and below we review the most intriguing ones.

1.2.1 Sensor data collection

The first step of learning is to collect data by sensing the environment. Depending on the applications, there are multiple configurations. A sensor can capture discrete events (e.g., user check-in) or sample from a continuous signal (e.g., user locations). The inference can depend on a single sensor or on a distributed sensor array. The collected signal can vary in dimensionality. The sensors can be static or mobile with or without control over mobility. Moreover, it is infeasible to place sensors at every location and sample continuously due to massive deployment cost, high energy requirement, and huge resulting data size. Therefore, challenges are to decide sensor locations, sampling frequency, and compressing the collected data. Following problems discuss these challenges in more detail. However, none of these problems are addressed in this thesis.

Deciding the sampling frequency. It is a common practice to use a fixed sampling frequency for ease of sensor configuration and deterministic performance in terms of both energy consumption and data size. The frequency value is naturally derived in many settings, for example, wireless network nodes (e.g., WiFi, Bluetooth) can fix their duty cycles bounded by the wireless protocol. Popular Nyquist Theorem asks to sample at least at twice the rate of the highest frequency component in the signal. It provides a conservative measure for perfect reconstruction. More sophisticated methods reduce the rate using non-uniform sampling (Venkataramani and Bresler, 2001). However, deciding the frequency is nontrivial for sensors where the exact reconstruction of the signal can be avoided (Candes, 2006). Therefore, an interesting research question is to determine the sampling frequency such that the resulting data size is small and yet contains adequate information to be useful in further analysis.

Compressing collected data. We can compress the data while it is being collected (online), or after it is collected (offline). Data compression is well studied in multiple fields and usually has two major variations – reducing dimensionality and reducing the number of data points.

The compressive sensing framework proposes to compress the data to a low dimensional representation with the possibility of approximate reconstruction. It has been successfully used across fields for sensing traffic congestion (Zhu et al., 2013), monitoring environmental signals (Yan et al., 2012a), etc. Apart from that, a large body of literature is available for reducing dimension using PCA, SVD,

factor analysis, etc., and selecting a subset of dimensions. Topological methods are also studied to find and preserve persistent features in the data (Katsikouli et al., 2014). There has been also research on smoothing signals (Hershberger and Snoeyink, 1994b), which essentially compress the data.

Coresets (Bachem et al., 2017; Frahling and Sohler, 2008) reduce the data-set size by keeping a subset of the data points. The constructions are application specific and offer theoretically guaranteed accuracy on the targeted applications. Clustering is useful for summarization where the data points are grouped and representative samples from clusters are retained in the summary (Kleindessner et al., 2019). Submodular optimization is also relevant to summarize data by finding maximally dissimilar data points (Mitrovic et al., 2018).

Placing spatially distributed sensors. Spatially distributed sensors can be placed at static locations, attached to controlled mobile objects, or crowd-sourced. They have different opportunities and challenges, for example, static sensors are often accurately calibrated, but have installation and maintenance cost, whereas crowd-sourced data is imprecise, but is cost-effective.

Many practical signals such as cellular signal strength, temperature, crowd density have correlated values at spatially nearby places. To place static sensors, most frameworks use this structure. They first model the spatial correlation among n possible sensor locations, then select a subset of k locations that maximize an objective, such as, uncertainty among sensor locations, coverage, the mutual information between directly observed and unobserved locations, etc. This is a variant of the well known NP hard maximum set cover problem and many approximation methods are proposed using submodular maximization (Mirzasoleiman et al., 2016; Krause et al., 2008), active learning, etc. However, these theoretical frameworks assume simplistic models for the spatial correlation, thus are less optimal in practice.

Motion planning for controlled vehicles is also studied in the literature (Kolyaie and Yaghooti, 2011). Another setup is to attach sensors to buses and trains (Elmokashfi et al., 2017). An interesting research question is how to select the buses and trains to minimize the number of sensors attached. Moreover, the routes may change frequently due to roadblocks, environmental phenomena, and sensors may fail; thus, a related question is how to make the selection of routes robust.

In the crowd-sourced setting, user agents collect and report sensing data. The sampling decision can be made by the user or a server knowing the location of the

user. In this configuration, along with the obvious objective of maximizing data quality, one has to consider that no individual user should be asked to collect data many times. This setting depends on predicting the agents' motion (explore vs exploit trade-off), mitigating the low quality sensing from commodity devices, possible attrition, and privacy concerns.

1.2.2 Learning from location and time stamps

Depending on the applications, inferences are learned from sensor data in various settings, streaming vs offline; at individual sensors vs aggregated over multiple sensors, etc. In the following, we describe multiple fundamental problems regarding learning from sensor data.

Similarity measure. Similarity measures between data points are at the heart of all machine learning and data mining methods.

Multiple methods exist to compute the distance between time series by comparing the signal values at corresponding time steps, using the coefficients in frequency domains, etc. Categorical sequences are popularly compared using edit distances.

Distances between curves are popularly computed using Hausdorff, Fréchet , and Dynamic Time Wrapping. For discrete curves, these distances measure the maximum distance between matched data points. To match the data points (e.g., each point in one curve to the nearest point in the other), these methods need computation time quadratic in the number of data points. Although there are several variations of these measures, they still have super linear compute time complexity (Chambers et al., 2010). Moreover, the Hausdorff and Fréchet distances do not form normed spaces and DTW is not even a metric. Therefore, these distances are not suitable for existing Euclidean learning methods. More distances like area between curves (Chambers and Wang, 2013) are also studied. We survey related works in Chapter 4.

Kernel methods are popular in machine learning for measuring distances in point clouds, and recently they are being explored for sequential data (Király and Oberhauser, 2019). Customized locality sensitive hashing schemes are also designed for mobility traces (Astefanoaei et al., 2018).

Another way to find similarity is to first map sequential data to a geometrically "nice" space, then do further analysis using the embeddings. Using this

philosophy, Chapter 4 maps mobility traces as fixed dimensional Euclidean vectors preserving their topological properties. Further, we analyze mobility traces using the vector representations. This speeds up trajectory comparison as it uses Euclidean distances, and enables all Euclidean learning tools.

Modeling a sequence. A generative model for sequential data is useful for characterizing and forecasting. Point process models are well studied in statistics for modeling discrete event streams, for example, Poisson point process models uniformly random occurrences of events, Hawkes process (Parmar et al., 2017) suits self-exciting events, etc. We have used Poisson Process to model the point events in Chapter 2 and 3.

Periodic process is pervasive in event streams, however, periodicity analysis in noisy streams is not well understood, especially when the periodicity and phase change over time. Realistic signals often have these characteristics, for example, delays between heart beats and foot-steps accumulate over time and that changes the phase of the signal. Chapter 2 proposes a periodicity detection algorithm for binary event streams with such noise. The proposed algorithm also handles false positive events in the stream.

Markov models (Murphy, 2012) are popular for modeling latent states from observations in a time series. These methods are extensively studied to better understand, control, and forecast various signals (Jurafsky and Martin, 2014; Rabiner and Juang, 1986; Xiao et al., 2017; Jia et al., 2017; Goldberg, 2017; Hallac et al., 2017). These models are appropriate for random walks where the next state depends only on the current one, however in many practical cases, the future value depends on longer history (e.g., mobility). Neural networks based models have recently become popular to model sequential data (Wu et al., 2017), however, they are tuned to specific tasks and not suitable for general mining and learning. We address this problem in Chapter 4 by encoding longer location history using fixed dimensional topological signatures.

Although, several data driven methods for mobility modeling are proposed in the literature (Barbosa et al., 2018; Rezaei et al., 2018), there is a lack of a comprehensive reliable model. Therefore, the problems of predicting travel time, estimating popular paths, generating synthetic trajectories are hard and need further study.

Learning applications. Here, we briefly describe the major learning applica-

tions for sensor data.

Mining statistics from categorical streams is well studied. Many interesting randomized methods are proposed to estimate moments, find heavy hitters, etc (Leskovec et al., 2014). However, all the methods in this genre either assume events in synchronous rounds or do not depend on timing. In this dissertation, we are concerned about events with associated timings generated in an asynchronous setting.

Clustering is a fundamental operation in machine learning. This is relevant to many applications, for example, grouping similar trajectories for ride sharing. Clustering time series and trajectories have been studied in the literature using different techniques (Buchin et al., 2011; Pokorny et al., 2016). We address this problem using topological signatures in Chapter 4.

Classification, grouping objects according to their labels, is ubiquitous, for example, classifying modes of transportation, user activities, etc. Several regression techniques like ARIMA (Liu et al., 2016), Gaussian Process Regression (HajiGhassemi and Deisenroth, 2014), etc., have also been studied to predict future values in a time series.

1.2.3 Preserving Privacy

Privacy is a natural concern in user centric sensing because nontrivial sensitive inferences are possible from location and time contexts. In the literature, there are two fundamental approaches to preserve privacy – anonymization and statistical privacy.

Anonymization. Anonymization is a common practice to make a dataset private by taking out the obvious user identifiers or replacing them with random values. However, it is shown to be possible to re-identify individuals considering auxiliary knowledge from other publicly available datasets. For example, a user can be characterized by time independent frequent visit locations (Pan et al., 2013), and with the knowledge of home and work locations, individuals can be re-identified. Moreover, (De Montjoye et al., 2013) showed that four spatiotemporal points are enough to uniquely identify 95% of individuals. They further showed that even with reduced resolution in spatial and temporal dimension privacy improves a little.

Popular k-anonymity provides privacy by making the sensitive record in-

distinguishable with $k-1$ other records and has been successful for relational databases (Sweeney, 2002). Although this is used for location privacy (Gramaglia et al., 2017; Gramaglia and Fiore, 2015), fundamentally it is not suitable for spatial and temporal data, because these types of data are real valued and need large perturbation. Again, k-anonymity protects against re-identification with probability $1/k$, but does not essentially protect the sensitive information. For example, suppose an adversary is interested to know whether a user u visited the hospital at a certain time. Then, knowing that one of k trajectories going to the hospital belongs to u is vulnerable.

Publishing anonymized event timings can leak user identity or sensitive information about an individual, for example, knowing that a user opens a medicine website regularly may reveal the sensitive medical state, exact timing of a call or message can reveal delicate dependence on sensitive incidents. The topic of anonymization is not investigated in this dissertation.

Statistical privacy. A stronger privacy guarantee is achievable using statistical privacy frameworks, such as differential privacy (Dwork et al., 2009). This is now considered as the gold standard for privacy preservation to answer aggregate queries. It probabilistically perturbs query results to blur the participation of any individual in the dataset. For this purpose, a differential privacy mechanism adds noise proportional to the worst case change in the query result in the absence of any individual in the dataset. It protects any individual against the strongest adversary who knows all sensitive information for all the participants except for the one participant he is interested in.

Differential privacy is extended to support continuous queries in streaming settings (Chan et al., 2011) and to accommodate data generation process into the framework using Pufferfish privacy (Kifer and Machanavajjhala, 2014a). In Chapter 3, we use the Pufferfish privacy framework to publish event timings and answer temporal range queries. There we protect the exact timings of events and their occurrence.

Privacy concerns for location tracking are omnipresent, however, location based systems need to know the user's location to produce useful results. Users may not trust the service providers or possible third party agents involved in the process (e.g., advertisements). A considerable amount of research has been done to protect the exact location of the users and yet enable the location based systems to return useful results (Andrés et al., 2013). We study the problem

of protecting privacy of location data in a distributed sensor network setting in Chapter 5 using the differential privacy framework.

Protecting privacy of trajectories is hard because users have unique mobility (Barbosa et al., 2018). (Xu et al., 2017) demonstrated that even without any prior knowledge, individual users' trajectories can be reconstructed from aggregated data like the number of people served by a cellular tower at specific timestamps. There have been multiple studies using k-anonymity (Gramaglia and Fiore, 2015), plausible deniability (Bindschaedler and Shokri, 2016), etc. for providing trajectory privacy. But, all these methods need much noise because of their spatiotemporal uniquness, continuity of a trajectory, and correlation between trajectories; So, further in-depth study in this topic is required to reduce the amount of noise needed and thus preserve better utility.

1.3 Summary

This section summarizes the major contributions of this thesis. It has two parts discussing analysis and privacy aspects of temporal and spatial data.

1.3.1 Learning From Temporal Streams

In this part, we focus on sequences of discrete events at real valued timestamps. These events are produced by sensors, for example, gait, heart beat, check-in, usage of apps in a phone, etc. Depending on the application concerned, these events can naturally be discrete, like check-ins, or extracted from the real valued signals using suitably chosen peaks. Patterns in the timestamped events are essential to learn for personalization and service optimization. However, these events contain sensitive personal attributes, and thus raise privacy concerns in such data collection. This thesis addresses the following specific problems in this regime.

Tracking periodicity in noisy event streams. (Ghosh et al., 2017) Detecting periodicity in noisy streams is challenging – especially when periodicity and phase drift over time and the stream has false positive events. These characteristics are common in many real datasets such as footsteps, heartbeats, daily habits, periodic surges in traffic, etc.

Chapter 2 proposes a generalized formal framework for periodicity and a novel

probabilistic model for periodic events in both idealized and realistic noisy scenarios. To estimate the periodicity, a particle filter-based algorithm is proposed. The algorithm initially guesses a few periodicity values and iteratively refine them based on real events. Experiments on simulated and real datasets show that the method outperforms existing methods in both accuracy and efficiency.

Private sensing of asynchronous event sequences. (Ding et al., 2019) Densely deployed sensors provide opportunities for large scale monitoring of home, workplace and public domains. Such data are shared with service providers and possibly with third parties (Chen et al., 2017; Ganti et al., 2008) – for research, environmental monitoring and other purposes. In the process of sharing and use of IoT data, sensitive private information such as activities of an individual can leak. Existing privacy mechanisms only consider events captured in synchronous rounds and require high sampling rate to support dense events. As a result, these methods introduce a large amount of noise globally.

Chapter 3 develops two mechanisms for protecting privacy of event timings. The first algorithm publishes event timings by perturbing them using Laplace distribution to hide exact event timings from an adversary. Further, to hide the occurrence of an event, the second algorithm augments the event stream with fake events in such a way that no adversary can be sure (e.g., with high probability) if an observed event is real. The standard deviation of the Laplace distribution and the rate of fake events are adjusted according to the privacy parameter and real event rate. Both of these methods achieve ε-Pufferfish privacy and preserve better utility for range queries than existing algorithms. In this chapter, we also discuss design choices to implement a sanitization service on the mobile phone such that all sensing applications in the phone can sanitize their data.

1.3.2 Learning From Spatial Data

Spatially distributed sensors collect data with location attributes, for example, user check-ins at points of interests, trajectories of vehicles, etc. Location tracking applications localize individual users using positioning systems, like GPS, call records, WiFi associations, etc. Applications range from learning individual mobility (e.g., predicting future location) to aggregate behavior (e.g., finding popular paths).

However, location data is among the most sensitive attributes being collected

with the possibility of social, economic, and physical inference and vulnerability. For example, one can infer a user's non-trivial medical condition from his regular visit to a certain part of the hospital. Despite its importance, until recently, location privacy did not tract the attention of research or industry due to the difficulty of tracking an individual's movements. But, recent technological growth with mobile phones, IoT devices, and GPS equipped vehicles made location data abundant, and therefore location privacy is of paramount importance.

Mobility mining using topological analysis. (Ghosh et al., 2018) Chapter 4 develops an efficient framework to analyze spatial trajectories. The analysis is from the perspective of the obstacles in the domain and it uses differential topology to map the trajectories to Euclidean vectors, called topological signatures. In a domain with k obstacles, the signatures have k dimensions; Each dimension characterizes how the trajectory navigates the corresponding obstacle.

Topological signatures provably preserve homotopy properties of the trajectories and support similarity measures between arbitrary trajectories. They enable Euclidean mining and learning methods to complex trajectories, e.g., nearest neighbor search using locality sensitive hashing, clustering, regression, density estimation, etc. Standard regressors using signatures can predict direction at large scale (e.g., $500m$) more accurately and efficiently than even complex neural network based models on raw location data. Extensive experiments on GPS taxi trajectories demonstrate that the signatures are useful for analyzing real datasets.

Publishing Differentially Private spatial data from distributed sensors. (Ghosh et al., 2019) Events captured by spatially distributed sensors are often subject to aggregate query over multiple sensors. For example, a range query on a check-in dataset measures crowd density. However, such an aggregate query needs an aggregator service. Users may not trust the aggregator, or the communication medium connecting the sensors to the aggregator, therefore, the sensors should sanitize the data before it reaches the untrusted entity. Existing mechanisms either assume centralized operation, add noise after aggregation or add too much noise to support distributed operation.

In Chapter 5, we propose multiple differentially private algorithms to publish event locations and support real-time analysis using range queries. Proposed methods are based on fake event augmentation and perturbation of event origins using a random walk in the sensor network. These mechanisms achieve (ε, δ)

differential privacy and preserve better utility for spatial range queries than competing methods.

Part I

Learning from Temporal Streams

Chapter 2

Periodicity in Noisy Event Streams

In this chapter, we describe a model of periodic events that covers both idealized and realistic scenarios characterized by multiple kinds of noise. The model incorporates false-positive events and the possibility that the underlying period and phase of the events change over time. We then describe a particle filter that can efficiently and accurately estimate the parameters of the process generating periodic events intermingled with independent noise events. The system has a small memory footprint, and, unlike alternative methods, its computational complexity is constant in the number of events that have been observed. As a result, it can be applied in low-resource settings that require real-time performance over long periods of time. In experiments on real and simulated data we find that it outperforms existing methods in accuracy and can track changes in periodicity and other characteristics in dynamic event streams.

2.1 Introduction

Here, we will study discrete event streams that exhibit *approximate* periodicity. These sequences contain noise events interleaved with the periodic events, together with variations in the times that events are observed, and variations in the period itself.

The presence of noise events, or false positives, is common in sensor data and other data streams that are subject to inaccuracies and calibration issues. An example is shown in Figure 2.1, where we use the output of an accelerometer on a phone to detect footsteps as a person walks. The steps are indicated by large spikes in acceleration, but for any threshold that reliably detects actual steps,

extraneous spikes in acceleration create false detections – or noise events. The challenge here is to detect the periodic events against the backdrop of these false positives.

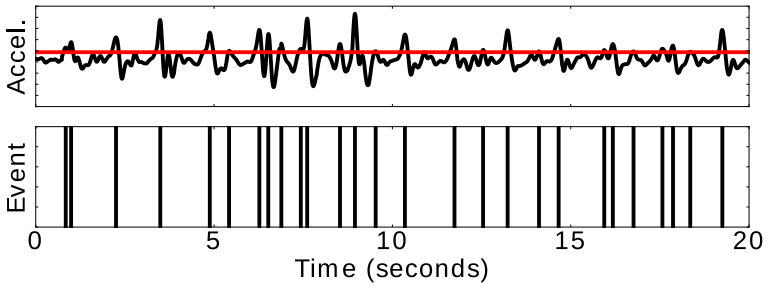

Figure 2.1: Noise events in footstep detection. Top plot: Accelerometer signal (Euclidean norm of acceleration given by 3-axis accelerometer on mobile phone), with event detection threshold in red. Bottom plot: Detected events. Some of the detections are noise events, produced by inter-footstep accelerations that exceeded the threshold.

Another common property of approximately periodic sequences is that even for events originating in the periodic process, the event times can be subject to noise or drift. While footsteps are periodic, they do not follow a perfect lock-step pattern – a person may pause, speed up, or slow down. These temporal offsets can accumulate, causing the periodic signal to depart from its original phase and/or period. Figure 2.2 shows an example of this behavior. A change in phase can throw off classical methods such as Fourier transform, which has been used to detect periodicity in discrete event streams in previous works (Jindal et al., 2013).

We thus need methods to find noisy patterns that are functions of time itself from an event stream. Some methods have been developed in the past to solve the problem of detecting discrete periodic events (e.g., (Li et al., 2012, 2015b; Indyk et al., 2000)) but these methods cannot handle sequences with variability in inter-event time and consequent phase changes. We will discuss flexible designs to accommodate this variability as well as noise events, while being computationally efficient for long streams of events.

Our contribution. We define a model of discrete signals with approximately periodic sequences embedded in them. The model is described in Section 2.3, and includes a periodic component with probabilistic inter-event time, and a Poisson

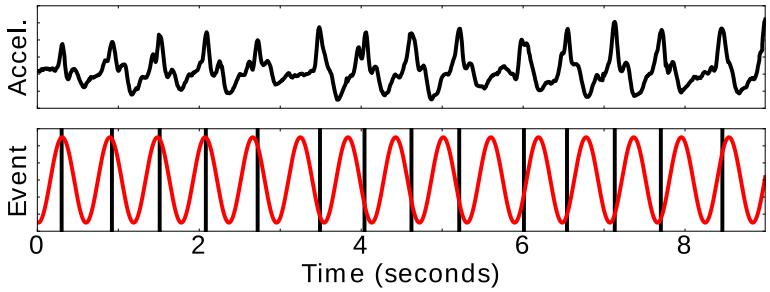

Figure 2.2: Top plot: Acceleration signal during walking. Bottom plot: Black lines denote local maxima in acceleration above a threshold, corresponding to individual footsteps; red line shows a sinusoid that is matched to the initial period of footsteps, demonstrating phase drift (or noise in inter-event delays) over time.

process modeling the aperiodic false positive noise events. It generalizes previous systems (Han et al., 1999; Indyk et al., 2000).

Section 2.4 describes the design of a particle filter system based on this model, which can identify the periodic events from the sequence in an online fashion. In addition to predicting events, it infers parameters of the underlying process such as the local period, the rate at which the period changes, and the rate at which noise events tend to occur. The particle filter system works with a collection of *particles* or *hypotheses*. Each hypothesis includes guesses about the parameters of the model, such as the period. With each new event, the system evaluates the current set of particles and assigns a weight to each depending on how well it has predicted the latest events. Based on these weights, the model occasionally rejuvenates particles to retain a diverse and plausible set of hypotheses and improve long-run accuracy.

To handle noise events, each hypothesis in the particle filter identifies the most recently observed event as either a periodic event or a noise event, in addition to tracking the overall rate of noise events. In systems where almost all events are due to noise, identification of periodic events is costly and error-prone, while the predictability of periodic events loses much of its utility as noise events overwhelm periodic events. In order to achieve high performance and a low memory footprint in contexts where periodic event detection is possible and useful, our particle filter incorporates the assumption that tractable noise rates are more likely.

The system works in an online or incremental manner, in that it only requires knowledge of events up to a point in time, without the need to know the entire event stream. Thus it can be used to track events in real time – even as the period

changes. We show it can operate accurately with relatively few particles and thus can be used at a low computational cost to analyze large volumes of data in a single pass. The particle filter processes events as they occur, and incurs no cost for the quiet periods between them. Thus the cost of the method depends only on the number of events, and is independent of the total duration of the event sequence or the sampling rate.

Experiments in Section 2.5 show that the system can accurately estimate the period of an event-generating process on both synthetic and real-world data. Existing methods are not designed to handle shifts in phase (Figure 2.2) and noise, as a result, they perform relatively poorly in these cases. Each hypothesis includes expectations about when future periodic events will occur, so the system can be used to predict upcoming events. Our experiments show that these predictions are accurate and robust to noise and changing periods. Moreover, the experiments show that our system works well with sparse data, converging to accurate estimates after observing only a few events.

2.2 Related works

Time series analysis has traditionally considered real-valued functions. Fourier transform is a natural tool for detecting periodic patterns in real-valued signals, and has also been applied to detect periodicity in binary event streams (Jindal et al., 2013). However, as observed in (Li et al., 2012), it does not perform well in data with noise, missing signals and other errors. It also does not lend itself to online inference, which is one of our main desiderata. Further, Fourier transform aims to fit a global phase and periodicity to the data. In our model, where phase can drift, the signal can easily go out of phase with the basic sine wave (Figure 2.2).

A *sketch* based approach in (Indyk et al., 2000) uses random linear projection over windows of time series data to compress them for easier comparison. This makes comparison between windows easier, but does not easily extend to detecting periodic events at arbitrarily large scales. More recently, Gaussian processes with periodic and Fourier kernels have been used to detect such periodic patterns (Ghassemi and Diesenroth, 2014; Osborne et al., 2008). These methods can detect periodic relationships in real-valued signals, but it is unclear how they might be extended to accommodate point events or online inference; the

cost of inference scales at least linearly with the number of data points being considered (and is $O(N^3)$ in naive implementations), falling short of our goal of constant-time inference per new event.

More relevant to our topic, Li et al. (Li et al., 2012) and its extension (Li et al., 2015b) have recently considered detecting periodicity in binary event sequences with noise. This approach is based on the intuition that the histogram modulo the correct time period will show peaks corresponding to true periodic events. This trial for various candidate periods, however, makes the method computationally expensive and difficult to adapt to streaming data. This method also is based on the model of a system with a fixed phase and thus fails when applied to more dynamic models.

Periodicity in sequences of symbols or strings has been considered in various other contexts. A filtering method based on the "apriori property", is described in (Han et al., 1999). It aims to find frequent periodic sequences in strings, which is computationally expensive. Other methods for periodicity in symbol sequences including gene sequences are considered in (Yang et al., 2003; Junier et al., 2010).

None of these existing methods can handle input with intrinsic variability which can cause the phase of the periodicity to change. As a result, as we saw in our experiments, these methods are not suitable for online operation or tracking rapidly changing periods of signals.

2.3 Model and problem description

In this section, we will develop a model that allows noise in periodic event sequence – both in the period itself and in occurrence or observation of individual events. Then we discuss how this model relates to different real scenarios.

Periodic events often arise because some recurring process takes a roughly uniform amount of time to finish and yield an observable event. Examples include heartbeats, volcanic geysers or steps taken by a walking person. In these systems an event may sometimes be delayed due to irregularities of the intervening process, resulting in a shift of phase as shown in Figure 2.2.

If such a system is perfectly regular, then every event $i+1$ occurs at time x_{i+1}, exactly T time units after event i, that is, $x_{i+1} = x_i + T$. The effect of the irregularity is then modeled using a Gaussian of variance σ^2 and zero mean added to T, giving us $x_{i+1} \sim \mathcal{N}(x_i + T, \sigma^2)$. Here T is the fundamental *period*

or inter-event interval parameter, while σ can be seen as the "noisiness" of the period over time.

Other than the intrinsic irregularity of the process, the data can reflect noise events. Noise events may either come from the observation mechanism affecting both record of true events as we have seen in Figure 2.1, or it may represent a different or spurious source of events.

We model this noise sequence as a Poisson process, i.e., a sequence of events $z_1, z_2, ...$ where $z_{i+1} = z_i + \delta$, and δ follows an exponential distribution with rate parameter λ; a higher lambda implies a greater rate, or shorter expected durations between false positive events.

Thus in our model, the overall sequence $y = y_1, y_2, \ldots$ can be partitioned into two subsequences[1]:

- A sequence x of periodic events, where $x_{i+1} \sim \mathcal{N}(x_i + T, \sigma^2)$.
- A sequence z of noise events given by $z_{i+1} = z_i + \delta$, where δ follows an exponential distribution with an expectation of $(\lambda)^{-1}$, for a rate parameter $\lambda > 0$.

Problem statement. Given a sequence of event times $y_{1:n} = y_1, \ldots, y_n$, we wish to infer the period T, which is the fundamental parameter that describes the behavior of the system. We would also like to know the parameters σ and λ that determine the extent and nature of the noise in the system.

As an additional feature, we want the algorithm to be *online*, meaning that it processes the sequence one item at a time, updating its estimates with each input without requiring that the system store or process the full event history. The ideal algorithm will make inferences with $O(1)$ time and memory complexity after each event, and can thus remain responsive even after processing arbitrarily large numbers of events.

Generality of the model and local fit with input. This model incorporates quite general scenarios. It does not make any assumption about there being a set of "true" signal events to detect as opposed to observational noise. It assumes that all events may be generated by the same underlying process, and aims to detect the presence of a periodic subsequence. The Gaussian distribution of inter-event

[1] A subsequence of a sequence is a subset of the events, not necessarily contiguous, in the same order as in the original sequence.

time represents a sum of unknown variables that may cause the local variations in the period.

As shown in Figure 2.1, the threshold for an "event" determines the noise rate. It is possible to set a high threshold to ensure very few noise events, at the risk of missing some fraction of periodic events. However, lower thresholds are more desirable – they may include more noise, but will not miss the periodic events. Our model is designed with this setup in mind – that periodic event information is preserved, even at the cost of more noise events. The parameter λ as part of the hypothesis learns this noise rate. Poisson processes are commonly used for such models, as they only assume that the noise occurs at a certain uniform rate in any temporal locality.

Note that the system operates in terms of a set of evolving hypothesis and can adapt to changing model parameters online as the system behavior changes. Thus, it is not required that the model fits the global data over long periods of time, only that it fits the system approximately, over any short period of time. Experiments show that in fact this model successfully adapts to periodic events and tracks them closely with changes in the system. Its performance remains consistent when the noise and inter-event variability are generated using distributions other than the ones assumed in the model.

Discussion and variations of the model. There are various common scenarios where periodic events are generated by processes that are special cases or variations on the model above. The simplest is what we will call *strict periodicity*, where successive events are separated by an exact time interval T, such as clock ticks, or events tied to clock-like sequences. Formally, $x_i = \phi + iT$, if all events are due to a strictly periodic process. We get this behavior in our model above by setting $\sigma = \lambda = 0$.

Strict periodicities are easy to capture, by simply observing the interval between successive events. A variant of this is *partial periodicity*, where a strict periodic function is mixed with noise. This was considered in (Han et al., 1999).

Certain sequences like heartbeats or volcanic geysers satisfy $\lambda = 0; \sigma > 0$ – they are not tied to a clock, but depend on a build up in the intervening process that can have some variability, and change in phase or even dynamic change in the period itself.

There are systems where noise in the periodicity exists, that is $\sigma > 0$, but phase does not not change. Example would be daily activities of a person –

such as checking the news in the morning – which may not have a strict inter-event time, but still around a particular time in the morning. These can be modeled by adding *observational noise* to strict periodicity: $x_i \sim \mathcal{N}(\phi + iT, \hat{\sigma}^2)$. The variation in inter-event time does not affect the phase ϕ here. This type of sequences have been addressed in a recent work (Li et al., 2012). The approach there is to consider the histogram of events modulo a number W, which produces a pronounced peak at the correct value of $W = T$. We discuss this and other related methods in Section 4.2.

2.4 Particle filter design

In this section, we describe a particle filter based system to detect periodicity in noisy and approximately periodic event sequences. The next subsection briefly summarizes particle filters, which form the foundation of our approach, and lists our notations. Following this, we describe the details of our design to adapt particle filters to the current problem.

2.4.1 Particle filters and importance sampling

Particle filters, or sequential Monte Carlo methods, are a popular family of online methods for making inferences about latent variables in noisy environments. They have been applied to diverse problems, including locating and tracking objects using sensor data (e.g., (Stewart and McCarty, 1992)), machine vision (e.g., (Nummiaro et al., 2003)), and natural language processing (e.g., (Canini et al., 2009)).

The essential idea is that each *particle* is a point sample in the space of possibilities of all the parameters in question. We interchangeably use the term *hypothesis* to mean that each particle is one of our guesses of the true configuration of the system.

Our goal is to determine the period T of an approximately periodic sequence. In probabilistic terms, we want to obtain a posterior distribution over possible values of T_n: the period after the n^{th} event, given a vector of observed event timestamps $y_{1:n} = \{y_1, ..., y_n\}$ up to that point. The period is not the only salient feature of the event-generating process, so we will use h_n to denote the ensemble of features, which includes the period, variance σ^2, rate of noise events

Symbol	Description
$f(x;\mathcal{D})$	Probability of random variable $R \sim \mathcal{D}$ taking value in small neighborhood of x.
$F(x;\mathcal{D})$	Probability of random variable $R \sim \mathcal{D}$ taking value $\leq x$.
$\exp(\lambda)$	Exponential distribution with rate λ.
y_i	i^{th} Event timestamp.
$h_i^{(j)}$	j^{th} hypothesis (also called as particle) after observing i^{th} event timestamp.
$\mathcal{L}_i^{(j)}$	Likelihood weight of $h_i^{(j)}$.
Hypothesis parameters of $h_i^{(j)}$	
$T_i^{(j)}$	Period parameter value.
$\sigma_i^{(j)}$	Standard deviation for Gaussian distribution of period variability.
$\lambda_i^{(j)}$	Rate of false positive noise events.
$\hat{z}_i^{(j)}$	Latest event timestamp marked as noise event
$\hat{x}_i^{(j)}$	Latest event timestamp marked as periodic event

Table 2.1: Definition of useful symbols

λ and whether an event is periodic (from the subsequence x) or is noise (from subsequence z).

With a posterior distribution over h_n, we can draw probabilistic conclusions about any of these variables. The probability of h_n cannot be computed exactly because it requires solving intractable integrals, but we can efficiently approximate its distribution in constant time per incoming event, by using a simple recursive Bayesian algorithm known as a *bootstrap filter* or *sequential importance sampler*. This idea is closely related to conditional density estimation in machine vision. We refer the reader to (Doucet et al., 2001; Thrun et al., 2005) for a de-

tailed explanation, restricting our attention to a brief summary in Algorithm 1, along with the distributional assumptions that allow us to apply it to the current problem.

In this algorithm, we need to keep track of our estimates of various parameters after each event. Thus we use subscript i to represent value of variables after event i. Further, each hypothesis or particle has its own estimate of variables, thus we use superscript (j) to represent the estimate of the variables in particle (j). Table 2.1 summarizes all the symbols used in this section, while Algorithm 1 presents the basic operation of a bootstrap filter.

Algorithm 1: Sequential Monte Carlo with resampling

Particle filter *(Event timestamps $y_{1:n}$)*
begin
Initialize k hypotheses $h_0^{(1)}, \ldots, h_0^{(k)}$ by sampling from a prior distribution over hypothesis parameters.
for *(time step i in $1, \ldots, n$)* **do**
for *(particle j in $1, \ldots, k$)* **do**
sample $h_i^{(j)}$ from $p(h_i|h_{i-1}^{(j)})$
Likelihood weight $\mathcal{L}_i^{(j)} = p(y_i|h_i^{(j)})$
end
Normalize likelihood weights: $\tilde{\mathcal{L}}_i^{(j)} = \frac{\mathcal{L}_i^{(j)}}{\sum_{j=1}^{k} \mathcal{L}_i^{(j)}}$
Resample k hypotheses with replacement according to normalized weights $\tilde{\mathcal{L}}_i^{(j)}$.
end
end

Algorithm 1 processes each event as follows. It initializes several hypotheses from the distribution over features for each particle. Then at every event, it checks how likely the new event is for each of these hypotheses, and uses that as a "score", $\mathcal{L}^{(j)}$, for each particle. Next, it normalizes the scores to turn them into probabilities, and resamples the set of hypotheses according to these to get the set of particles for the next round, effectively favoring neighborhoods of particles that have matched better with recent events. At any time, the estimate for a parameter is the expectation of the parameter over all particles weighted by their current scores.

2.4.2 Particle filter for discovering periodicity

A hypothesis h_n contains the estimated characteristics of the periodic signal after n events. The periodic characteristics are specified using the period T_n, and standard deviation σ_n for Gaussian distribution of period variability. Our hypothesis h_n also includes the last periodic event $\hat{x}_n$ in the sequence. We have included the rate of background noise events λ_n, and the timestamp of the last event that was attributed to noise, $\hat{z}_n$ in our definition of h_n. We will use i to index event timestamp, y_i, where $1 \leq i \leq n$.

Under this model, each event y_i originates from either the periodic signal or false positive noise. We introduce $r_i \in \{0, 1\}$ to track event provenance, where $r_i = 1$ represents the case where the i^{th} event comes from the periodic process. This auxiliary variable facilitates efficient inference: using r_i, we obtain a closed-form solution for the density of periodic events conditional on the last periodic event, and noise density conditional on the last event. Calculating $P(r_i|y_{1:i}, h_{0:i-1}, r_{1:i-1})$ exactly is expensive, as the number of states involved increases exponentially as we observe more events, but we can augment our sampling procedure to reflect the posterior distribution of r_i. For simplicity we omit (j) superscripts where they are clear from context.

The bootstrap particle filter algorithm requires us to specify three probability distributions:

- A prior over hypotheses for initialization of $h_0^{(j)}$.
- A likelihood function adjusting the weight of a hypothesis given observed events.
- A distribution defining how hypotheses change between events.

We specify the distributions as follows:

Priors. For each hypothesis $h^{(j)}$ we sample the initial period $T_0^{(j)}$ and noise event rate $\lambda_0^{(j)}$ from exponential distributions, and sample the standard deviation $\sigma_0^{(j)}$ uniformly from the interval $[0, T_0^{(j)}]$. At the initialization stage, we know nothing about the periodicity value or noise event rate other than that they are positive, thus we use exponential distribution as a maximum entropy guess for the distribution. Both $\hat{x}_0^{(j)}$ and $\hat{z}_0^{(j)}$ are assumed to start at zero.

Likelihood weighting. Given a hypothesis h_i, the likelihood of event i occurring

at time y_i is equal to $\mathcal{L} = \sum_{r_i \in 0,1} p(y_i, r_i | h_i)$. The periodic signal's contribution to this sum is $\mathcal{L}_{per} = p(y_i, r_i = 1 | h_i)$, and is the product of two terms:

- Density function from the previous periodic event, assuming that $\hat{x}_{i-1}$ is known. Since the time of a periodic event is subject to additive Gaussian noise, we represent this density as

$$p(y_i | h_i^{(j)}) = \mathcal{N}(T_i^{(j)} + \hat{x}_{i-1}^{(j)}, \sigma_i^{(j)}). \tag{2.1}$$

- A term based on the observation that $r_i = 0$ if and only if there are zero noise events in the time between $\hat{z}_{i-1}$ and y_i, inclusive. If a Poisson process generates noise events, then that probability is $e^{-\lambda_i (y_i - \hat{z}_{i-1})}$.

The false positive noise's contribution to the total likelihood is $\mathcal{L}_{bg} = p(y_i, r_i = 0 | h_i)$. Here, we have a product of two terms:

- An exponential distribution, with its origin at $\hat{z}_i$ and a rate equal to the noise rate.

- The cumulative probability that no periodic event occurred between $\hat{x}_{i-1}$ and y_i. We approximate this probability by the complementary cumulative density of periodic events between y_i and $\hat{x}_{i-1}$ by evaluating the complementary cumulative density function for the distribution in Equation 2.1.

A pseudo code of of the likelihood weighting is presented in Algorithm 2. The components of the likelihood function are illustrated in Figure 2.3.

Hypothesis updates. With each iteration, the hypothesis distribution is updated according to the prior over state changes. We obtain $h_i^{(j)}$ by sampling from $p(h_i | h_{i-1}^{(j)})$, where $p(h_i | h_{i-1}^{(j)})$ implements for each parameter in $h_i^{(j)}$, a sampling from a Cauchy distribution centered at the previous value of the parameter. For example, $T_i \sim \text{Cauchy}(T_{i-1}, b)$ where b is a tunable scale parameter. The period (T), periodic deviation (σ), and noise rate (λ) (truncated at zero) are updated according to the said Cauchy distribution.

Note that these updates make it possible to iteratively refine parameter estimates, in addition to tracking the dynamics of the system, e.g., when the period or phase changes over successive events.

The $\hat{z}_{i-1}$ and $\hat{x}_{i-1}$ terms are updated differently depending on whether the provenance of the latest event is the periodic or noise process. Given that y_i is

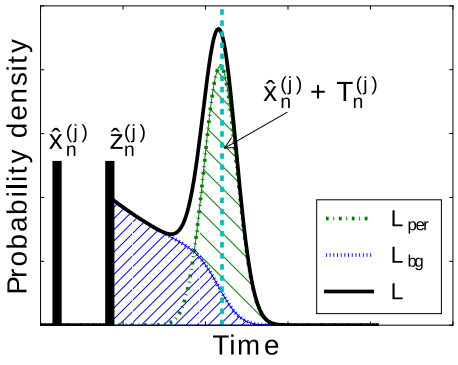

Figure 2.3: Periodic and false positive noise's contribution to the likelihood of hypothesis j. The periodic contribution $\mathcal{L}_{per}$ is centered around $T_n + \hat{x}_n$ where $\hat{x}_n$ denotes the last periodic event and the noise contribution $\mathcal{L}_{bg}$ starts from the last noise event $\hat{z}_n$.

Algorithm 2: Likelihood Weighting of j^{th} hypothesis $h_i^{(j)}$ on observing i^{th} event timestamp y_i.

Likelihood Weight $(h_i^{(j)}, y_i)$

begin

$$\mathcal{L}_{per} = f\big(y_i; \mathcal{N}(\hat{x}_{i-1} + T_i, \sigma_i)\big) \times \big(1 - F\big(y_i - \hat{z}_{i-1}; \exp(\lambda_i)\big)\big)$$

$$\mathcal{L}_{bg} = f\big(y_i - \hat{z}_{i-1}; \exp(\lambda_i)\big) \times \big(1 - F\big(y_i; \mathcal{N}(\hat{x}_{i-1} + T_i, \sigma_i)\big)\big)$$

$$\mathcal{L} = \mathcal{L}_{per} + \mathcal{L}_{bg}$$

return $\mathcal{L}$

end

observed, we can use $p(y_i, r_i|h_i)$ to obtain a conditional distribution for r_i: $p(r_i = 1|y_i, h_i) = \frac{p(y_i, r_i=1|h_i)}{p(y_i, r_i=1|h_i)+p(y_i, r_i=0|h_i)}$. We can then sample r_i from this Bernoulli distribution, and by extension $\hat{x}_{i-1}$ and $\hat{z}_{i-1}$: if $r_i = 1$ then, $\hat{x}_i = y_i$ and $\hat{z}_i = \hat{z}_{i-1}$. Otherwise, $\hat{x}_i = \hat{x}_{i-1}$ and $\hat{z}_i = y_i$.

Output: period estimate. After seeing n events, the expected period of the event sequence is $\mathbb{E}[T_n] \approx \sum_{i=1}^{k} \tilde{\mathcal{L}}_n^{(j)} T^{(j)}$, and represents an estimate of the period. More generally, we can take the expectation of arbitrary functions $f(.)$ of hypotheses by replacing $T_n^{(j)}$ with $f(h_n^{(j)})$, to obtain estimates of other parameters such as noise rate and period variability. In our experiments, we use the weighted median as a more robust estimate of parameters.

2.4.3 Practical optimizations for noisy environments

The algorithm presented in the previous section can detect the period of a noisy sequence of events, but can require a large number of hypotheses to do so reliably; the particle filter needs a considerable number of hypotheses to ensure that several occupy high-probability regions of the parameter space. If we use a small number of hypotheses, then the particle filter will occasionally provide poor or high-variance estimates, especially when the period or dynamics are extreme or a priori unlikely. In this section, we present a modification our basic algorithm that preserves accuracy while using fewer hypotheses.

A pragmatic observation from an end-user's point of view is that if the number of noise events in a sequence is much greater than the number of periodic events, then the period value of the signal is not useful for predicting future events, and periodic event detection may become infeasible. Motivated by this observation, we can modify the likelihood weighting strategy for the previous algorithm to capture the assumption that we are facing an estimation problem for which there exists a *useful* solution. In so doing, we improve our ability to obtain useful solutions if they exist, and incur negligible costs if they do not.

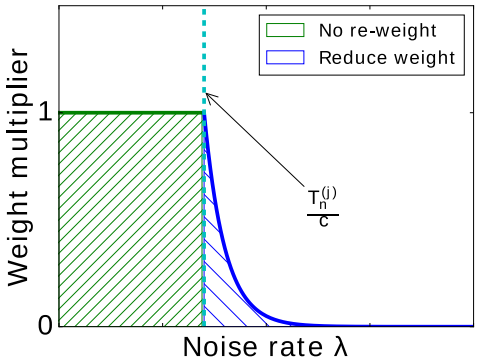

Figure 2.4: Re-weighting function.

We fix an application specific input parameter c to our algorithm, expressing a ratio of the number of noise events to the number of periodic or regular events, above which useful inferences are likely to be elusive. Parameter c can be tuned for specific applications, but in practice the value 2 works well across the settings for all of our experiments. We assign lower probabilities to hypotheses that have higher noise event rates than c, reducing the weights of the hypotheses for which $\lambda_i^{(j)} \times T_i^{(j)} < c$ according to an exponential decay function. The start location of the exponential decay function is set to be $\frac{c}{T_i^{(j)}}$, and the rate depends on the

importance of the assumption of limiting noise rate. We multiply the likelihood of a hypothesis derived as described in the previous section by a value drawn from a function as represented in Figure 2.4. With this strategy, we ensure low weights for the hypotheses which have large periods and high noise event rates that would lead to poor predictive accuracy.

2.5 Experimental evaluation

We tested the performance of our particle filter and compared it with existing ideas on real human gait data and human pulse data. We also created several sets of artificial data with different values of intrinsic variability, noise event rate, and period to precisely characterize the detection accuracy. Overall, we found that:

- In presence of noise events and phase drifts the particle filter method outperforms other techniques in accuracy.
- With higher noise event rates and phase drift, only the particle filter produces reasonably accurate and reliable results.
- The particle filter method can operate with a reasonable and constant number of about 256 particles to give good results.
- The particle filter runs more efficiently than competing methods, and thus is suitable for operation in an online environment to produce increasingly accurate results.
- On data with rapidly changing periodicity, the method can track the period closely. We show this by applying the technique to human step data to determine changing gait rate.
- The method applied to real data such as human pulse and gait data accurately detects periodicity.

The following subsections first describe the competing techniques for periodicity detection, and then the detailed experimental results.

2.5.1 Comparison algorithms

The following popular methods for detecting periodicity are compared with the particle filter algorithm.

Fourier Transform: The frequency with highest spectral energy in Fast Fourier Transform algorithm is a reasonable candidate for the true frequency of the system. This technique has been used in the past as a practical method for detecting periodicity (Jindal et al., 2013).

Autocorrelation: The cross-correlation of the input signal with the signal itself with different amounts of offsets, thus building the autocorrelogram can be used to find period of a signal. The delay of the signal where the cross-correlation value reaches its maximum value can then be treated as the period of the signal (Vlachos et al., 2005). A linear search on period values is required to find this maximum.

Segmentation based algorithm: The method described in (Li et al., 2012) detects periodicity in face of approximate periodicity and noise, as described in Section 2.3. This algorithm operates by checking all possible periods by computing the histogram of events modulo the period, and looking for a "peak" in this histogram. This checking of all possible periods makes it inefficient on large datasets.

2.5.2 Sensitivity to noise and model parameters

To gain understanding of the basic operation of the system in noisy environments with variability in period and presence of noise events requires data with precisely known values of these parameters. We thus simulated artificial data based on the models described in Section 2.3.

2.5.2.1 Generation of synthetic data

With fixed values for parameters: period T, deviation of periodic events σ, and noise event rate λ, we generated two separate sequences: the periodic events and the noise events, and merged them in sorted order.

Periodic event sequence (x). The first periodic event x_0 is set to 0. Each subsequent periodic event i is designated to occur at time x_i given by $x_i = x_{i-1} + \delta_{per}$. The distance between two consecutive periodic events, δ_{per} is drawn

form the Gaussian distribution $\mathcal{N}(T, \sigma^2)$. While drawing the samples δ_{per}, we make sure that the $(i-1)^{\text{th}}$ periodic event always precedes i^{th} periodic event, i.e. $x_{i-1} < x_i, i > 0$, by re-sampling δ_{per} from the Gaussian distribution.

False positive noise event sequence (z). Similar to periodic event sequence, the first noise event, z_0 is assumed to occur at time 0. Each subsequent noise event time z_i is constructed using recursive function $z_i = z_{i-1} + \delta_{bg}$. The inter-event distance between two consecutive noise events, δ_{bg} is drawn from an exponential distribution with rate λ.

The final event sequence y is a merge of the two event sequences in sorted order.

2.5.2.2 Performance evaluation of accuracy

The evaluations are based on the signal characteristic parameters: period T, the relative variance of periods ($\frac{\sigma}{T}$), and ratio of the frequency of noise events to frequency of periodic events in the signal.

For a signal with period T, let us denote the period predicted by an algorithm in consideration by $\hat{T}$. We define the relative error ξ as:

$$\xi = \left| \ln \frac{\hat{T}}{T} \right| \tag{2.2}$$

This measure is symmetric with respect to multiples of T. That is, an estimate of αT is considered equally erroneous as an estimate T/α.

For all the experiments, unless mentioned otherwise, we use a signal with 40 periodic events; the total number of observed events varies according to the noise event rate. In all experiments, the particle filter assumes that the rate of noise events rarely reaches twice the rate of periodic events. This assumption is not critical in practice as we show in our results in Figure 2.7(b). All experiments are repeated 16 times with independently generated synthetic data.

Effect of number of particles. Particle filters involve a tradeoff between efficiency and accuracy. Increasing the number of particles increases accuracy, but the computational cost increases linearly with number of particles. As expected, larger particle counts lead to lower average error (Figure 2.5). The error decreases steadily with increasing number of particles and we find that the error is quite low at about 256 particles, beyond which the gains are small. Thus, in the rest of the experiments, we use 256 particles. Note that computational cost for using

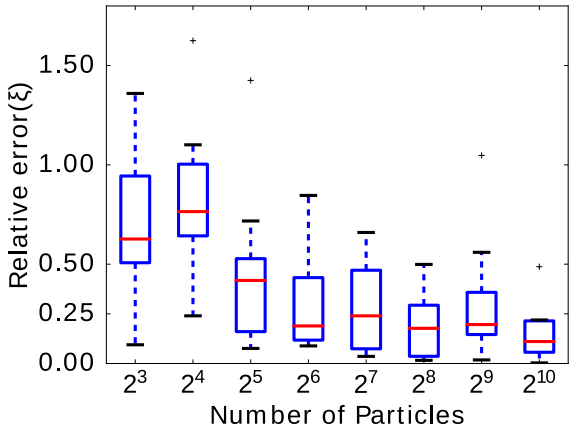

Figure 2.5: Error in period detection decreases with number of particles. 256 particles is a reasonable tradeoff for practical use where error is low and number of particles is small. Signal parameters: period T=10, relative deviation $(\frac{\sigma}{T}) = 0.6$, and average number of noise events per periodic event $= 1.5$.

256 particles is nominal in comparison to other algorithms as discussed later in this section.

All the box plots in this chapter have bottom and top boundaries as 0.25 (Q_1) and 0.75 (Q_3) quartiles of the relative error ξ. The middle line in the boxes represent the median values (Q_2) of the relative error. The whiskers are represented as 0.15 times the inter quantile range, e.g. $Q_3 + 1.5 \times (Q_3 - Q_1)$. Values appearing outside these ranges are considered as outliers and represented as individual points.

Effect of relative deviation of periodic events ($\frac{\sigma}{T}$). The deviation that the periodic signal can have, given by the standard deviation σ of the normal distribution, determines how fast the phase can drift away from the original configuration. Figure 2.6 shows that as σ increases relative to T, other methods perform poorly for even small values of σ, and do increasingly worse. The particle filter achieves reliable results even at high variance. This is in part due to the fact that unlike other methods, the particle filter is designed to be adaptive to change in phase and period and does not attempt to fit a single global model, including phase, to the entire signal.

Effect of noise events. Figure 2.7 shows that the particle filter based method has the lowest period detection error among all other methods for all noise event

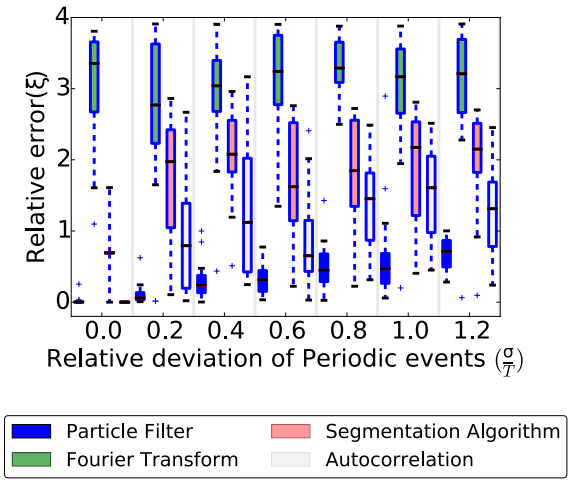

Figure 2.6: Base signal parameters: period $T = 10$. Average number of noise events per periodic event $= 0.05$. Relative error in period detection for different deviations of periodic events (σ/T). Noise rate is low to focus on the effect of σ. Even for large σ, particle filter shows small error and high reliability.

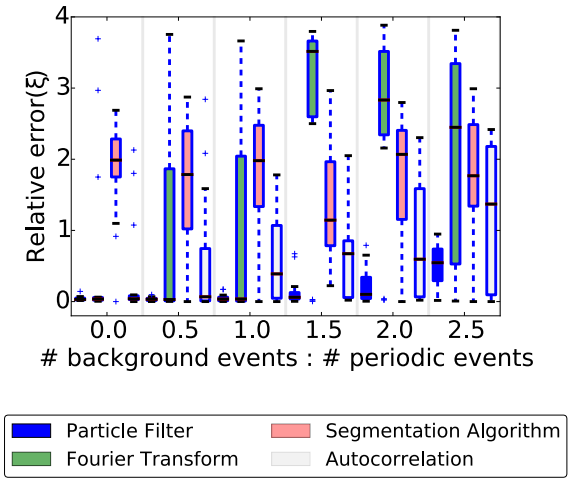

Figure 2.7: Base signal parameters: period $T = 10$. Relative deviation of periodic events 0.1. Period detection error with increasing rate of noise events relative to periodic events. Particle filter performs significantly better for reasonably large error sizes.

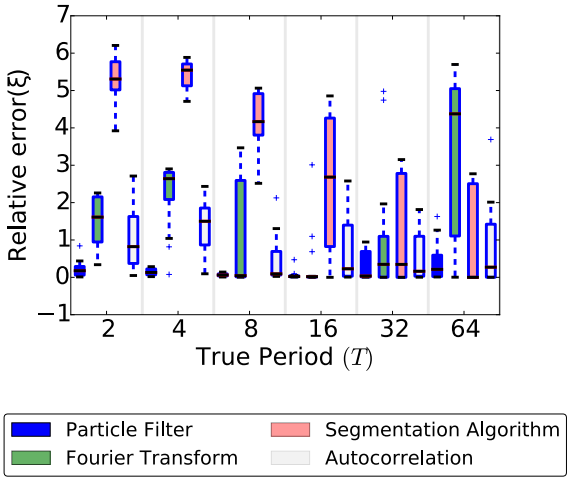

Figure 2.8: Base signal parameters: Average number of noise events per periodic event $= 0.05$. Particle filter has lowest period detection error over varying periods.

rates starting from no noise event up to a rate of 2.5 times periodic events. In this case, other methods perform well for few noise events, but with increase of noise events, their relative errors rise rapidly. Note that our parameters are set to assume that noise rates of over twice the periodic event rates are unlikely. However, at a rate of 2.5 times the errors for particle filter are still lower than other methods.

Effect of period (T) The period T itself is not expected to have any significant effect on the relative error. Our experiments show in Figure 2.8 that while all methods have a general increase in variance, particle filter is by far the most accurate across the spectrum.

Effect of number of observations. Figure 2.9 shows that particle filter based method converges with minimum number of observations in comparison to other methods. In this experiment, Fourier transform and autocorrelation algorithm never converge to low error. The fast convergence of particle filter implies that it can work with smaller quantities of data and does not require long observation sequences.

Tracking rapidly changing periods. In this experiment, we fix the noise parameters while changing the periodicity of the signal. In Figure 2.10, we observe that the period estimate of the particle filter closely follows the true period changing curve, whereas other algorithms perform badly with changes in the period value. Particle filter algorithm also converges quickly to the true period after

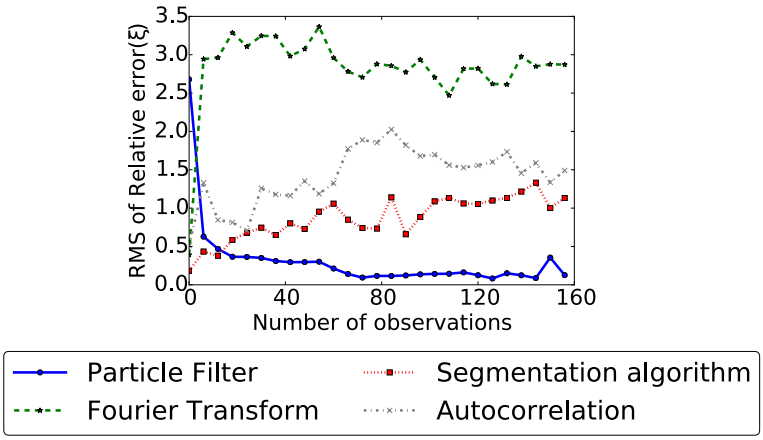

Figure 2.9: Base signal parameters: relative deviation of periodic events $= 0.2$, and relative amount of noise events to the periodic events $= 0.01$. Periodicity of the signal is set to 10.0. Experiment plots RMS error from 16 iterations. Particle Filter based method converges faster than other algorithms.

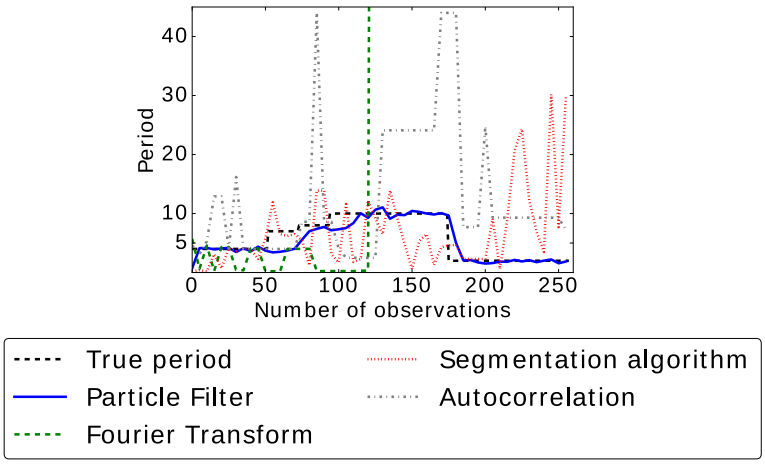

Figure 2.10: Base signal parameters: relative deviation of periodic events $= 0.2$, and relative amount of noise events to the periodic events $= 0.01$. Periodicity of the signal is set to 10.0. Particle filter based method successfully tracks changing periodicity of the signal. Period estimate for Fourier Transform algorithm is not shown completely as it is too large beyond certain point.

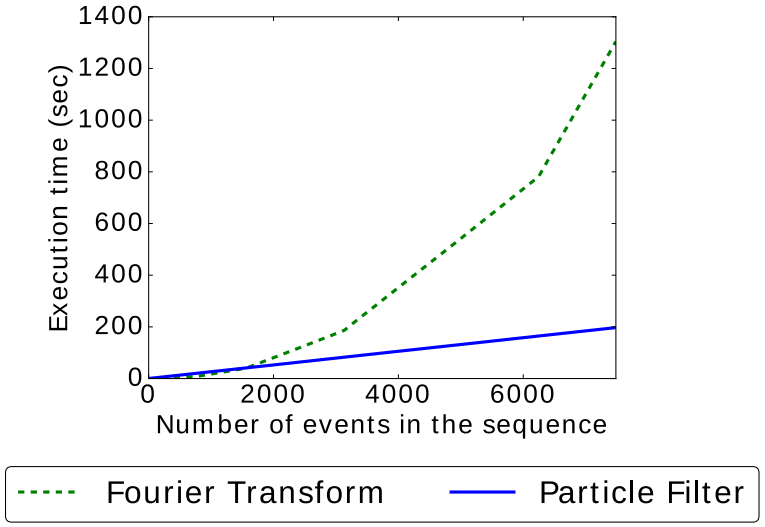

Figure 2.11: Particle filter based method needs less time to process large event stream compared to Fourier Transform. Particle filter based method execution time increases linearly with number of events.

the true period changes which enables it to catch rapid dynamics of a system. We note that similar behavior is noticed in our experiments with human steps as walking speed changes in section 2.5.3.1.

In Figure 2.12, we tested the system on data generated under different models – with different distributions (normal, Laplace, gamma, etc., with different parameters) for noise rate and inter-event time, and found that the system detects periodicity accurately. As explained in Section 2.3, this is due to the fact that for the sake of adaptability, the system prioritises local features over global ones, and thus is not greatly affected by differences in global models.

2.5.2.3 Execution time comparison.

We measured the time taken to run the particle filter on datasets of various sizes, and found that computing based on 256 particles is quite efficient and takes less time to process a large event stream compared to Fourier Transform algorithm and other algorithms.

The particle filter operates with constant amount of computation per event, thus its execution time increases linearly with the number of events, while Fast Fourier Transform takes $O(n \log n)$ time to process a signal of length n. Thus, the FFT execution time increases at a superlinear rate. Figure 2.11 shows that as expected, the particle filter requires less time to process large event stream

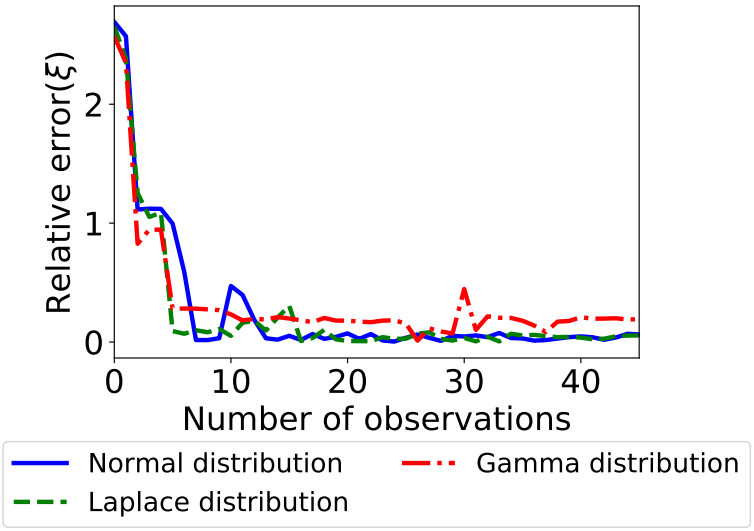

Figure 2.12: Period estimation error of our particle filter based method converges when the periodicity deviation is modeled using different distributions, such as Laplace, Gamma, etc.

compared to Fast Fourier Transform. The Segmentation based algorithm and autocorrelation check for all possible period values and require substantially larger execution times, and are omitted in this plot. The plot is based on a period value to 10, relative deviation of periodic events to 0.2, and relative amount of noise events to the periodic events to 0.05. We used particle filter based method implemented using Java 1.7 in Linux and Fast Fourier Transform functionality available in Apache math library [2]. We run these two algorithms in a typical desktop machine with 8GB primary memory and Intel $i5$ processor.

One of the advantages of the particle filter is that it processes events only as they happen, and does not perform computations in their absence. In contrast, the complexity of methods like Fourier transform and autocorrelation scale with the duration of the sequence, as opposed to number of events. Thus in systems with sparse events, or with very high sampling rates, these methods incur high cost for the quiet regions, while the cost of particle filters are independent of these parameters and depend only on the number of events. We believe that the particle filter can be made more efficient than this prototype implementation with suitable code optimizations. Although the code optimizations are not investigated as a part of this thesis, efficient sampling from the probability distribution and making likelyhood computation distributed would make the system more efficient.

[2]https://commons.apache.org/proper/commons-math/

2.5.3 Experiments on real datasets

We found that the particle filter can closely track changing periodicity in human gait data in comparison to other algorithms and accurately predict next human pulse event with low error.

2.5.3.1 Periodicity in human step data

We compared the performance of the particle filter based algorithm with other algorithms described in subsection 2.5.1 for tracking changing periodicity in human steps. We collected accelerometer signals using mobile phones while users walk at their own pace, varying their walking speed between walking segments. An accelerometer measures acceleration of a user giving a three dimensional signal S^x, S^y, and S^z. The Euclidean norm represents the magnitude of the signal at time t: $S_t = \sqrt{(S_t^x)^2 + (S_t^y)^2 + (S_t^z)^2}$, followed by smoothing using a Gaussian filter and normalizing around its mean. All peaks in the normalized signal above a predefined threshold are considered as discrete step events. Taking different values for threshold results in different rates of noise events as we have seen in Figure 2.1. We calculated the ground truth of step periodicity as the average time taken per step over a segment. A segment is the time duration when the user conciously maintains his walking speed almost a constant. The data is annotated by the user himself while walking. He presses a button in the app at the time of changing walking speed; thus, the segments can be identified later. The ratio of the duration of a segment and the number of steps in that segment denotes the ground truth walking speed.

Tracking a single walking trace. Figure 2.13 shows that the estimated period from the particle filter closely tracks the changing curve of ground truth step periodicity as it changes between segments. Here we used the threshold as the half of the standard deviation of the smoothed magnitude signal to detect step events. Figure 2.14 shows that due to its local adaptive nature, the particle filter has the lowest periodicity estimation error among all algorithms. Figure 2.15 shows the CDF of error over twelve traces collected from six different people.

The particle filter method is robust to different choices of thresholds for extracting step events from the accelerometer signal. This is shown in Figure 2.16 for different choices of threshold.

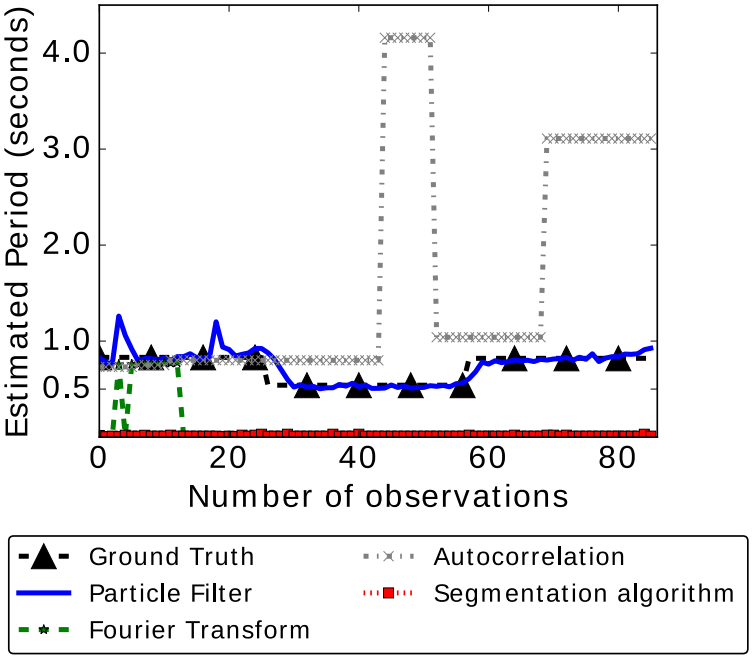

Figure 2.13: Periodicity estimation on human step data. Particle filter based method closely follows changing periodicity.

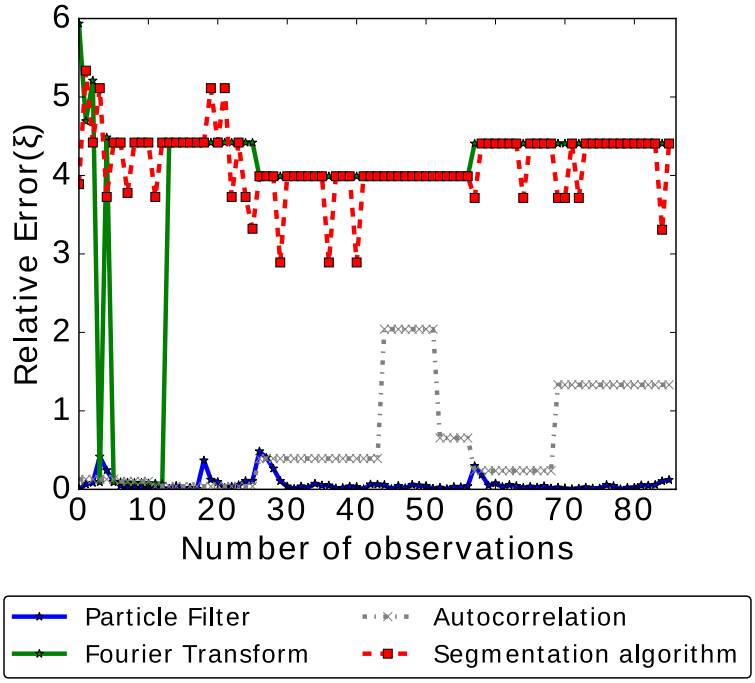

Figure 2.14: Error in period estimation in human gait data. Particle filter based method has lowest periodicity detection error.

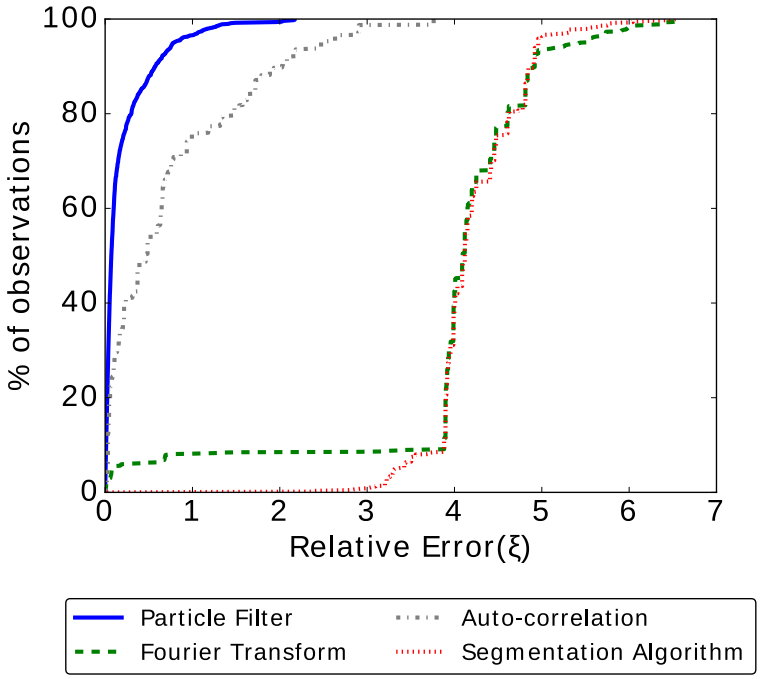

Figure 2.15: Estimating periodicity for steps from 6 subjects. Particle filter based algorithm has small periodicity estimation error for all the users.

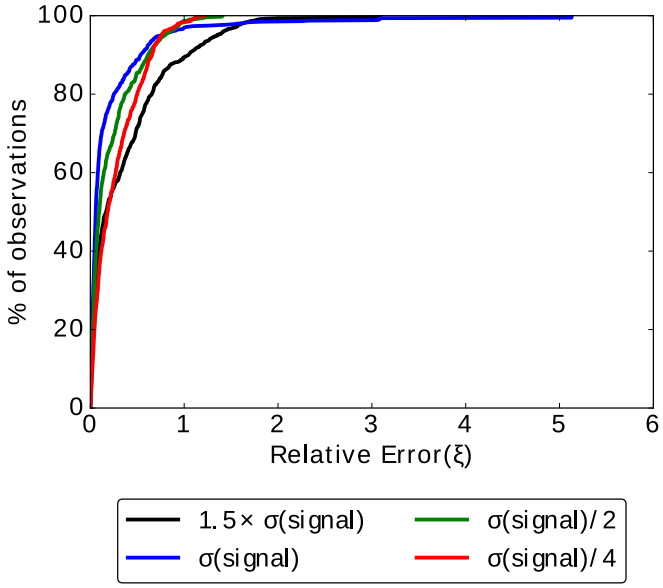

Figure 2.16: CDF of particle filter error, where event detection thresholds are multiples of the standard deviation of a preprocessed accelerometer signal, showing low estimation error in all cases. However, with decreasing threshold (increasing false positive events) the error naturally increases.

2.5.3.2 Pulse prediction.

The particle filter can reliably predict upcoming events in a noisy sequence. For this experiment we collected videos of users' fingertips, and used the red color component as a signal for pulse events. We applied similar preprocessing on the pulse signal as we did for accelerometer signal.

The estimate of period by the particle filter gives an estimate of the next event time. We measured the next pulse event prediction error as the absolute difference in predicted and actual event times. Figure 2.17 shows that the particle filter quickly converges to reliably predict the pulse event and consistently performs better than other algorithms. The larger errors (e.g. at around 55 second mark) represent sudden changes in heart rate due to change in user's activity (a spot jump otherwise the user was standing still).

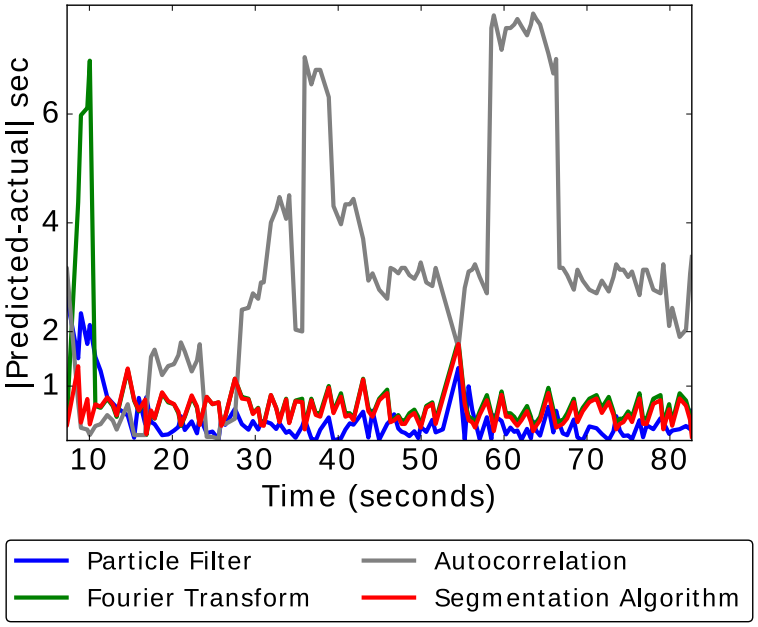

Figure 2.17: After a small number of events, the next pulse event prediction error (|predicted event time − actual event time|) is generally lower for the particle filter compared to other algorithms.

Chapter 3

Private Sensing of Asynchronous Event Sequences

In this chapter, we provide a rigorous study of the privacy of event timestamps, which are particularly sensitive attributes. Our privacy approach is specially tailored to discrete point events with varying rates and asynchronous operation, which is shown to be more effective than existing synchronous methods. We propose new privacy mechanisms, including temporal perturbation and inclusion of fake events. These methods provide provable guarantees against the adversary deducing time of events, identifying events with timing correlation attacks and inferring temporal ordering of events. We describe the implementation of data privatization as a system service on Android. Experiments on public datasets and locally collected data show that the privacy mechanisms are found to protect utility by preserving the overall distribution of events.

3.1 Introduction

Densely deployed sensors and IoT devices provide opportunities for large scale monitoring of home, workplace and public domains (Chen et al., 2017; Ganti et al., 2008). In the process of sharing and use of IoT data, protection of sensitive information related to activities of an individual has become an important research topic. In this paper, we consider the privacy issue in publishing timestamps of sensing events.

Consider sensors or mobile phones detecting specific events and activities of users and later reporting these behavior statistics to a service provider for usage

analysis. Timestamp information can imply correlation, association and causality between events, and thus are sensitive attributes. An adversary who has access to details of certain external events can cross-query the datasets and associate users with external events. For example, timing information of online activities and web browsing can be used to perform timing correlation attacks to deduce visits to sensitive web sites. Precise timing information are known to even compromise cryptographic protocols (Wong et al., 2009). In the following we discuss some domains where privacy of timestamp is critical.

Mobile phone data. Activity timing information from a mobile phone can paint very accurate pictures of someone's habits. Recent advances in activity and context recognition exacerbate the sensitivity of this information (González et al., 2009; Song et al., 2010).

Social information. The reach of sensing data goes beyond individuals and reveals information about social contacts and social life. Persons frequently found at the same location at the same times are likely to be socially connected, which is also a concern in crowd-sensing approaches (Miao et al., 2015). Analogously, individuals frequently using the same chatting app at the same time are likely to be friends.

Timing information in networks and web. Data from network routers as well as website access logs are frequently used for analytics. Suppose an adversary has knowledge that a web site (or service) X was accessed at exact times t_1, t_2 and t_3, and now gains information that a user u triggered a browser session (or relevant application) shortly before each time. The adversary can then associate u with X. Such timing attacks are known even to compromise the anonymity of mixing networks like Tor (Levine et al., 2004).

Motivated by these considerations, we specifically study the privacy of event timestamps. A full solution of privacy of multi-attribute sensor data will require a multitude of considerations and various application dependent attributes that are beyond the scope of any single project. However, in many analytic applications, such as packet arrivals or connection requests at routers, or visitor check ins at venues, unlabelled point event sequences are themselves a subject of study, which is the focus of this paper.

To protect private information from unknown users and inadvertent leakage, statistical privacy mechanisms (Dwork et al., 2006; Kifer and Machanavajjhala,

2014a) have been designed. The core idea of these methods is to perturb information before sharing it, so that precise facts about individuals in the database cannot be inferred, yet the aggregate result or statistical pattern is well approximated.

An example of timing information leakage and the action of our mechanism is shown in Figure 3.1. Figure 3.1(a) is the Fourier transform of the sequence events of a user opening the weather app on the phone. The data is taken from the LiveLab dataset (Shepard et al., 2011). Figure 3.1(a) shows a clear energy peak at 24 hours, which reveals the user's habit of checking the app at the same time. Applying the sanitization methods described in this paper, we get the Fourier transform in 3.1(b), where the periodic behaviour has vanished, and therefore the precise time of checking the weather app is no longer so predictable. An overview of our techniques and contributions follow.

Our Contributions. Statistical privacy is a non trivial concept. The most popular statistical privacy technique is Differential Privacy (Dwork and Roth, 2014; Dwork et al., 2006). The idea is to prevent inference of a particular data item being present in the dataset. We describe in Section 3.3 why this approach and existing differential privacy based algorithms operating in synchronous rounds are unsuitable for publishing events over long duration of time – they add too much noise which reduces data utility. In distributed sensor databases, asynchronous operation is particularly desirable, since synchronization is non-trivial to maintain, and the frequency requirements can vary by system. Our approach, thus, is to use the Pufferfish setup which can quantify privacy in the asynchronous setting.

The overall model of operation and the adversarial knowledge is considered in Section 3.4. Here we describe three fundamental problems we wish to solve.

1. Obscuring event times so that they cannot be inferred to a precision greater than Δ.

2. Obscuring the presence of events so that an adversary cannot be sure whether some event occurred within a particular interval of size Δ.

3. Obscuring event times so that relative order of events that take place within a short time of each other cannot be inferred.

The statistical mechanisms that solve these problems are intuitive. For prob-

lems 1 and 3, we present a perturbation of the event time by a real number chosen uniformly from $[-k\Delta/2, k\Delta/2]$, which suffices to achieve Pufferfish privacy. For Problem 2, we show that adding fake events with a suitable rate achieves privacy, while the error in a range query can be shown to be bounded. These mechanisms are easy to implement for temporal data in a continual release scenario – when one reports the cumulative event count continuously. In statistical privacy, a major challenge always is to ensure that the privacy of the mechanism can be quantified in a formal sense. All our solutions admit provable privacy guarantees, which are deduced along with the mechanisms in Section 3.5.

Along with privacy guarantee, our main concern is preserving the utility of data. Our methods introduce only small perturbations, so that the data retains its statistical properties. In experiments (Section 3.7), we measure this quality using range queries over time intervals and demonstrate that the perturbation caused by our privacy mechanisms do not substantially change the utility in range queries. Figure 3.2 shows an example for the same weather app usage data (Shepard et al., 2011) for multiple people. Figure 3.2(a) shows that after sanitization, the estimation of the periodicity has large errors, which means that the habits of users are not revealed. Meanwhile, Figure 3.2(b) shows that the density of events in given ranges does not change substantially, which means the utility is well preserved.

Section 3.6 describes implementation of a data sanitization service for mobile phones, along with the design considerations for such a service. A discussion of the various implications of Pufferfish privacy, distributed operations, and publishing latency are presented in Section 3.6.

3.2 Related Work

Releasing continual counts for temporal event streams with differential privacy guarantees have been studied in (Chan et al., 2011; Dwork et al., 2015, 2010; Xiao et al., 2011). More data-dependent works on continual aggregate statistics release of stream data can be found in (Chen et al., 2017; Kellaris et al., 2014). All these works assume a suitable sampling frequency for obtaining the event stream in the first place. As we argued in the Section 3.4, these methods fail where event density varies.

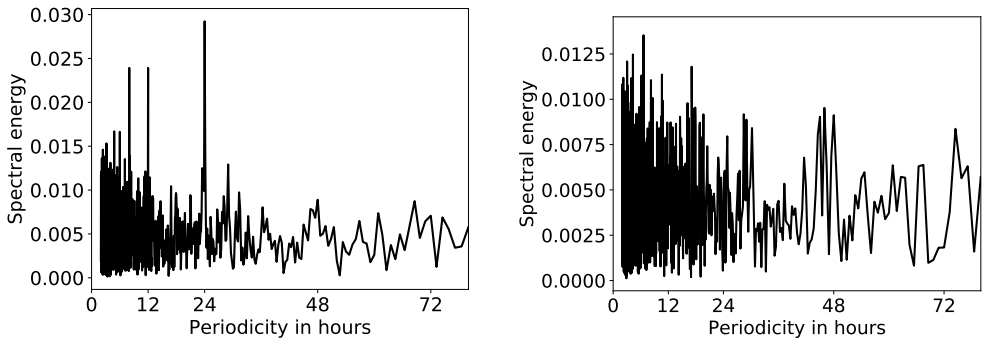

(a) (b)

Figure 3.1: Periodicity analysis on when a user opens weather app. **(a)** Fourier periodogram of original time series shows clear periodicity of 24 hours - the user checks the app at the same time every day. **(b)** After events are sanitized using Mechanism 1.3 in 3.5.1, periodic pattern vanishes.

(Rastogi and Nath, 2010) transformed the time series into frequency domain using discrete Fourier transform and applied sanitization to the k Fourier coefficients with highest spectral energy. This method achieves ε-differential privacy with error of approximately $O(k/\varepsilon)$. However, this algorithm does not suit our setting as it releases data only once.

(Fan et al., 2013) proposed an adaptive system to release real time aggregate traffic statistics under differential privacy using sampling and filtering. This algorithm is data-dependent, but, without theoretical guarantee. (Ganti et al., 2008; Ahmadi et al., 2010) have proposed to generate fake time series from the same distribution as the original data. This method solves a related but a different problem than ours, as the goal is to protect re-identification of a time series, but do not hide individual events in a series.

(Song et al., 2017) discussed privacy preservation in presence of correlation in the data. Activities of a user over time are modeled as a Markov chain and sanitized using Pufferfish privacy. (Kifer and Machanavajjhala, 2014a; Niu et al., 2019) designed a time-series data trading system with Pufferfish privacy under temporal correlations. However, the method does not trivially translate to privacy of individual event timings as we consider in this paper. Blowfish (He et al., 2014) is another instantiation of the Pufferfish framework for use on continuous variables, which however does not apply to discrete abstractions like event ordering. Differential privacy is also being explored for correlated time series data (Cao

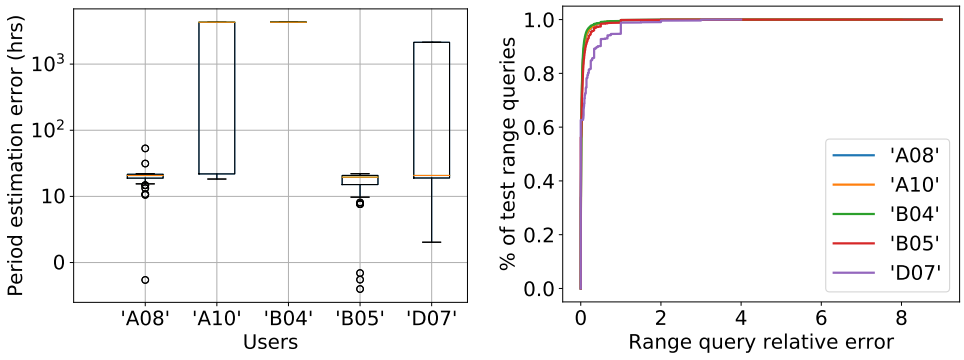

(a) (b)

Figure 3.2: Experiment on opening weather app from 5 users. All users here have 24 hours periodicity. **(a)** Periodicity estimation using Fourier transform on sanitized events has large error in the order of several hours. Notice that the y-axis is on an exponential scale. **(b)** Range queries count number of events in queried intervals still have relatively low error.

et al., 2018).

Various methods have been proposed to protect user level and activity level privacy. Differential privacy frameworks for protecting specific inference from the data is investigated (Saleheen et al., 2016) using dynamic Bayesian networks to capture the adversary's knowledge. The proposed method first infers latent states and then protects them. Continual adaptive release of histogram statistics is considered (Li et al., 2015a) to protect users to be re-identified. Unlike these works, the goal of the current paper is to protect individual event timings.

3.3 Statistical Privacy and Challenges in Streaming Event Data

We will start the section with an overview of statistical and differential privacy. Readers familiar with the basics may want to skip ahead to Subsection 3.3.1.

Let us consider a dataset D which contains some sensitive attributes. An adversary who does not have access to D, may still be able to infer sensitive information if we answer some queries on the dataset. The trivial method to prevent such unintended inference is to disallow any query that uses the sensitive

attributes, but that renders the data useless.

To preserve utility of the database and simultaneously protect sensitive information, statistical privacy methods work by creating uncertainties about the original data. For example, if we are asked for the count of items in a dataset, we can add noise – a small random number – to the count, and return this noisy value. An adversary receiving this noisy value is uncertain about the true count, which provides us with privacy.

This privacy has a tradeoff against utility of the query for legitimate use and is a central issue in statistical privacy. For example, a small noise provides little privacy, but largely preserves utility – as a user can make use of an approximate result. A large noise creates larger deviation from truth, and destroys utility, but provides greater privacy.

Quantifying privacy. Suppose there is a fact s about the database D that we wish to keep secret, and $\mathcal{A}$ is a randomized algorithm (such as adding a type of noise) that we use to answer a query. The fundamental idea is that the probability of $\mathcal{A}$ producing a particular output w should be similar irrespective of $s =$TRUE or $s =$FALSE. This property ensures that from the output w. the adversary cannot gain much information. For example, if the probability of $\mathcal{A}$ producing w is exactly the same irrespective of s, then observing w gives no information about the truth of s. Based on this idea, Differential privacy was defined in (Dwork et al., 2006; Dwork, 2006), as follows.

Definition 1 (Differential Privacy)**.** *Suppose D' is a dataset that is different from D in the presence of a single element x. Then randomized algorithm $\mathcal{A}$ is called ε-differentially private, if for all such pairs (D, D') and all $w \in$ Range$(\mathcal{A})$, the algorithm $\mathcal{A}$ satisfies: $\frac{P(\mathcal{A}(D)=w)}{P(\mathcal{A}(D')=w)} \leq e^{\varepsilon}$.*

Here the secret is the presence of item x in the dataset, and the definition asserts that the presence or absence of any x does not change the probability of the output w by more than a small factor e^{ε}. A smaller ε implies greater privacy. We expect a positive fractional value: $0 < \varepsilon \leq 1$.

Differentially private algorithms depend on a quantity called sensitivity of a query function f. It is defined as the maximum possible change to $f(D)$ due to presence or absence of any single element x:

Definition 2 (Sensitivity)**.** *The sensitivity of f, denoted as Δf, is defined as $\Delta f = \max \|f(D) - f(D')\|$.*

When f is the counting query, $\Delta f = 1$, since a single element can change the count only by 1. The sensitivity determines the noise we need to add to obscure the presence of an element. If sensitivity is high, more noise is needed to ensure that an element is hidden. The most common method used to add noise based on sensitivity is called the Laplace mechanism, and uses the Laplace distribution as a source of noise. A Laplace distribution of mean zero and variance $2b^2$ is written as $\text{Lap}\,(b)$, and its probability density at x is given by $\frac{1}{2b}e^{-\frac{|x|}{b}}$.

Laplace mechanism. Suppose $f : D \to \mathbb{R}$ is a query function. Then the corresponding ε-differentially private Laplace mechanism (Dwork et al., 2006; Dwork, 2006) is given by $\mathcal{A}(D) = f(D) + \xi$ where $\xi \sim \text{Lap}\left(\frac{\Delta f}{\varepsilon}\right)$ is a random number drawn from the Laplace distribution of variance $2(\frac{\Delta f}{\varepsilon})^2$.

In the counting problem, since sensitivity is 1, this mechanism is equivalent to adding a random number from the distribution $\text{Lap}\left(\frac{1}{\varepsilon}\right)$ to the count before returning the result. The corresponding guarantee is that inclusion or exclusion of any single element to the dataset changes the probability of observing the same output by at most a factor of e^{ε}.

3.3.1 Continuous Publication of Events

Suppose we monitor a sequence of events, and publish the time at which events take place. All other attributes are either removed or unknown – such as arrivals of vehicles at a junction, entry of people at a venue etc. Such sequences are of interest in mining temporal patterns of events.

For simplicity, operation in synchronous rounds is often used – at each round t, we publish the count $c(t)$ of events. A particular variant of this problem was considered by Chan et al. (Chan et al., 2011) where in each round there is zero or one event. A basic method described in (Chan et al., 2011) is to publish the count with a Laplace noise: $c(t) + \xi(t)$, where $\xi(t) \sim \text{Lap}\left(\frac{\Delta f}{\varepsilon}\right)$. In any individual round, the presence or absence of an event is obscured by the noise.

The difficulty of this method is that over time, the noise builds up. Over T rounds, T different values of ξ are added, and the total of published counts can deviate rapidly from the true count – see Figure 3.3. The problem becomes more severe when events are sparse and there are many rounds without any events. Such empty rounds add to the noise and inaccuracy, but the true count does not increase. Figure 3.3(b) shows a case where the round frequency is high,

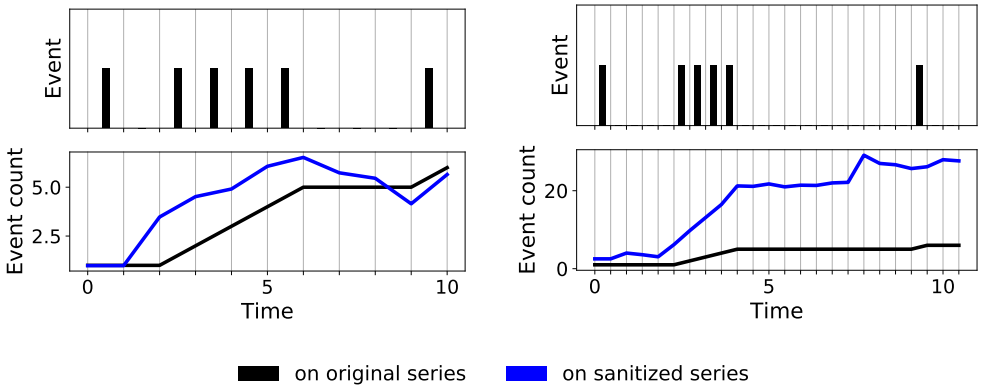

(a) (b)

Figure 3.3: Synchronized privacy frameworks in (Chan et al., 2011) need discrete time rounds with suitable sampling rate. Here $Lap(1)$ noise is added to the data at each time slot. **(a)** Low sampling frequency is enough, and synchronized privacy mechanisms would add reasonable noise as shown in the count below. **(b)** High density need high sampling rate for dense region and thus introduces many units of noise in sparse areas, diverging from true count. Synchronized privacy mechanisms would add noise so large that the output becomes useless.

but events occur sparsely in bursts. The noise dominates the true total count. Chan et al. (Chan et al., 2011) go on to describe hierarchical methods that can reduce the contribution of the noise to $O(\frac{1}{\varepsilon}(\log T)^{1.5} \log \frac{1}{\delta})$ with probability at least $1 - \delta$. See Section 4.2 for other related results. However, these approaches do not eliminate the issue of accuracy decreasing with time.

As a practical matter, the round frequency, and therefore the temporal resolution of data in this design is hard to choose as a universal parameter. The event density and required temporal resolution can vary by application (e.g. human behaviour in seconds, versus network measurements in milliseconds) can be unknown, or can vary within the same application.

Thus, we would like to avoid rigid synchronous rounds, and use an asynchronous setup, where the published timestamp of an event can be real number. Our objective is to publish all events with approximately correct time, in a way that the adversary cannot guess the true time accurately. For example we can publish all events, with small noises added to their timestamps.

The privacy of such a method is difficult to define in the differential privacy paradigm, because differential privacy, as we saw, hides the possible presence

of an item, not its value. We will resume this discussion in Section 3.4; in the following subsection, let us introduce Pufferfish privacy, which is a more versatile framework.

3.3.2 Pufferfish Privacy

The Pufferfish Privacy framework (Kifer and Machanavajjhala, 2014b) allows us to define any set of facts to be regarded as secret, and protect them probabilistically. To define the Pufferfish privacy, we first introduce the following sets.

- The set of secrets $\mathcal{S}$ to be protected within dataset $\mathcal{X}$,
- How the secrets shall be protected against each other: by specifying discriminative pairs $\mathcal{Q}$ of secrets,
- And the prior knowledge of the adversary, written as a set Θ of prior distributions, essentially representing how the data is generated.

A discriminative pair can be written as $(s_i, s_j) \in \mathcal{Q}$, where s_i and s_j are elements of $\mathcal{S}$, and represents two facts that we do not want the adversary to be able to distinguish.

A randomized mechanism M satisfies ε-*Pufferfish* privacy if for $s_i, s_j \in \mathcal{S}$, $(s_i, s_j) \in \mathcal{Q}$, $\theta \in \Theta$ and $w \in Range(M)$ the following holds:

$$e^{-\varepsilon} \leq \frac{P(M(\mathcal{X}) = w|s_i, \theta)}{P(M(\mathcal{X}) = w|s_j, \theta)} \leq e^{\varepsilon} \tag{3.1}$$

assuming $P(s_i|\theta) \neq 0$ and $P(s_j|\theta) \neq 0$. Similar to differential privacy, a smaller ε implies greater privacy.

The definition is in the Bayesian philosophy. It implies that the truth of s_i versus s_j does not make a significant difference to the probability of observing any particular output w. Therefore, when w is in fact observed, the adversary does not gain any significant certainty whether s_i or s_j is true, compared to what he already knew based on prior knowledge θ. As we will see in the next section, the generic nature of secrets and discriminative pairs lets us define privacy for properties like event ordering and event times.

The interpretation of the prior Θ is that it represents the underlying distributions generating the data, for example, the vehicle density at a crossing at night, morning or rush hour, or the distribution of certain events being performed on a

mobile phone. Pufferfish allows this distribution to be known to the adversary, but not true times of actual events.

3.4 Model and problem statements

We want to publish timestamps of events recorded by sensors. We are interested in publishing data continuously, but not in real time. Events can be assumed to be published in batches, for example, once in an hour or a day, and taken together form a stream lasting over long time spans.

The sensors send their data to an aggregator service such as a cloud server, which then publishes the data. Depending on whether the sensors trust the cloud server or not, there can be different approaches to publishing.

Labelled and unlabelled event sets. Labelled events are those that carry IDs or other attributes that can potentially identify events uniquely. Unlabelled events are those that carry no such attributes or carry the same attributes making them indistinguishable. Unlabeled events can occur in various time series datasets, such as vehicles arriving at a crossing, anonymized access logs of a web site, etc. Privacy implications of event sets can vary by their label status. Since we are interested in the timestamp attribute of events, our event sets can be regarded as unlabeled unless mentioned otherwise.

3.4.1 Sensing Data Collection and Trust Relations

If the devices (or their owners) trust the aggregator and the communication channel, they can transmit all data to the aggregator, who then sanitizes (privatizes) and publishes it at suitable time.

If the channel or the aggregator is not trusted, then the devices must take care of sanitization by themselves. In differential privacy terms, this is called *local privacy* (Kasiviswanathan et al., 2011).

All algorithms in this paper can be applied locally, where a device detecting events can apply sanitization before transmission to the aggregator. This approach has the advantage that the data transmitted is guaranteed to be private, since data sanitized by suitable statistical methods are known to be immune to post processing (Dwork and Roth, 2014). Once the data has been modified by the mechanism, they carry the privacy guarantee irrespective of how the data is

used. This is particularly useful in sensor data that may be shared with various public and private organisations.

3.4.2 Utility: Range Queries

To ensure that the sanitized data is useful, we measure its utility in terms of accuracy of range queries. Given a time interval T, the range query asks for the number of events recorded inside T. The motivation for using range queries as test of utility is that it is akin to preserving the large scale probability distribution that generates the data. If the count of events in different ranges is preserved, it implies that the statistical properties of data are preserved.

3.4.3 Adversary Model and Problem Statements

We assume that the adversary can observe the published events. Note that the adversary may or may not be able to compromise the communication channel or aggregator – this is not relevant for us, since we aim to create algorithms with local privacy. We do, however, assume that the adversary cannot compromise the distributed devices themselves to observe events as they happen.

As is standard in security and privacy, we assume that the privacy algorithms and parameters are known to the adversary. However, the random choices – such as the random numbers generated during an execution are not known.

Under these capabilities of the adversary, we consider the following types of data protection. More details will be presented in Section 3.5 along with algorithms.

Problem 1: Protecting the time of a published event. In this problem, we publish events along with timestamps. However, we do not wish the adversary to know the true time of the event. Now, in most cases, the adversary does not need to know the precise number – narrowing the time down to a small interval of the true time suffices. For example, for human activities like checking into a venue, accuracy within a few minutes of the true time can be considered accurate enough.

Thus for an event e at time t, we want to prevent an adversary from gaining accuracy to within an interval of size Δ around the true time.

Problem 2: Protecting existence of an event. Suppose we have a sequence

of unlabeled events, such as arrival of cars at a crossing, or a person's access to a website. Such events are known to follow Poisson process models.

Definition 3 (Homogeneous Poisson Process)**.** *A homogeneous Poisson process with intensity λ is one where the number of events X in any unit interval follows a Poisson distribution:*

$$P(X = K) = e^{-\lambda} \cdot \frac{\lambda^K}{K!}.$$

The expected value of X is λ. The definition extends naturally to larger intervals: the number of events in an interval B follows a Poisson distribution of intensity $|B| \cdot \lambda$.

In general, events may not have a uniform rate at all times. Such variable rates are described by *non-homogeneous* Poisson processes:

Definition 4 (Non-homogeneous Poisson Process)**.** *In a non-homogeneous Poisson process defined over an interval A with intensity function $\lambda : A \to \mathbb{R}_{\geq 0}$, the number of events $X(B)$ in any subinterval B of the domain follows a Poisson distribution:*

$$P(X(B) = K) = e^{-\Lambda(B)} \cdot \frac{\Lambda(B)^K}{K!},$$

where $\Lambda(B) = \int_B \lambda(t)\, dt$ is called the mean rate in B.

By using a function $\lambda(t)$ that may vary in time, the Poisson process can be used to generate almost any desired distribution of events.

Let us suppose that the adversary suspects the presence of an event inside a small time interval of size Δ, and wishes to verify that such an event did in fact take place. Our objective is to prevent such an inference in a statistical privacy sense.

Problem 3: Protecting Event ordering. Relative ordering of events can reveal sensitive information. For example, if A leaves a restaurant shortly after B enters, that reveals that A and B are likely to have met. Thus, in this problem, we wish to protect the relative ordering of two events that take place within an interval of size Δ.

3.5 Privacy mechanisms

In this section, we discuss how to achieve statistical privacy of event e_i with respect to any choice of time interval I of size Δ. In some cases the detailed technical proofs are replaced by their sketches in the interest of space.

3.5.1 Problem 1: Protecting Event Times

First we consider that the adversary has the knowledge of a temporal domain of W, bounded and large, within which an event e_i of interest is known to have taken place.

Let t_i be the time of event e_i. Assume that t_i follows a uniform distribution over W. This constitutes the prior knowledge θ about the data known to the adversary. This assumption is for simplicity of analysis – we will discuss later how the mechanisms work with more general distributions.

The secret we wish to protect here is $s : t_i \in I$. The discriminative pair is $(s, \neg s)$. The objective is to obtain ε-*Pufferfish* privacy for $(s, \neg s)$ – thus making the adversary uncertain between the two possibilities. Note that we are not trying to obfuscate presence of the event, only its time.

To warm up, let us discuss a trivial mechanism:

Mechanism 1.1: Given an event e_i with true time t_i, the mechanism outputs $M(e_i) = \xi$, where ξ is selected uniformly at random in the interval W.

It is easy to argue privacy for this method. Suppose that in a particular run of the algorithm, $M(e_i) = w$. In this case, $P(M(e_i)) = w$ is independent of the truth of s_i, therefore, $P\big(M(e_i) = w|s_i, \theta\big) = P\big(M(e_i) = w|\neg s_i, \theta\big)$, and the mechanism satisfies 0-*Pufferfish* privacy. Essentially implying that it adds nothing to the knowledge of the adversary.

The mechanism is unsatisfactory in the sense of utility. It is in fact completely independent of the actual value t_i – it samples a time from W, which is known, so it does not add anything to the knowledge of legitimate users either. When W is large, the perturbation to the event time is large, resulting in poor utility. Next we consider a mechanism with better utility. Here, we provide the main results and sketches of the proofs. The detailed proofs are in Section 3.8.

Mechanism 1.2: M outputs $M(e_i) = t_i + \xi$, where ξ is selected from the uniform distribution over $[-k\Delta/2, k\Delta/2]$.

This method is more useful since it restricts $M(t_i)$ to a smaller interval around t_i. It can be be shown to have ε-*Pufferfish* privacy for a suitable choice of k.

Theorem 1. *Mechanism 1.2 satisfies ε-Pufferfish privacy for* $k = \dfrac{|W|}{e^{\varepsilon}\Delta}$.

The sketch of the proof is that we compute the probability of the output $M(e_i)$ being in $[t_i - k\Delta/2, t_i + k\Delta/2]$, under the respective conditions of s_i being true

and $\neg s_i$ being true. Their ratio can be shown to be bounded by e^{ε}, which gives ε-*Pufferfish* privacy.

3.5.1.1 Priors of Laplace distribution

Now we relax the requirement for the bounded window W. The adversary's prior hypothesis is that the timestamp t_i of event e_i follows a Laplace distribution centered at μ, where $|\mu - t_i| \leq k\Delta$.

Mechanism 1.3: $M(e_i) = t_i + \xi$, where $\xi \sim \text{Lap}\left(\frac{k\Delta}{\varepsilon}\right)$. That is, a Laplace noise similar to differential privacy is added.

Theorem 2. *A perturbation with* $\text{Lap}\left(\frac{k\Delta}{\varepsilon}\right)$ *guarantees* ε*-Pufferfish privacy.*

The proof follows from the definition of Laplace distributions that if the mean of two Lappace distributions with same variance are separated by distance x, then at any point their probability densities differ at most by e^{ε}. The details is in Section 3.8.

3.5.2 Problem 2: Protecting event existence in Poisson processes

For this problem, we consider Poisson processes with event rate λ in a unit interval. The events are assumed to be unlabeled. Remember that the adversary wishes to confirm the existence of some event in the interval I of size Δ, where the adversary has some reason to suspect the presence of an event in I. For example, this interval may be based on the adversary's knowledge of external related events. The adversary also knows the Poisson rate λ.

Let us write $\Delta = c/\lambda$. In a Poisson process, the expected interval between events is $1/\lambda$. If $c >> 1$ and therefore $\Delta >> 1/\lambda$, then there is likely to be multiple events in I, and presence of an event is not informative for the adversary. However, when for $c \leq 1$ – when the adversary has fairly accurate information of the event's possible time, and other events are unlikely in the interval, a small Δ can *isolate* the event – it gives the adversary reasonable confidence that any event in the interval is the one of interest.

In the Pufferfish model, the secret can be defined as $s := (\exists i : t_i \in I)$ – representing the fact that some event e_i has occurred in the small neighborhood I of size Δ. The discriminative pair is $(s, \neg s)$, where $\neg s$ means that no event has

taken place in I. For this problem, we describe a mechanism using fake events. The main intuition is that if we add many fake events to the sequence, then any interval I is likely to consider events, and thus the presence of events in I does not give much information to the adversary.

Mechanism 2.1: Introduce a fake event sequence with unit time event rate $\Lambda = \frac{\lambda}{c} \ln \frac{e^\varepsilon}{(e^\varepsilon - 1)}$, and publish both true and fake event times.

The greater rate of this Poisson process ensures that it is likely that one or more events will be present in the interval, and thus the adversary cannot be certain of the presence of a true event.

Theorem 3. *Fake event rate* $\Lambda = \frac{\lambda}{c} \ln \frac{e^\varepsilon}{(e^\varepsilon - 1)}$ *provides* ε*-Pufferfish privacy for existence of events.*

Proof. Let η be the situation that an event is seen in I in the stream after adding fake Poisson events. When s is not true, there is no fake event generated by the Poisson process. We have $P(\eta \mid \neg s, \theta) = 1 - e^{-\Lambda\Delta}$. When s is true, η is always true, thus $P(\eta \mid s, \theta) = 1$. When $\Lambda = \frac{\lambda}{c} \ln \frac{e^\varepsilon}{(e^\varepsilon - 1)}$, we have $\frac{P(\eta|s,\theta)}{P(\eta|\neg s,\theta)} \leq e^\varepsilon$. □

In this setting, a range query on an interval $[x, y]$ can be answered as follows. If the total number of events (real and fake) in $[x, y]$ is I, then a range query on $[x, y]$ is estimated as $\mathcal{A}(x, y) = n - \Lambda \cdot (y - x)$. That is, from the total number of events in the interval, we subtract the expected number of fake events, to get an unbiased estimate. The following theorem shows that the error in range counting introduced by this approach is not large.

Theorem 4. *If* $\Lambda = \frac{\lambda}{c} \ln \frac{e^\varepsilon}{(e^\varepsilon - 1)}$*, we get an estimation of the count of real events in a interval with length* L *with error bounded by* $O\left(\sqrt{\Lambda L \log \frac{1}{\beta}}\right)$*, with probability* $1 - \beta$*.*

This mechanism has the nice property that if each device j applies the mechanism with respect to its local Poisson rate λ_j, then the aggregate global event stream has the same privacy guarantee with respect to the global Poisson event rate. This result follows from the Superposition Theorem (Kingman, 1992; Grimmett and Stirzaker, 2001) – that the union of Poisson processes is still a Poisson process.

3.5.3 Problem 3: Privacy of event order

Suppose the adversary knows a window W, and knows that events e_a and e_b occurred within a short time difference Δ of each other. The adversary wants to know if e_a occurred before e_b or not. So, the secret is $s_{a<b} : t_a < t_b$.

Mechanism 3.1: Apply the uniform mechanism (same as in 1.2): $M(e_i) = t_i + \xi$, where ξ is chosen uniformly from $[-k\Delta/2, k\Delta/2]$.

Theorem 5. *$k \geq \frac{3+e^{\varepsilon}}{e^{\varepsilon}-1}$ gives ε-Pufferfish privacy with respect to event ordering.*

The sketch of the proof considers two cases depending on whether the sanitized events preserve the order. In each case, it looks at both possibilities of the secret. To compute probabilities of the form $P(M(t_a) < M(t_b)|s_{a<b}, \theta)$ we need to consider three regions where the events can be perturbed to, namely $[t_a - \frac{k\Delta}{2}, t_b - \frac{k\Delta}{2}], [t_b - \frac{k\Delta}{2}, t_a + \frac{k\Delta}{2}]$, and $[t_a + \frac{k\Delta}{2}, t_b - \frac{k\Delta}{2}]$. Considering the fact that the event ordering can only change based on in which region the sanitized events are placed, we can get the theorem.

This implies that a simple mechanism provides a guarantee against inference of precise ordering of nearby events. Note that events that are far separated in time are not covered under this model, since any modified assignment of timestamps that modifies the ordering of distant events will effectively randomize the the data completely, destroying all utility.

In Subsections 3.5.1 and 3.5.3 we have used a uniform distribution for simplicity of demonstration. The mechanisms can be easily adapted and implemented for non-uniform distributions, albeit with a more complex analysis.

3.6 Privacy service design and implementation

To achieve private publishing of data, we designed and implemented a service in Android. The service accepts raw data from an application, and returns sanitized data. The same service can of course also be run on a central server to sanitize data from multiple events. The following discussion applies to both cases. An application may choose one of the mechanisms described in Section 3.5 to apply to its data. Along with each event time, it passes the parameters for privacy as arguments.

The privacy arguments and return values are shown in Table 3.1. We have presented versions where privacy constraint ε is passed as argument, while the

Table 3.1: Callable mechanisms, their arguments and return values in sanitization service.

Mechanism	**Arguments**	**Returns**
Mechanism 1.2	$(t_i, \Delta, W, \varepsilon, \dots)$	$(M(t_i), k, \dots)$
Mechanism 1.3	$(t_i, \Delta, k, \varepsilon, \dots)$	$(M(t_i), k, \dots)$
Mechanism 2.1	$(t_i, \lambda, c, \varepsilon, \dots)$	$(\text{List}(t_i, \Lambda, \dots))$
Mechanism 3.1	$(t_i, \Delta, W, \varepsilon, \dots)$	$(M(t_i), k, \dots)$

derived quantity k or Λ are returned along with sanitized values. It is possible to have versions where the roles of these parameters are switched. In case of mechanism 2.1, the return value consists of a list of event times instead of a single time, since this mechanism generates fake events.

The service operates in batch mode, which is more efficient when sanitizing large number of events. The ellipsis represents that the application can optionally pass event id or other attributes. The service includes these attributes as is in the returned set. This feature is useful in research where it is of interest to observe the sanitized timestamp of an input event. In case of mechanism 3.1, the fake events carry empty attributes. In case of real usage, it is the responsibility of the application to remove these attributes before or after the call to the service, or to set a flag remove_labels = True.

Time of event publication. Beyond getting data sanitized by the service, the application needs to take care in when the timestamp of an event is published, since in temporal privacy, the time of publication may reveal information about the true event time. In case of mechanisms 1.2 and 3.1, we recommend publishing event time stamps after the time window W. In case of mechanism 2.1, events can be published as soon as real time has passed the timestamp of the event.

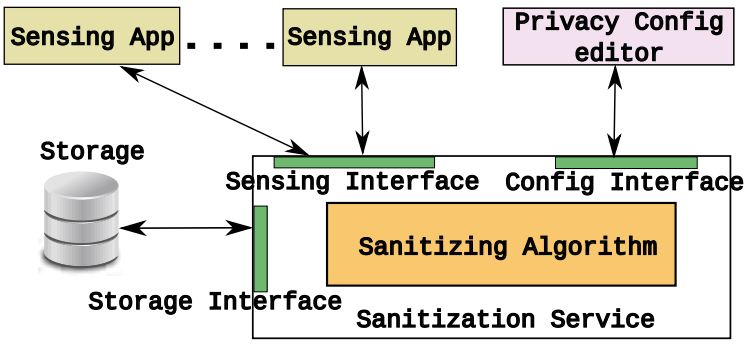

Figure 3.4: System design for sanitization module. The service exposes APIs for sanitizing events, configuring privacy parameters, and storing configuration parameters. The design is flexible to have the components be part of a single process or from different processes.

3.6.1 System design as background Android service

Our implemented service uses Java Apache math library[1] for sampling and randomization. The other aspects of the service are shown in Figure 3.4.

Sensing apps. Each app may have different privacy configuration and they can register and unregister the settings as default.

Privacy configuration editor. Users can view and edit the privacy settings for various apps.

Persistent storage. The privacy configuration for different apps are stored in a secure file system.

The sanitization service offers separate interfaces to the sensing apps, privacy configuration viewer and editor, and storage module. Below are the details of the interface functions. This is of a proof of concept implementation, and can be modified as appropriate in different circumstances.

3.7 Experiments

This section describes experiments showing that the privacy preserving mechanisms preserve utility for practical purposes. Highlights of the results are the following.

[1] http://commons.apache.org/proper/commons-math/

- Sanitized event timings support accurate range queries.
- The proposed methods preserve utility better than competing methods in terms of range queries.
- Privacy preserving mechanisms work in real event streams of check-ins, app-usages, and phone unlock events.

3.7.1 Experimental Setup

Datasets. Our experiments use three real world event timing dataset. (*i*) The check-in dataset[2] consists of 12,372 check-ins at Akihabara station, Tokyo by Foursquare users. (*ii*) Events occur in the app-usage dataset (Shepard et al., 2011) when a user opens one of his 10 most frequent apps, e.g., SMS, mail, Facebook, etc. (*iii*) Event occurs when a user unlocks the phone. Whereas, the first two datasets contain data for about an year, the last dataset has data of a week. Further, the last two datasets have data for a single user and the first dataset include data from $1k$ users.

Measuring utility. Utility of the sanitized data is measured using range queries. Each experiment uses 5000 random query ranges and repeated 10 times. If the range count in the original event stream is n and in the sanitized event stream is $\tilde{n}$, then the relative error is $\xi = \frac{|n-\tilde{n}|}{n}$ The relative error is symmetric with respect to addition, i.e., estimating $n + \Delta$ and $n - \Delta$ incur same error.

3.7.2 Evaluating Event Time Privacy

Figure 3.5(a) and (b) show the distribution of events in the check-in dataset overlaid in a single day for actual stream and the sanitized stream respectively using Mechanism 1.3. Visually, the sanitization preserves the critical features in the distribution, e.g., the peak.

Mechanism 1.2 is evaluatede in Figure 3.5 by varying ε and the error is small for small values of ε. Figure 3.7(a,b,c) and (d,e,f) evaluate Mechanism 1.3 and show natural privacy-utility tradeoff by varying Δ and ε respectively – with increasing Δ and decreasing ε, privacy increases and the error increases.

[2]https://www.kaggle.com/chetanism/foursquare-nyc-and-tokyo-checkin-dataset

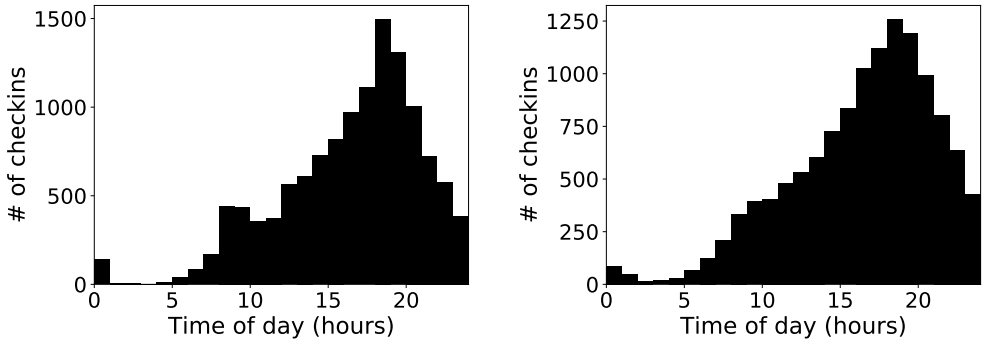

(a) (b)

Figure 3.5: **(a)** Temporal distribution of check-in events at Akihabra station in Tokyo. The dataset features typical behavior of a point of interest – gradually gets busy during day and idle during early morning. **(b)** Temporal distribution of sanitized events using mechanism in 3.5.1 with $\Delta = 1$ hour and $\varepsilon = 1$. Sanitized data preserves the overall temporal pattern.

3.7.3 Evaluating Event Existance – Mechanism 2.1

The fake event rate at each hour is set according to Theorem 3. The event rate at an hour is simply the number of events occured at that hour and $c = 1$. To answer a range query we count total number of events in the range, n, and get Λ by integrating $\lambda(t)$ over the query range. The true count is then estimated as $n - \Lambda$. Figure 3.8 (d,e,f) confirm usual ε behavior.

3.7.4 Comparison with existing methods.

The p-sum mechanism described in (Chan et al., 2011) and briefed in Section 3.3.1 is applied to event series with different resolution. Originally, the checkin-dataset has resolution in seconds, and the coarser resolutions are prepared by suitable binning. As we see in Figure 3.6 (a) our mechanism 1.3 is more accurate than the p-sum mechanism for recording events every minute which is necessary for many practical applications.

3.7.5 Time efficiency

Both Laplace perturbation and fake event augmentation method operate at constant cost per event, and threfore are efficient to sanitize large event datasets as shown in Figure 3.6 (b). The algorithms implemented using Python and executed

in a Ubuntu desktop machine with $i5$ processor and 8GB memory. The execution time grows linearly with the size of the dataset.

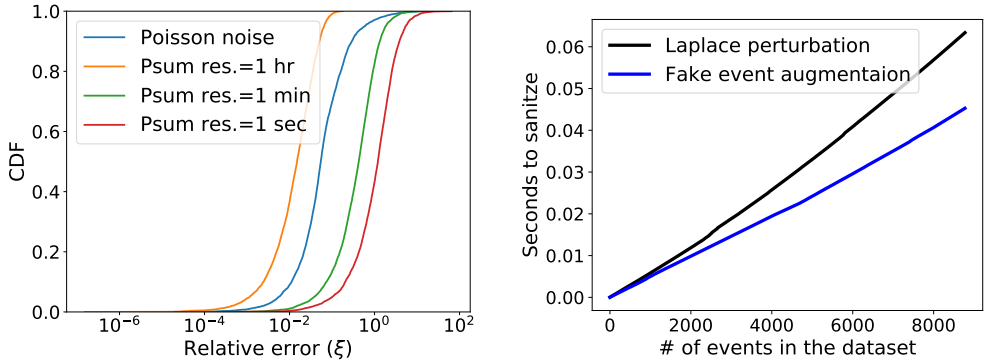

(a) (b)

Figure 3.6: **(a)** Real-time temporal range queries are more accurate for our Poisson process based method than p-sum mechanism on time series with finer resolution than a minute.**(b)** Both the privacy preserving methods using Laplace perturbation and Fake event augmentation are efficient for large dataset. Sampling from Laplace distribution is slightly slower than sampling from Poisson and Uniform distribution in numpy Python library, therefore the Laplace perturbation method takes a bit longer time to execute.

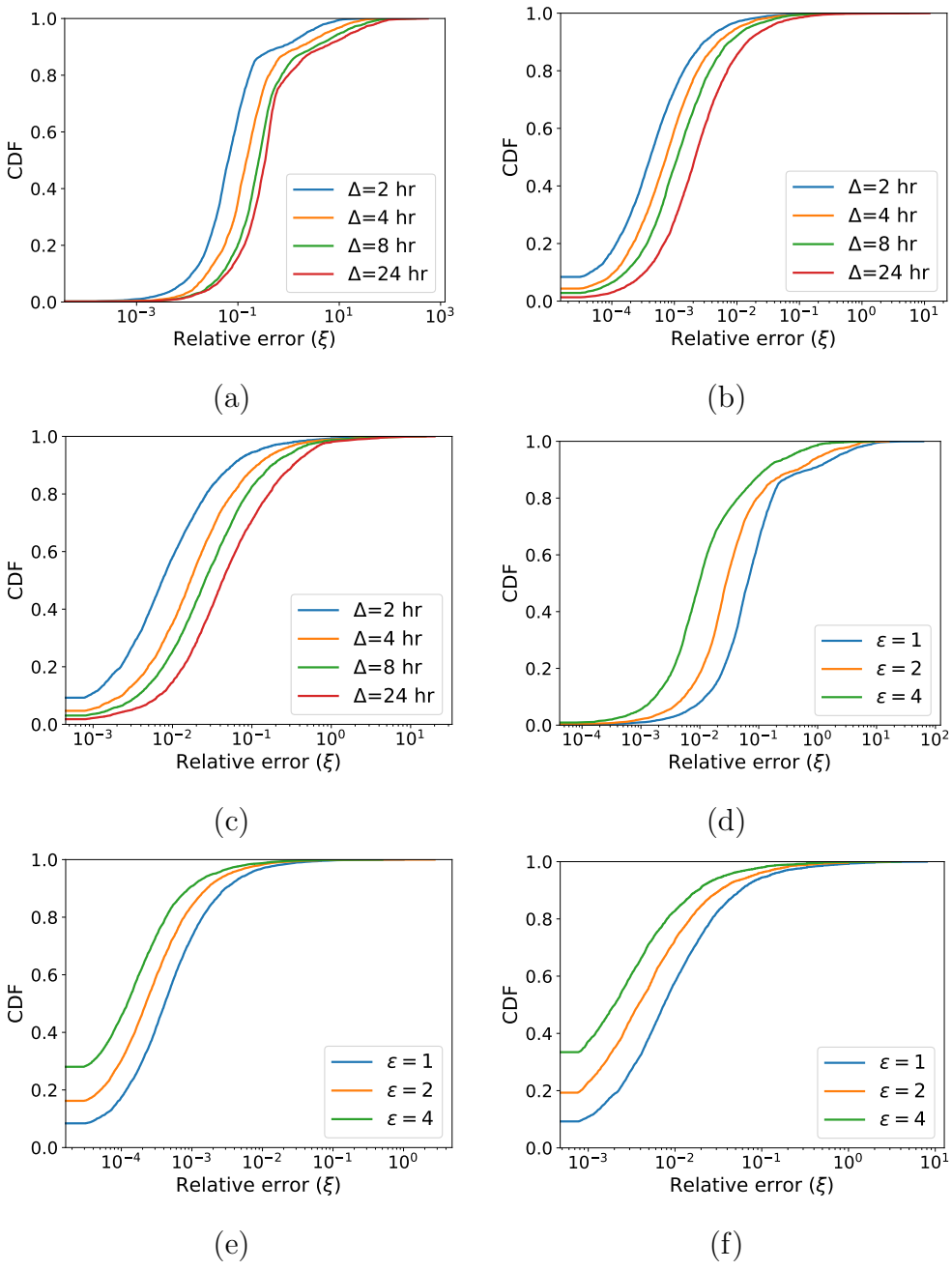

Figure 3.7: Evaluating Mechanism 1.3. **(a,b,c)** vary Δ with fixed $\varepsilon = 1$ and **(d,e,f)** vary ε with fixed $\Delta = 2$ hours. (a, d) use check-in dataset,(b, e) use app-usage dataset, and (c, f) use phone unlock dataset. For all configurations, the sanitized dataset achieve high utility and they show natural privacy-utility tradeoff.

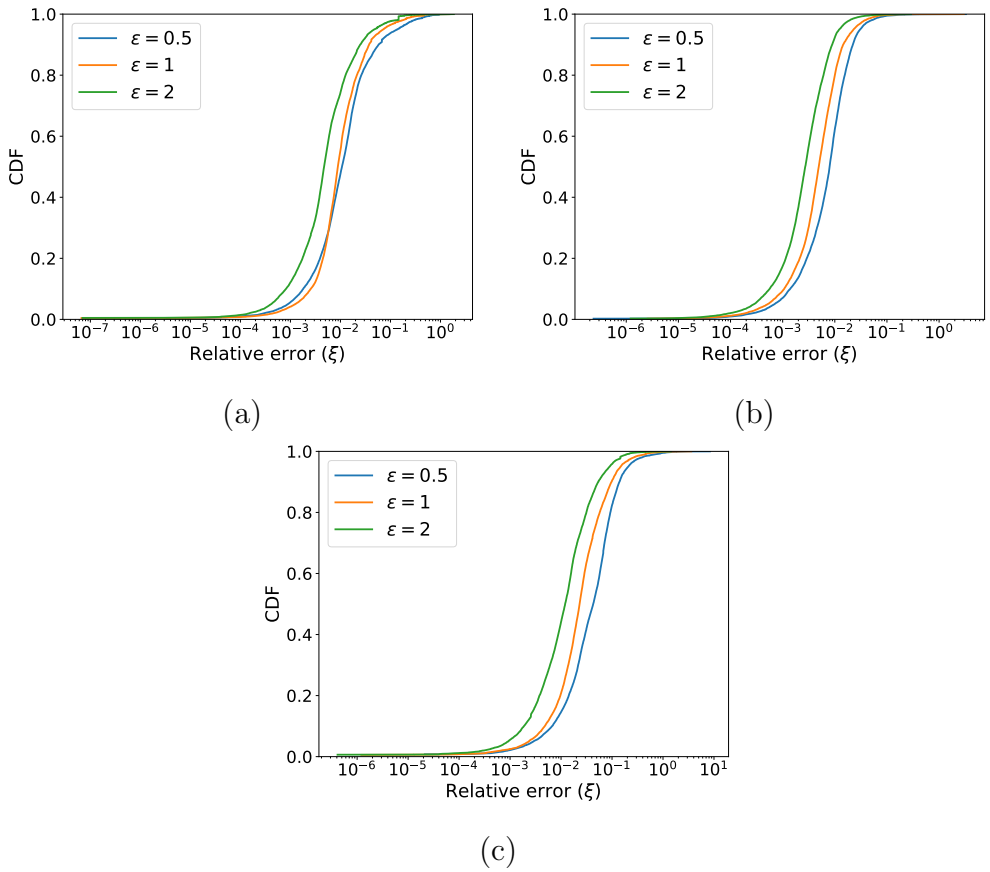

Figure 3.8: Evaluating Mechanism 2.1. **(a,b,c)** vary ε for check-in dataset, app-usage dataset, and phone unlock dataset respectively. The mechanism preserve high utility for all ε and with decreasing ε, error increases.

3.8 Proofs of the Theorems

3.8.1 Proof of Theorem 1

Proof. Following the definition of Pufferfish privacy, for an event e_i occuring at t_i, $M(e_i)$ needs to be checked for two types of ranges – i) when $M(e_i) \in I$ and ii) when $M(e_i) \notin I$. Assume $\delta > 0$ is a very small constant.

Event E_1 denotes $e_i \in I_1$, event E_2 denotes $e_i \in I_2$, and E_3 denotes $e_i \in I_3$.

Case (i) When the sanitized event is placed in the Δ sized neighbourhood I, i.e., $M(e_i) \in I$.

It is easy to see that, $Pr(M(e_i) \in I|s, \theta) = \frac{\Delta}{k\Delta} = \frac{1}{k}$.

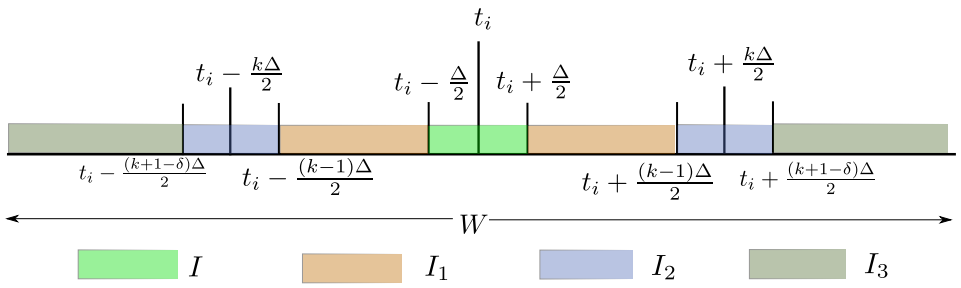

Figure 3.9: Setup for the proof of Theorem 1

$$
\begin{aligned}
Pr\big(M(e_i) \in I|\neg s, \theta\big) &= Pr\big(M(e_i) \in I, E_1 \cup E_2 \cup E_3|\neg s, \theta\big) \\
&= Pr\big(M(e_i) \in I, E_1|\neg s, \theta\big) + Pr\big(M(e_i) \in I, E_2|\neg s, \theta\big) \\
&\qquad + Pr\big(M(e_i) \in I, E_3|\neg s, \theta\big) \\
&= Pr\big(M(e_i) \in I|E_1, \neg s, \theta\big).Pr(E_1|\neg s, \theta) \\
&\qquad + Pr\big(M(e_i) \in I|E_2, \neg s, \theta\big).Pr(E_2|\neg s, \theta) \\
&\qquad\qquad [\text{Using } Pr\big(M(e_i) \in I|E_3, \neg s, \theta\big) = 0, \text{ and independence.}]
\end{aligned}
$$

Now the adversary's prior knowledge is that the events occur with uniform distribution, therefore $Pr(E_1|\neg s, \theta) = \frac{(k-1)\Delta - \Delta}{W - \Delta} = \frac{(k-2)\Delta}{W-\Delta}$. And $Pr\big(M(e_j) \in I|E_1, \neg s\big) = \frac{1}{k}$. So,

$$Pr\big(M(e_i) \in I|E_1, \neg s, \theta\big).Pr(E_1|\neg s, \theta) = \frac{(k-2)\Delta}{k(W-\Delta)}$$

.

Again, $Pr(E_2|\neg s, \theta) = \frac{(2-\delta)\Delta}{W-\Delta}$, and
$Pr\big(M(e_i) \in I|E_2, \neg s, \theta\big) \geq \frac{\delta\Delta}{2k\Delta} = \frac{\delta}{2k}$. Therefore,

$$\frac{\delta(2-\delta)\Delta}{2k(W-\Delta)} \leq Pr\big(M(e_i) \in I|E_2, \neg s, \theta\big).Pr(E_2|\neg s, \theta) \leq \frac{(2-\delta)\Delta}{k(W-\Delta)}$$

Now adding the probabilities for E_1 and E_2 we get,

$$
\begin{aligned}
\frac{\delta(2-\delta)\Delta}{2k(W-\Delta)} + \frac{(k-2)\Delta}{k(W-\Delta)} \leq Pr\big(M(e_i) \in I|\neg s, \theta\big) \leq \frac{(2-\delta)\Delta}{k(W-\Delta)} + \frac{(k-2)\Delta}{k(W-\Delta)} \\
\frac{(2\delta - \delta^2 + 2k - 4)\Delta}{2k(W-\Delta)} \leq Pr\big(M(e_i) \in I|\neg s, \theta\big) \leq \frac{(k-\delta)\Delta}{k(W-\Delta)}
\end{aligned}
$$

So,

$$\frac{(W-\Delta)}{(k-\delta)\Delta} \leq \frac{Pr\big(M(e_i) \in I|s,\theta\big)}{Pr\big(M(e_i) \in I|\neg s,\theta\big)} \leq \frac{2(W-\Delta)}{(2\delta-\delta^2+2k-4)\Delta} \tag{3.2}$$

Case (ii) When the sanitized event is placed in the Δ sized neighbourhood N, i.e., $M(e_i) \notin I$.

It is easy to see that, $Pr(M(e_i) \notin I|s,\theta) = \frac{k-1}{k}$. Again, similar to the above case,

$$Pr\big(M(e_i) \notin I|\neg s,\theta\big) = Pr\big(M(e_i) \in I, E_1 \cup E_2|\neg s,\theta\big) + Pr\big(M(e_i) \notin I, E_3|\neg s,\theta\big)$$

Now, $Pr(E_1 \cup E_2|\neg s,\theta) = \frac{\Delta(k-\delta)}{W-\Delta}$.
Again, $\frac{k-1}{k} \leq Pr\big(M(e_i) \notin I, E_1 \cup E_2|\neg s,\theta\big) \leq \frac{k-\delta}{k}$, therefore,

$$\frac{(k-1)(k-\delta)}{k(W-\Delta)} \leq Pr\big(M(e_i) \notin I, E_1 \cup E_2|\neg s,\theta\big) \leq \frac{(k-\delta)^2\Delta}{k(W-\Delta)}$$

It is easy to see that, $Pr\big(M(e_i) \in I|E_3,\neg s,\theta\big) = 1$. Now, $Pr(E_3|\neg s) = \frac{W-(k+1-\delta)\Delta}{W-\Delta}$. Therefore, $Pr\big(M(e_i) \in I, E_3,|\neg s,\theta\big) = \frac{W-(k+1-\delta)\Delta}{W-\Delta}$. Hence, we get the following,

$$\frac{(k-1)(k-\delta)}{k(W-\Delta)} + \frac{W-(k+1-\delta)\Delta}{W-\Delta} \leq Pr\big(M(e_i) \notin I|\neg s,\theta\big) \leq \frac{(k-\delta)^2\Delta}{k(W-\Delta)}$$

$$Or, \quad \frac{(k-1)(k-\delta)+Wk-k\Delta(k+1-\delta)}{k(W-\Delta)} \leq Pr\big(M(e_i) \notin I|\neg s,\theta\big) \leq \frac{Wk+\delta^2\Delta-k\Delta(1+\delta)}{k(W-\Delta)}$$

Combining the results for $E_1 \cup E_2$ and E_3, we get,

$$\frac{(W-\Delta)}{(k-1)(Wk+\delta^2\Delta-k\Delta(1+\delta))} \leq \frac{Pr\big(M(e_i) \notin I|s,\theta\big)}{Pr\big(M(e_i) \notin I|\neg s,\theta\big)} \leq \frac{(W-\Delta)}{(k-1)[(k-1)(k-\delta)+Wk-k\Delta(k+1-\delta)]} \tag{3.3}$$

Combining the lower bound of Equation 3.2 and Equation 3.3 we get.

$$\min\left(\frac{(W-\Delta)}{(k-\delta)\Delta}, \frac{(W-\Delta)}{(k-1)(Wk+\delta^2\Delta-k\Delta(1+\delta))}\right) \leq \frac{Pr\big(M(e_i)=w|s,\theta\big)}{Pr\big(M(e_i)=w|\neg s,\theta\big)} \leq \max\left(\frac{2(W-\Delta)}{(2\delta-\delta^2+2k-4)\Delta}, \frac{(W-\Delta)}{(k-1)[(k-1)(k-\delta)+Wk-k\Delta(k+1-\delta)]}\right)$$

$$Or, \frac{\Delta}{2Wk^2} \leq \frac{Pr\big(M(e_i)=w|s,\theta\big)}{Pr\big(M(e_i)=w|\neg s,\theta\big)} \leq \frac{2W}{k\Delta} \text{ when } W \geq 2\Delta$$

$$Or, e^{\varepsilon} \geq \frac{2W}{k\Delta} \text{ and } e^{-\varepsilon} \leq \frac{\Delta}{2Wk^2} \text{ [from Pufferfish privacy defination.]}$$

$$Or, k \geq \frac{2W}{e^{\varepsilon}\Delta}$$

□

3.8.2 Proof of Theorem 2

Proof. Similar to the above proof, for an event e_i occuring at t_i, $M(e_i)$ needs to be checked for two types of ranges – i) when $M(e_i) \in I$ and ii) when $M(e_i) \notin I$.

Case (i) When the sanitized event is placed in the Δ sized neighbourhood I, i.e., $M(e_i) \in I$.

$$\int_0^{\Delta} Lap(x;0,b)dx \leq Pr(M(e_i) \in I|s,\theta) \leq \int_{-\Delta/2}^{\Delta/2} Lap(x;0,b)dx$$

$$Or,\ -\frac{1}{2}\Big[e^{-x/b}\Big]_0^{\Delta} \leq Pr(M(e_i) \in I|s,\theta) \leq 2.\int_0^{\Delta/2} Lap(x;0,b)dx$$

$$Or,\ \frac{1}{2}[1-e^{-\Delta/b}] \leq Pr(M(e_i) \in I|s,\theta) \leq \Big[e^{-x/b}\Big]_0^{\Delta/2}$$

$$Or, \frac{1}{2}[1-e^{-\Delta/b}] \leq Pr(M(e_i) \in I|s,\theta) \leq (1-e^{-\Delta/(2b)}) \tag{3.4}$$

Now, for the secret $\neg s$, when event e_i does not occur in I,

$$\int_{k\Delta-\Delta}^{K\Delta} Lap(x;0,b)dx \leq Pr(M(e_i) \in I|\neg s,\theta) \leq \int_0^{\Delta} Lap(x;0,b)dx$$

$$Or, \frac{e^{-k\Delta/b}}{2}(e^{\Delta/b}-1) \leq Pr(M(e_i) \in I|\neg s,\theta) \leq \frac{1}{2}(1-e^{-\Delta/b}) \tag{3.5}$$

Combining Equation 3.4 and 3.5, we get the following,

$$\min\left(\frac{e^{k\Delta/b}(1-e^{-\Delta/b})}{e^{\Delta/b}-1}, 1, \frac{2e^{k\Delta/b}(1-e^{-\Delta/(2b)}}{e^{\Delta/b}-1}, \frac{2(1-e^{-\Delta/(2b)})}{1-e^{-\Delta/b}}\right)$$
$$\leq \frac{Pr(M(e_i)\in I|s,\theta)}{Pr(M(e_i)\in I|\neg s,\theta)} \leq$$
$$\max\left(\frac{e^{k\Delta/b}(1-e^{-\Delta/b})}{e^{\Delta/b}-1}, 1, \frac{2e^{k\Delta/b}(1-e^{-\Delta/(2b)}}{e^{\Delta/b}-1}, \frac{2(1-e^{-\Delta/(2b)})}{1-e^{-\Delta/b}}\right)$$
$$1 \leq \frac{Pr(M(e_i)\in I|s,\theta)}{Pr(M(e_i)\in I|\neg s,\theta)} \leq e^{k\Delta/b} \tag{3.6}$$

Case (ii) When the sanitized event is placed in the Δ sized neighbourhood I, i.e., $M(e_i) \notin I$.

For the case with secret s,

$$2\int_{\Delta/2}^{k\Delta/2} Lap(x;0,b)dx \leq Pr(M(e_i)\notin I|s,\theta) \leq$$
$$\int_{-(k-1)\Delta/2}^{0} Lap(x;0,b)dx + \int_{\Delta}^{-(k+1)\Delta/2} Lap(x;0,b)dx$$
$$Or,\ e^{-\Delta/(2b)} - e^{-k\Delta/2b} \leq Pr(M(e_i)\notin I|s,\theta) \leq$$
$$1/2\big(1+e^{-\Delta/b} - e^{-(k-1)\Delta/(2b)} - e^{-(k+1)\Delta/(2b)}\big) \tag{3.7}$$

And for the case with secret $\neg s$,

$$\int_{0}^{k\Delta} Lap(x;0,b)dx + \int_{k\Delta/2}^{(k+2)\Delta/2} Lap(x;0,b)dx$$
$$\leq Pr(M(e_i)\notin I|\neg s,\theta) \leq$$
$$\int_{-(k-1)\Delta/2}^{0} Lap(x;0,b)dx + \int_{\Delta}^{-(k+1)\Delta/2} Lap(x;0,b)dx$$
$$Or,\quad 1/2(1+e^{-(k+2)\Delta/(2b)} - e^{-k\Delta/(2b)} - e^{-k\Delta/b})$$
$$\leq Pr(M(e_i)\notin I|\neg s,\theta) \leq$$
$$1/2\big(1+e^{-\Delta/b} - e^{-(k-1)\Delta/(2b)} - e^{-(k+1)\Delta/(2b)}\big) \tag{3.8}$$

Now the ratio of Equation 3.7 and 3.8 is bounded by the following.

$$\frac{e^{-\Delta/(2b)} - e^{-k\Delta/2b}}{1/2\big(1 + e^{-\Delta/b} - e^{-(k-1)\Delta/(2b)} - e^{-(k+1)\Delta/(2b)}\big)}$$
$$\leq \frac{Pr(M(e_i) \notin I|s,\theta)}{Pr(M(e_i) \notin I|\neg s,\theta)} \leq 1$$
$$Or, \qquad e^{-k\Delta/b} \leq \frac{Pr(M(e_i) \notin I|s,\theta)}{Pr(M(e_i) \notin I|\neg s,\theta)} \leq 1 \tag{3.9}$$

Finally we combine Equation 3.6 and 3.9 and get the following.

$$e^{-k\Delta/b} \leq \frac{Pr(M(e_i) = w|s,\theta)}{Pr(M(e_i) = w|\neg s,\theta)} \leq e^{(k-1)\Delta/b}$$

From the Pufferfish privacy definition,

$$e^{-\varepsilon} \leq e^{-k\Delta/b} \leq \frac{Pr(M(e_i) = w|s,\theta)}{Pr(M(e_i) = w|\neg s,\theta)} \leq e^{(k-1)\Delta/b} \leq e^{\varepsilon}$$

Which gives the bound $b \geq \frac{k\Delta}{\varepsilon}$.

□

3.8.3 Proof of Theorem 4

To proof the theorem we need the following lemma first.

Lemma 1. *Goldreich (2017) If a random variable Y follows a Poisson distribution with mean Λ_Y, $P(|Y - \Lambda_Y| \geq \alpha) \leq 2\exp\left(-\frac{\alpha^2}{2(\Lambda_Y+\alpha)}\right)$.*

Proof. Given a interval $[x, y]$ with length L, denote the count of real events as n^*. $\mathcal{A}(x, y) - n^* = n - n^* - \Lambda \cdot (y - x)$. Notice that $n - n^*$ is the count of fake events, following the Poisson with mean $\Lambda \cdot (y - x)$. Applying the Lemma 1, for any β, we set $\alpha \geq \log\frac{2}{\beta} + \sqrt{\log^2\frac{2}{\beta} + 2\Lambda\log\frac{2}{\beta}}$, and we have

$$P\left(|\mathcal{A}(x, y) - n^*| \leq \log\frac{2}{\beta} + \sqrt{\log^2\frac{2}{\beta} + 2\Lambda\log\frac{2}{\beta}}\right) \geq 1 - \beta.$$

Rearranging, we get the theorem.

□

3.8.4 Proof of Theorem 5

Proof. For simplicity of calculation let us assume $\Delta = 1$ (we can scale everything to make this happen). Form the figure, $|I_2| = (k - 1)$. For two events e_a and e_b

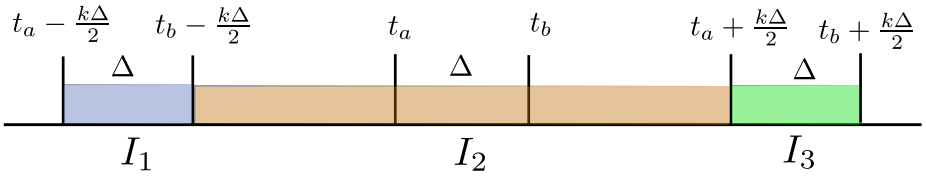

Figure 3.10: Setup for the proof of Theorem 5

occuring at time t_a, t_b, the situation E denotes that the fact that $M(e_a) \leq M(e_b)$, and $\neg E$ denotes the complement of this situation. Therefore,

$$\begin{aligned} Pr(E|s,\theta) \leq & Pr(M(e_a) \in I_1) + Pr(M(t_a) \in I_3) \\ & + Pr(M(e_a) \leq M(t_b), M(e_a) \in I_2, M(e_b) \in I_2) \\ Or, \quad \leq & \frac{2}{k} + \frac{(k-1)^2}{k^2}\frac{(k-1)+1}{2(k-1)} \\ \leq & \frac{2}{k} + \frac{k-1}{2k} \\ \leq & \frac{k+3}{2k} \end{aligned} \tag{3.10}$$

For the lower bound we have t_a and t_b almost coencide, which makes the $R_3 \approx k$,

$$Pr(E|s,\theta) \geq \frac{k+1}{2k} \tag{3.11}$$

Now, combining Equation 3.11 and equation 3.10, we have the following.

$$\frac{k+1}{2k} \leq Pr(E|s,\theta) \leq \frac{k+3}{2k} \tag{3.12}$$

Again for the secret $\neg s$, we have the following.

$$\begin{aligned} \frac{(k-1)^2}{k^2}\frac{k-1+1}{2(k-1)} \leq & Pr(E|\neg s,\theta) \leq \frac{k+1}{2k} \\ Or, \quad \frac{k-1}{2k} \leq & Pr(E|\neg s,\theta) \leq \frac{k+1}{2k} \end{aligned} \tag{3.13}$$

Now, combining the Equation 3.12 and Equation 3.13 we have the following.

$$\begin{aligned}
&\min\left(\frac{k+1}{k-1}, \frac{k+1}{k+1}, \frac{k+3}{k-1}, \frac{k+3}{k+1}\right) \\
&\leq \frac{Pr(E|s,\theta)}{Pr(E|\neg s,\theta)} \leq \\
&\max\left(\frac{k+1}{k-1}, \frac{k+1}{k+1}, \frac{k+3}{k-1}, \frac{k+3}{k+1}\right) \\
&1 \leq \frac{Pr(E|,\theta)}{Pr(E|\neg s,\theta)} \leq \frac{k+3}{k-1}
\end{aligned} \tag{3.14}$$

Now, for the event $\neg E$ and secret s, we have the following.

$$\begin{aligned}
\frac{(k-1)^2}{k^2}\frac{k-1+1}{2(k-1)} \leq & Pr(\neg E|s,\theta) \leq \frac{k+1}{2k} \\
Or, \qquad \frac{k-1}{2k} \leq & Pr(\neg E|s,\theta) \leq \frac{k+1}{2k}
\end{aligned} \tag{3.15}$$

Again for the event $\neg E$ and secret $\neg s$, we have the following. This equation is same as the one in Equation 3.12 by simply considering opposite timing assignment of the events, i.e., event e_a occurs in t_b and event e_b occurs in time t_a.

$$\frac{k+1}{2k} \leq Pr(\neg E|\neg s,\theta) \leq \frac{k+3}{2k} \tag{3.16}$$

Combining Equation 3.15 and Equation 3.16,

$$\begin{aligned}
&\min\left(\frac{k-1}{k+1}, \frac{k-1}{k+3}, \frac{k+1}{k+1}, \frac{k+1}{k+3}\right) \\
&\leq \frac{Pr(\neg E|s,\theta)}{Pr(\neg E|\neg s,\theta)} \leq \\
&\max\left(\frac{k-1}{k+1}, \frac{k-1}{k+3}, \frac{k+1}{k+1}, \frac{k+1}{k+3}\right) \\
&\frac{k-1}{k+3} \leq \frac{Pr(\neg E|s,\theta)}{Pr(\neg E|\neg s,\theta)} \leq 1
\end{aligned} \tag{3.17}$$

Suppose, the ordering of the sanitized events $M(e_a)$ and $M(e_b)$ is denoted as $O(M(e_a), M(e_b)) \in \{M(e_a) \geq M(e_b), M(e_b) \geq M(e_a)\}$, Combining Equation 3.14 and Equation 3.17,

$$\begin{aligned}
\min\left(\frac{k-1}{k+3}, 1\right) \leq & \frac{Pr(O(M(e_a), M(e_b))|s,\theta)}{Pr(O(M(e_a), M(e_b))|\neg s,\theta)} \leq \max\left(1, \frac{k+3}{k-1}\right) \\
\frac{k-1}{k+3} \leq & \frac{Pr(O(M(e_a), M(e_b))|s,\theta)}{Pr(O(M(e_a), M(e_b))|\neg s,\theta)} \leq \frac{k+3}{k-1}
\end{aligned} \tag{3.18}$$

For ε-Pufferfish privacy we have $\frac{k+3}{k-1} \leq e^{\varepsilon}$, which gives $k \geq \frac{3+e^{\varepsilon}}{e^{\varepsilon}-1}$.

□

Part II

Learning from Spatial Data

Chapter 4

Topological Signatures For Fast Mobility Analysis

Analytic methods can be difficult to build and costly to train for mobility data. We show that information about the topology of the space and how mobile objects navigate the obstacles can be used to extract insights about mobility at larger distance scales. The main contribution of this chapter is a topological signature that maps each trajectory to a relatively low dimensional Euclidean space, so that now they are amenable to standard analytic techniques. Data mining tasks: nearest neighbor search with locality sensitive hashing, clustering, regression, etc., work more efficiently in this signature space. We define the problem of mobility prediction at different distance scales, and show that with the signatures simple k nearest neighbor based regression perform accurate prediction. Experiments on multiple real datasets show that the framework using topological signatures is accurate on all tasks, and substantially more efficient than machine learning applied to raw data. Theoretical results show that the signatures contain enough topological information to reconstruct non-self-intersecting trajectories upto homotopy type. The construction of signatures is based on a differential form that can be generated in a distributed setting using local communication, and a signature can be locally and inexpensively updated and communicated by a mobile agent.

4.1 Introduction

Location traces are computationally challenging to process. Distances between trajectories like Fréchet and Hausdorff distances (Alt and Godau, 1995) do not form a normed space, Dynamic time warping distance (Sakoe and Chiba, 1978) does not even form a metric (Driemel and Silvestri, 2017). As a result, typical computational methods are difficult to apply. Specialized techniques have been developed for location traces. Theoretical approaches such as locality sensitive hashing have to be tailored to trajectories for faster near neighbor search (Indyk, 2002; Driemel and Silvestri, 2017; Astefanoaei et al., 2018); computation of medians (Buchin et al., 2013), popular paths (Katsikouli et al., 2018) etc have also been considered.

Analysis and prediction of motion have been developed with Markov models (Xue et al., 2013; Ziebart et al., 2008; Liu et al., 1998) that assume motion to depend only on the current "state" of an agent and not on longer history. However, recent experimental results show that the memoryless assumption of Markov models does not hold in real location data, since agents do not execute a random walk, but move with the purpose to reach a destination (Srivatsa et al., 2013). Specialized neural network based models (Wu et al., 2017; Lv et al., 2018) with the power to encode longer history are shown in practice to be effective for next road segment prediction, although they do not provide rigorous models for other general tasks, e.g., search and comparison of trajectories. We instead seek a framework for interpretable encoding of large scale properties of trajectories, that is compatible with a range of analytic methods.

The motion of objects is determined by the major obstacles in the plane, which defines the geometry and topology of the space. However, considerations of topology raise complex issues, and traditional quantities like Fréchet distance are prohibitively expensive to compute in domains with obstacles (Chambers et al., 2010). Geometric algorithms thus usually assume motion in a simple plane, or of same topological type.

In past work, Hodge theory and relative homology from algebraic topology have been used for the purpose of topological classification (Yin et al., 2015; Pokorny et al., 2016). However, these approaches are only applicable to specific start and end points of trajectories, and yield only discrete classifications by homotopy type, which is not general enough for use in further analysis. They are

also expensive to compute. We intend to overcome these obstacles by using more flexible topological constructs.

Our contributions. This chapter shows that topological information can enhance mobility analysis by meaningfully encoding large scale patterns of movement, and demonstrates how the relevant information can be represented compactly.

The geometry and topology of the space of mobility itself can be discretized as a graph, where regions of zero or little activity are treated as obstacles or *holes*, and the remaining space is triangulated based on a suitable set of vertices.

Let us define a *discrete differential form* $\xi : E \to \mathbb{R}$ as a function that assigns values to directed edges. For any directed edge ab, the function ξ satisfies $\xi(ab) = -\xi(ba)$, that is, the values on an edge and its reverse are negations of each other (See Section 4.3). Further, the values on the edges sum to zero around any face of the graph, except possibly the obstacles. For each obstacle i, we define a differential form ξ_i such that around obstacle i, ξ_i on the edges sum to 1, and thus preserves topological information with respect to this obstacle.

For any mobility trace A, the differential form values along its directed edges are added to obtain $\xi_i(A)$. For a trajectory that goes around an obstacle i, $\xi_i(A) = 1$. In a space with k obstacles, the general differential form $\xi = \{\xi_1, \xi_2, \ldots \xi_k\}$ is a vector of length k.

The significant property here is that a signature element $\xi_i(A)$ can have a real numbered value when A is not a perfect loop. The signature $\xi(A) \in \mathbb{R}^k$ is a point in k dimensional space. Thus, beyond simple topological equality, the signatures can represent topological *similarity*. The mapping to a normed space enables standard analytic techniques like clustering, regression, density estimation, etc. We discuss the basic construction in Section 4.4 and the detailed technique in Section 4.5.

Summations over differential forms preserve only large scale properties, and are insensitive to noise that does not change topological type of a trajectory. As a result, the signatures are invariant to localization errors and GPS noise. They are compact compared to real trajectory data, and can be easily exchanged between mobile nodes to perform mobility comparison among nearby nodes. It is efficient to compute and to update incrementally as an object moves in the plane. Comparison between trajectories is now reduced to comparison of points in a low dimensional space. The signature of a simple trajectory contains sufficient

information to provably reconstruct it upto homotopy equivalence.

The knowledge of global topological behaviors of trajectories can be used to make predictions at larger scale beyond the next road segment. For this purpose, we define a notion of prediction at an arbitrary scale r. Motion prediction on larger scale can be useful in many applcations, e.g., to predict tourists visiting various attractions in a city. Simple k nearest neighbor regression on the signatures performs comparably to expensive and opaque neural network based methods, which suggests that the topological features are essential to understanding and prediction of motion.

Data mining techniques of locality sensitive hashing, dimension reduction, etc run efficiently and accurately on the signatures (Section 4.6). Experiments (Section 4.7) show that the dimensionality of the signatures can be reduced by selecting only a few obstacles from the domain, and this further increases the efficiency of the system. Based on how the trajectories traverse the domains, the obstacles themselves can be characterized by how they influence mobility.

Section 4.2 discusses some related works and how the new approach compares with them.

Before we move on with technical details, let us summarize our approach into the following steps: 1. Find obstacle as sparse regions of the plane 2. construct a differential 1-form for each obstacle. 3. As a mobile agent moves, use these forms to track how it circumnavigates each obstacle and get a point in Euclidean space, where each dimension represents behavior with respect to one obstacle. 4. Apply efficient analytic techniques treating trajectories as points in Euclidean space.

4.2 Related work

Hodge decomposition of a randomly generated vector field has been used in (Yin et al., 2015) to classify paths into homotopy types. This approach relies on a numerical process, and only applies to trajectories with same start and end points. This problem is avoided to an extent in (Pokorny et al., 2016), which uses relative homology, and marks certain regions of the space where start and end points lie, but other trajectories do not pass. Thus these approaches do not apply to general trajectory datasets of the type we have considered here. Both these methods are also computationally expensive.

In other works, topological characterization has been used to measure dis-

tances between curves (Chambers and Wang, 2013) but restricted to curves with same start and end points, since homotopy cannot be defined between open curves. A seminal work (Baryshnikov and Ghrist, 2009) Baryshnikov and Ghrist used integrals of Euler characteristics to compute number of mobile targets. Topological persistence can be used to simplify trajectories (Katsikouli et al., 2014). Discrete exterior calculus has been a subject of study in graphics, modeling and discrete geometry and developed in several different flavors (Hirani, 2003; Desbrun et al., 2008). In sensor network, it has been used for performing range queries of mobile objects (Sarkar and Gao, 2013).

Mobility modeling using (hidden) Markov models have been developed in (Xue et al., 2013; Ziebart et al., 2008; Liu et al., 1998) and other works, usually with the objective to predict the agent's next road segment. As mentioned earlier, the Markov assumption can be shown to be unrepresentative of typical trajectory datasets (Srivatsa et al., 2013). In line with recent developments in machine learning, Neural networks have been designed for the prediction task. Recurrent Neural Networks using Long Short Term Memory are considered useful in sequential data, and has been used in (Wu et al., 2017); we used a similar approach in our experiments, modified suitably for geometric trajectories in the datasets.

In contrast to these methods, our approach is computationally much more efficient in preprocessing, training as well as prediction query. It can be applied to road networks and geometric data alike. Unlike Markov and neural models that simply provide a prediction mechanism, the topological signatures reveal similarity between trajectories and reveal insights about how they traverse the domain. As a result, they can form the basis of search, clustering, prediction and other analytic tasks.

4.3 Theoretical background

Discrete differential forms and exterior calculus are a varied topic of study across many disciplines. This section presents a brief description of the main ideas relevant. A more formal treatment can be found in (Hirani, 2003). Readers familiar with the topic can consider skipping ahead to the next section.

Let us represent the space of motion using a simplicial complex or a cell complex. A two dimensional *simplicial complex* is a planar graph G with $0, 1$, and 2 dimensional simplices as vertices, edges, and triangles as shown in Figure 4.1(a).

A simplicial complex is built by attaching simplices together along subsimplices.

Orientation of a simplex is defined using ordering of constituent lower dimension simplices. E.g. ordering of two $0-$simplices $[v_0, v_1]$ produces an oriented $1-$simplex or a directed edge, e, while its opposite orientation is $-[v_0, v_1]$ or $-e$.

A linear combination of d dimensional simplices: $\sum_{i=0}^{k} \lambda_i \sigma_i$, where each λ_i is an integer, is called a d-chain. A trajectory or mobility trace can be seen as 1-chain.

The boundary ($\partial\sigma$) of an oriented $p-$chain σ is a $(p-1)-$chain that separates σ from rest of the complex and the orientation of the boundary is inherited from σ. Planar graphs are orientable, meaning that all its simplices can be oriented consistently (Kinsey, 2012). Here, all $2-$simplices or faces are assumed to be oriented counter clockwise. Consequently, the boundary of a summation of faces (2-chains) is the sum of their boundaries (1-chains); formally: $\partial(f_1 + f_2 + f_3 + \dots) = \partial f_1 + \partial f_2 + \partial f_3 + \dots$ (Figure 4.1(b)).

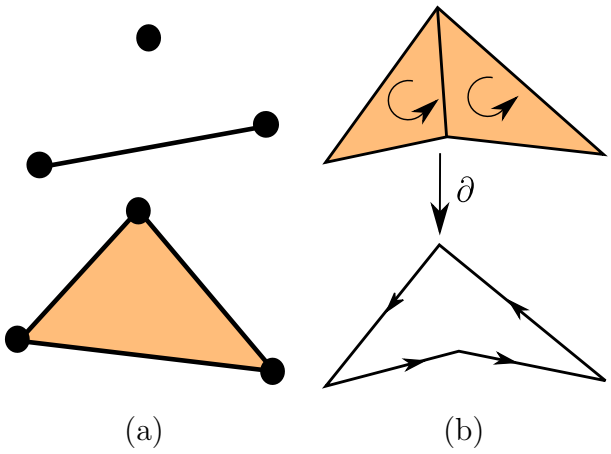

Figure 4.1: **(a)** $0, 1,$ and $2-$simplices **(b)** Boundary operation on a chain of 2-simplices

Cell complexes are a natural extension of simplicial complexes. The only difference meaningful to this context is that a two dimensional cell, or face, can be a simple polygon instead of a triangle, otherwise a cell complex retains all relevant properties of a simplicial complex. The area external to the planar graph is called the exterior face, or the *face at infinity*. The edges at the boundary of this face constitute the exterior boundary.

Dual complex. The dual of a simplicial complex G is a planar graph $\star G$ where a face σ in G corresponds to a node $\star\sigma$ in $\star G$ and an edge $\star e$ in $\star G$ exists between two nodes if the corresponding two faces in G are adjacent with shared edge e.

An example is shown in Figure 4.2(a).

4.3.1 Discrete differential 1-forms and co-chains

Differential forms are defined as functions over the directed cells of the cell complex. Specifically, 1-forms are values for the edge set E of a graph as $\omega : E \to \mathbb{R}$. The values are associated with directed edges, so that $\omega(ab) = -\omega(ba)$. Given a discrete trace written as $e_1 + e_2 + e_3 \ldots$, the integral of the form over it is now computed as sum of ω over the directed edges: $\omega(e_1) + \omega(e_2) + \omega(e_3) \ldots$.

The function ω thus defines a co-chain in $C^1(G; \mathbb{R})$ that maps 1-chains to real values. The entire construct translates to a dual with a dual function $\star\omega$ defined simply as $\star\omega(\star e) = \omega(e)$. Thus $\star\omega$, yields a differential form ω, which will be useful in the following section.

Sources and sinks. Suppose $X(v)$ is the set of edges of the type $(v, \circ)$ – that is, all edges incident on v, with orientation selected as pointing outward from v. Then we can compute the net *outflow* from v as $h(v) = \sum_{e \in X(v)} \omega(e)$. Depending on this value, v can be a:

- **Source:** net outflow $h(v) > 0$.
- **Internal or regular node:** net outflow $h(v) = 0$.
- **Sink:** net outflow $h(v) < 0$.

Observe the effect on the dual system. For a primal face f with dual vertex $\star f$, we have : $\sum_{\star e \in X(\star f)} \star\omega(\star e) = \omega(\partial f)$.

4.4 Topological signatures

The goal is to utilize differential forms to characterize the behavior of the traces with respect to obstacles in the domain. We assume that the obstacles such as buildings and lakes reside in the larger faces of the graph and the mobile objects move along the nodes and edges of the graph. The question of what constitutes important obstacles in a domain will be taken up later, for now assume that some faces are given to us to be treated as obstacles.

Dual sources. Each obstacle is a source of a dual vector field $\star\xi$. More specifically, given a face f with an obstacle, the corresponding dual node $\star f$ is the only

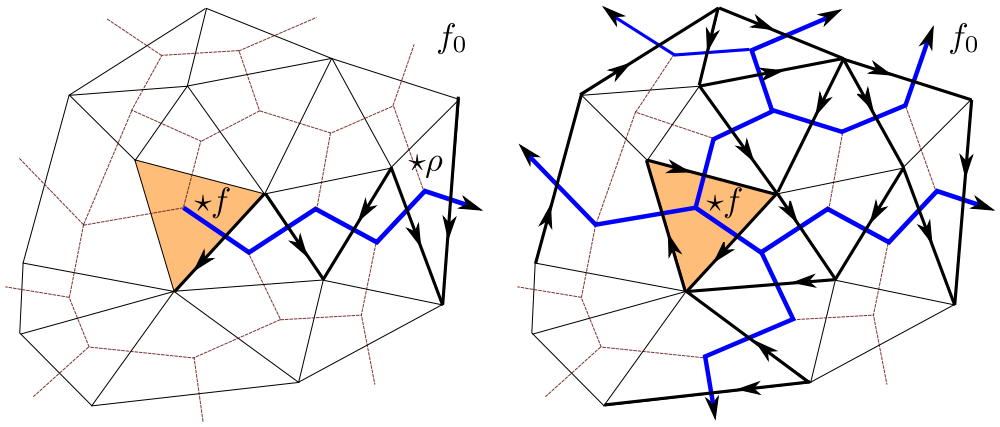

(a) (b)

Figure 4.2: **(a)** An example primal graph with a source face f. Dual path $\star\rho$ flows from $\star f$ to external node $\star f_0$.**(b)** Multiple dual paths from the source $\star f$ construct a differential form of non-zero integral around $\star f$.

source for $\star\xi$ in the dual graph. The external face, dual node $\star f_0$ is the only sink. A specific weight $h(\star f)$, usually set to 1, is associated with each source $\star f$.

The dual form with a value for each directed dual edge defines a differential form for the primal graph using $\xi(e) = \star\xi(\star e)$. For each face f_i that is an obstacle, we create one such differential form ξ_i, which equivalently sums to $h(\star f_i)$ around the boundary ∂f – representing a cyclic vector field along ∂f. We refer to these as the *signature forms* for the obstacles. The idea is shown in Figure 4.2.

The important property of this structure is that over any cycle γ surrounding f, the form sums to $\xi(\gamma) = \xi(\partial f) = h(\star f)$.

Theorem 6. *For a* $2-$*chain* U *with coefficients in* $0, 1$ *in* G *(excluding* f_0*) with a single source face* f_i*, the differential form* $\xi(\partial U) = h(\star f_i)$ *if* $f_i \in U$*, otherwise* $\xi(\partial U) = 0$.

The proof follows simply from the fact that for any face f, $\xi(\partial f) = h(\star f)$, and that $\partial(f_1 + f_2 + f_3 + \dots) = \partial f_1 + \partial f_2 + \partial f_3 + \dots$.

Topological signatures of trajectories. Using these differential forms, we can now define the topological signature of a trace. If there are k obstacles and corresponding signature forms, then for a trace T, we get a k dimensional vector $\theta(T)$. The component $\theta_i(T)$ represents to what extent T goes around obstacle i. If it forms exactly one complete cycle, then $\theta_i(T) = h(f_i)$.

The useful feature here is that even if T does not quite form a cycle, $\theta_i(T)$

still reveals valuable information. If the value of $\theta_i(T)$ is higher, it implies that t goes farther around the obstacle. This construction is more general than simple winding numbers, since the differential forms construction can assign arbitrary weights to individual edges, and can be made sensitive to specific mobile agents. From a computational point of view, it works directly on a discrete structure, with or without knowledge of locations. The symmetric nature of directed edges nullifies the effect of noisy GPS localization.

The signature $\theta : \mathcal{T} \to \mathbb{R}^k$ maps trajectories in set $\mathcal{T}$ to a k dimensional space.

4.5 Algorithms

This section describes how the mathematical construct of discrete topological signatures can be realized, including in a distributed environment.

4.5.1 Construction of planar graphs

The algorithms work on any planar graph on the mobility domain. Following are a few possible strategies varied by availability of mobility data and infrastructure.

Graphs from data. In many scenarios, road map data is available and directly yields a graph, where road intersections are vertices and road segments are edges. Alternatively, a simple model – a grid or a triangulation of randomly deployed point sets (vertices) may serve as the planar graph. In (Pokorny et al., 2016) a triangulation of the locations from the dataset itself is used as the discrete domain. A mobile trace is then converted to a sequence of edges in this graph. This can be done by simply mapping locations to nearby vertices. With sufficient data, it is also possible to construct a roadmap itself as is done in openstreetmap and other projects (Cao and Krumm, 2009).

Discrete sensor domains. In sensor networks and robotics, trajectories may be recorded by sensors. Such a trajectory may not have any localization at all, and is represented simply as a sequence of sensors that have detected the mobile object. For localized and unlocalized wireless sensor networks, there is a large body of research in topology control, localization and planar graph extraction, relying on the locality of wireless transmission. Depending on the network, such a technique can compute planar graph of the nodes (Sarkar et al., 2009; Funke

and Milosavljevic, 2007).

Our differential forms setup, as described in the previous section, works on the planar graph, without the need for an explicit embedding.

4.5.1.1 Obstacles and dual sources.

Having constructed the planar graph and map of trajectories to sequence of edges, we are left with the question of what are the 'obstacles' in the domain. In principle, every face can be an obstacle, but this is neither intuitive, nor informative to any algorithm operating on the data.

Instead, a face can be an obstacle if it is larger than a certain size, measured as area, diameter, or some other measure. The strength $h(\star f)$ of the source $\star f$, which is normally set to 1, can also be set to be proportional to the measure to reflect the weight of an obstacle. In unlocalized scenarios, there are techniques for detecting boundaries of large enough sizes (Wang et al., 2006), while a measure such as the number of edges on the face can be used to determine its weight.

Subsection 4.6.3 discusses more involved questions of determining the importance of an obstacle and dimension reduction techniques to merge nearby obstacles to simplify data.

4.5.2 Constructing signature forms

For each obstacle face f, our basic strategy is to take its dual face $\star f$, and start multiple walks in the dual graph. The walks spread in all directions, and end in the exterior face at infinity $\star f_0$. The total weight of the walks is $h(\star f_i)$. Having constructed walks of total weight of $h(\star f_i)$, the weight of each dual edge can be transferred to the corresponding primal edge as $\xi_i(ab) := \star\xi_i(\star ab)$.

In a distributed sensor network scenario, the operations of a dual node $\star f$, which is a face f in the primal, can be handled by an elected sensor node on its boundary. There are different ways to structure these walks and the corresponding differential form. Unless mentioned otherwise, the following mechanisms work in localized as well as unlocalized graphs.

Random walk in the dual. Starting from the dual node $\star f_i$, create several random walks that stop only when they reach $\star f_0$. Each walk has a weight w, and to each directed dual edge $\star ab$ it traverses, the weight is added as $\star\xi_i(\star ab) :=$

$\star\xi_i(\star ab) + w$. Note that this process preserves the strictly one source ($\star f_i$) and one sink ($\star f_0$) since at every other vertex it exits every time it enters. The walk is also allowed to pass through $\star f_i$ as well as any other dual vertex.

Shortest paths in the dual. Another possible way of constructing the signature forms is using shortest paths to the boundary faces, which are adjacent to the external face f_0.

From these boundary faces, select a subset either randomly or at some uniform separation. From the dual source node $\star f_i$, a shortest path in the dual is computed to each such boundary face $\star f_j$ and appended a final edge $(\star f_j, \star f_0)$ to complete the walk.

Following a straight line to the boundary. In scenarios with available locations, instead of selecting faces at the boundary, it is possible to select specific locations at the boundary and follow a straight line to them. By picking a location to place the dual nodes inside faces, e.g., at centroids, a line starts from a source location $\star f_i$. 'Following' a straight line in the dual graph is essentially choosing the next node in the path that minimizes the distance to the line segment (Nath and Niculescu, 2003).

4.5.3 Computing topological signatures

A trace consists of a sequence of edges, and for each edge e, the value $\xi_i(e)$ is computed corresponding to each obstacle i. Thus, for each e traversed by the trajectory T results in updates of the form $\theta_i(T) = \theta_i(T) + \xi_i(e)$.

In a distributed scenario, this works naturally, where for any edge ab, the ξ values for this edge are held by sensors a and b, and when a mobile object traverses this edge, it can obtain the values locally and maintain its own $\theta(T)$ vector. Or in a tracking scenario, the sensors as they track the object's motion can maintain and handoff this value.

While in principle $\theta_i(T)$ can take up any real value, the larger values of θ imply an agent circumscribing an obstacle many times. This is unlikely in many realistic scenarios such as trips in a city. In such cases, it is natural to assume that on a single trip an agent does not take sub-optimal self-intersecting paths that go all the way around the obstacle. Thus, for such trajectories, for any obstacle i, $|\theta_i(T)| < 1$, and let us refer them as simple trajectories. Theorem 7 shows that for simple trajectories, the signature uniquely determines their homotopy type.

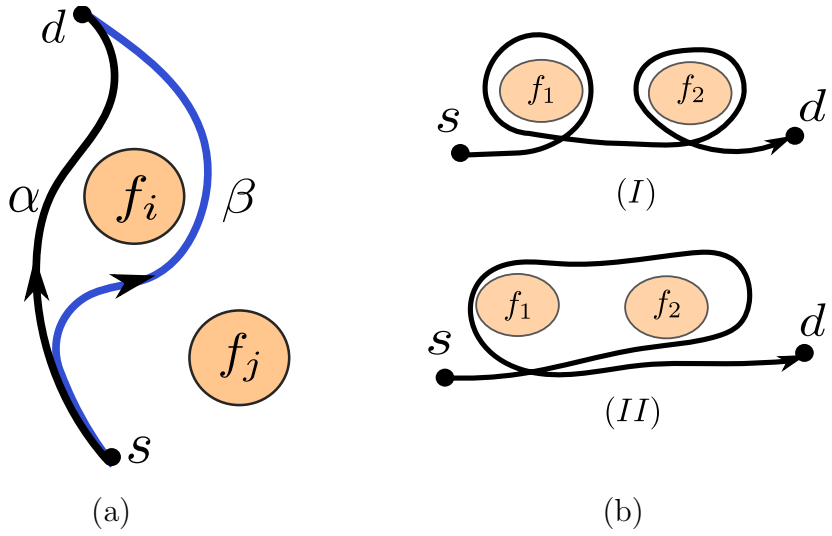

Figure 4.3: **(a)**Two simple trajectories α, β goes from s to d have same homotopy type w.r.t. source f_j, but different homotopy type w.r.t. f_i. **(b)** Two self-intersecting paths between same source and destination may have same signature value but different homotopy type.

Theorem 7. *For two simple trajectories α and β between same source s and destination d:*

$$\theta_i(\alpha) = \begin{cases} \theta_i(\beta) \text{ } \textit{If } \alpha, \beta \textit{ have same homotopy w.r.t. source } f_i. \\ \theta_i(\beta) \pm 1, \textit{ otherwise [assuming } h(\star f) = 1] \end{cases}$$

Proof. An example setup is shown in Figure 4.3(a). Where paths α and β have the same homotopy type with respect to f_j and different types with respect to f_i. The concatenation of α with $-\beta$ gives loop $\gamma = \alpha - \beta$.

The first claim simply says $\theta_j(\alpha) = \theta_j(\beta)$, since otherwise $\theta_j(\alpha - \beta) \neq 0$, contradicts Theorem 6.

For the second claim, any closed oriented one dimensional loop object $\hat{\gamma}$ in the two dimensional cell complex is the boundary ∂U of a chain U with coefficients in $[0, 1]$. Thus $f_i \in U$ implies $\xi(\hat{\gamma}) = 1$. Depending on the orientation of $\gamma = \alpha - \beta, \theta(\alpha - \beta) = \pm\theta(\hat{\gamma}) = \pm 1$, implying the second claim. □

Figure 4.3(b) shows an example where the above condition is violated, and trajectories of the same signature have different homotopy types.

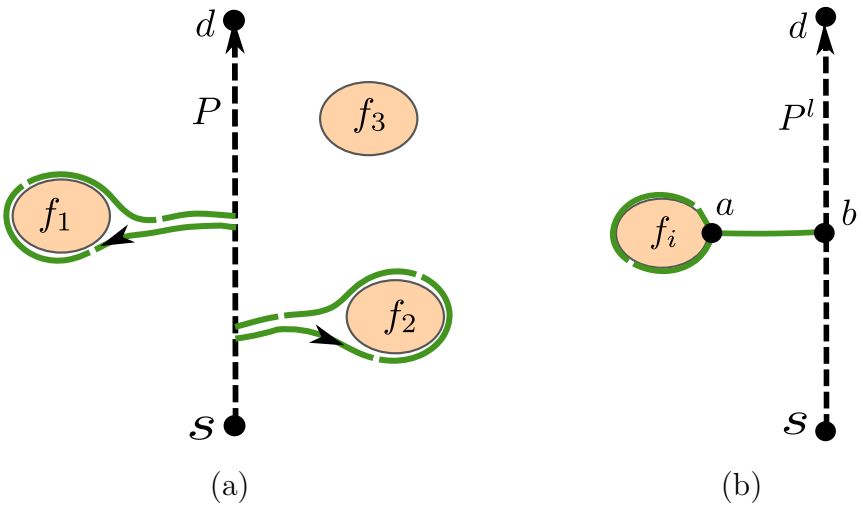

Figure 4.4: **(a)** Construction of homotopy equivalent path for desired signature value. **(b)** Realization of the idea by taking a path from the current path to the boundary of the obstacle.

4.5.4 Reconstructing traces from signatures

The following lemmas say that given a signature it is possible to check in polynomial time if such a trajectory exists, and if so it can be reconstructed up to homotopy equivalence in linear time.

Lemma 2. *Given a signature vector X, source s, and destination d; it is possible to find in linear time if there exists a homotopy class of simple paths going from s to d with the signature X.*

Proof. Consider the shortest path P from s to d as shown in Figure 4.4(a) and its signature $\theta(P)$. Using the result from Theorem 7, the only thing to test is if $(\theta_i(P) - X_i) \in \{0, 1, -1\}$ for all i. This can be done in linear time in the number of holes in the domain. □

Lemma 3. *Given signature vector X, source s, and destination d, there exists an algorithm to find a unique simple trajectory up to homotopy equivalence with signature X. The algorithm runs in linear time in the number of holes in the domain.*

Proof. A natural extension of Lemma 2 uniquely identifies the source faces f_i where we need to change the side by which P passes f_i – precisely where $(\theta_i(P) - X_i) \neq 0$. Next, these sources are fixed iteratively.

Initialize this process by setting the path P as the shortest path from s to d. Suppose at iteration l, the path is P^l and the next obstacle to fix is f_i. Consider an arbitrary node $b \in P^l$, and another arbitrary node $a \in \partial f_i$ as shown in Figure 4.4(b). Now P^{l+1} is the concatenation of the following path segments: s to b, b to a, a to a (along ∂f_i), a to b, and finally b to d. So, the path P^{l+1} has now right homotopy type w.r.t. f_i. □

This construction essentially determines the homotopy type from the signature. Given that, we can now compute a short path in that class using well known algorithms in computational geometry (Hershberger and Snoeyink, 1994a).

4.6 Applications and Optimizations

Here we discuss how the topological signatures can be designed and implemented for better applied analytics.

4.6.1 Nearest neighbor search and Locality Sensitive Hashing

A fundamental question in data analysis is the search for nearest neighbor, or k nearest neighbors, which forms the basis of several classification and clustering techniques and queries on noisy data. In case of trajectories, searching for nearest neighbors is expensive due to the fundamental cost of comparing two long trajectories (Alt and Godau, 1995).

Locality sensitive hashing (LSH) is used in data mining to accelerate the search for nearest neighbors. However, defining LSH for trajectories is a non trivial problem, as is constructing computationally efficient hash functions (Driemel and Silvestri, 2017). We want to instead use representations of trajectories as points in the Euclidean space, where good LSH techniques are known.

A standard LSH scheme (Datar et al., 2004) uses a hash function h constructed as follows. Select a random straight line in $\mathbb{R}^k$. Then project each data point linearly onto the line. Partition the line into segments of length w for some given w, and treat each segment as a "bucket". Nearby data points are likely to hash into the same bucket, while far apart points are likely to hash to different ones. Given a query point q, we can perform the same projection and hashing, and then search for its nearest neighbor in the bucket containing q. Expensive methods (Alt and Godau, 1995) can be used for this search since the pruned candidate set

is smaller. Repeating the process with multiple hash functions increases the probability to find the true nearest neighbor of q. Note that Euclidean hash is substantially more efficient than direct locality sensitive hashing of trajectories described in (Driemel and Silvestri, 2017; Indyk, 2002).

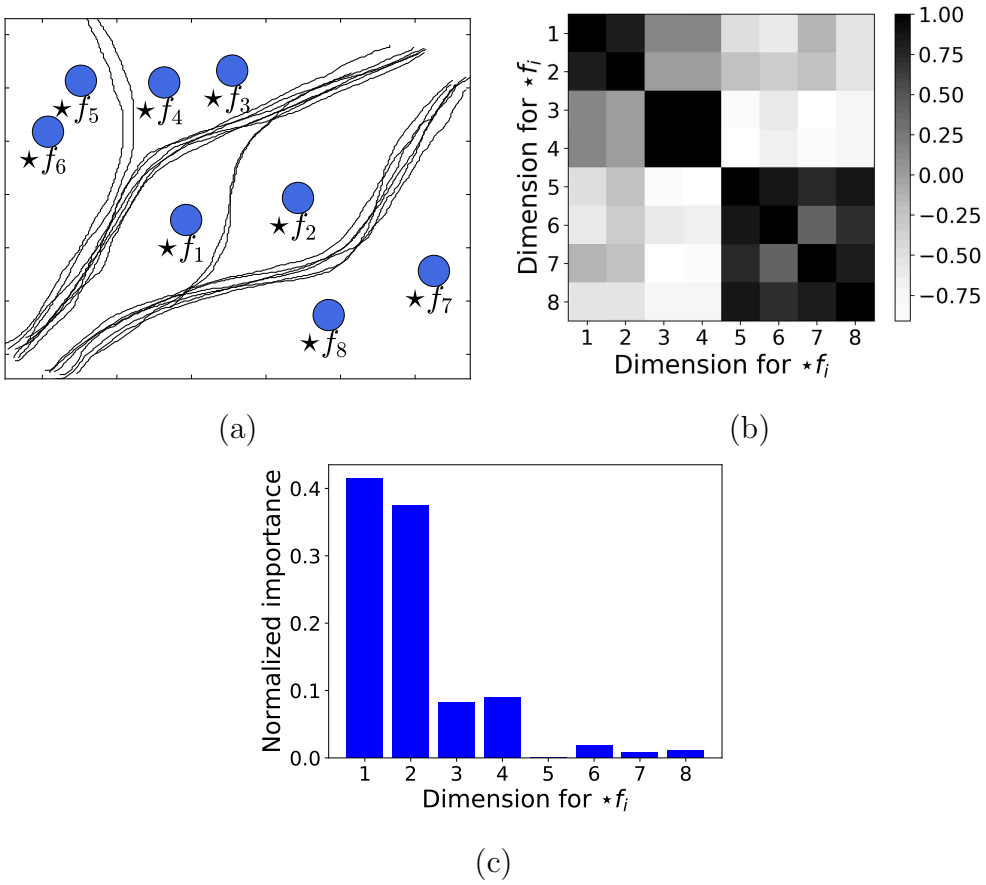

Figure 4.5: (a) Trajectory set with 8 obstacles. (b) Correlation matrix with respect to signatures of the trajectories. Darker shades imply higher correlation (c) PCA based importance ranking.

4.6.2 Predicting motion at large scales

Let us define motion prediction at scale r, where r is a given distance – e.g. 500 meters. We wish to ask where will a mobile object be, when it is at a distance r from its current location. Formally suppose o is the current location, C_r is the circle of radius r centered at o. Based on our mobility data, we can predict p on C_r as a point where the object's trajectory will exit (intersect) C_r.

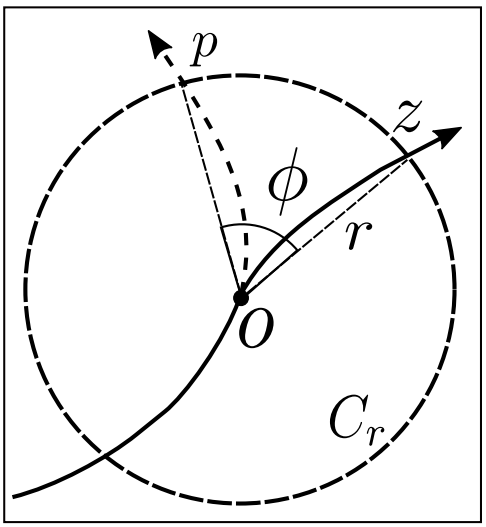

Figure 4.6: Given the history predict the next direction ϕ at current location p.

To measure the error in prediction, suppose the object actually exits the circle at point z. The prediction error is defined as the angle $\phi = \angle poz$. More accurately, it is $\min(|\phi|, |2\pi - \phi|)$. See Figure 4.6. Since the scale itself is given, the essential task here is to predict the right direction from o at scale r, which is represented as predicting the angle.

The motion prediction itself can proceed according to any machine learning method. Experiments in Section 4.7 demonstrate that standard prediction techniques based on k-nearest neighbors, linear regression, random forest, gradient boosting trees work well.

4.6.3 Dimension reduction, correlation and domain analysis

Given that the trajectories are now points in k dimensional Euclidean space given by $\theta(T)$, standard analytic techniques can be applied to better understand the trajectories, and to understand the underlying domain from the perspective of the given trajectories. We can ask, which obstacles are important, or which obstacles are similar with respect to actual mobility patterns?

Figure 4.5(a) shows a set of trajectories moving in the plane around obstacles $1, 2, \ldots, 8$. Clearly, there is a natural grouping of obstacles where obstacles 3 and 4 are similar in the sense that they act practically as a single obstacle, since every trace passes either to the right or left of both. The same holds for pairs $(5, 6)$ and $(7, 8)$. Obstacles $1, 2$ are also similar in the sense that most traces behave

similarly with respect to both, with only a few passing between them.

These intuitive results can be obtained from standard analytic and visualization methods. Figure 4.5(b) shows the correlation matrix of θ, where darker shades indicate higher correlation. The correlation lets us have a more abstract view of the domain, where related nearby holes can be viewed as one.

Techniques like Principal Component Analysis can be applied to the Euclidean data to determine which dimensions record larger variance – implying larger variability in how traces traverse the obstacles. We apply this idea to get the intuitive result in Figure 4.5(c) that obstacles 1 and 2 are clearly more significant than others as they split a large body of motions.

Greedy filtration of obstacles. A different strategy which is found effective in experiments, is to greedily select obstacles (dual sources) that maximize the accuracy for the task at hand.

For example, for nearest neighbor search, this accuracy can be defined as the fraction of times that the true Fréchet nearest neighbor is contained among the m nearest neighbors. The greedy strategy will iteratively select the obstacle that maximizes the total accuracy over all pairs, until it has selected some k obstacles. For scenarios with large number of obstacle, similar strategies can be implemented for distributed cluster computation (Mirzasoleiman et al., 2016). The benefit of this heavy computation is that the signatures become more compact and assuming the dataset is representative of typical motion, future computations of signatures, nearest neighbors, predictions etc will be more efficient.

4.6.4 Adaptive resolution signatures

It is natural to ask for representations that give greater weight to recent information and less weight to history, for example, for short term prediction. The signatures can be seamlessly adapted to achieve this using weighted averaging. Where for each edge traversed by the trajectory, we modify the update rule to be $\theta_i(T) = \beta.\theta_i(T) + (1-\beta)\xi_i(e)$ for a constant $\beta : 0 < \beta < 1$ that determines the weight of history in the signature.

In the example in Figure 4.7(a) at point o, the adaptively weighted signature finds the set γ to be currently more relevant to the query α.

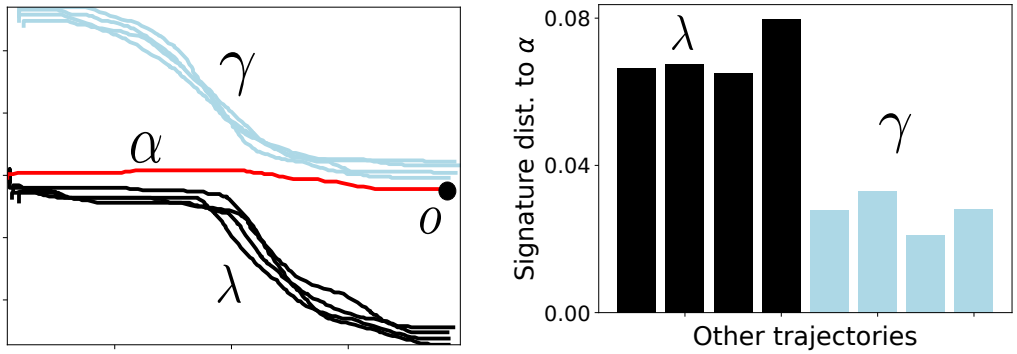

(a) (b)

Figure 4.7: **(a)** Trajectories flow left to right. (b) Distance of α's signature from others shows that in near future the set γ is more relevant than the set λ that have clearly diverged.

4.6.5 Composing signatures

The composability of differential forms means that a set of traces can be represented in the signature space as a linear combination of the constituent traces – such as the mean of all the signatures. This simplifies center computation by creating an abstract 'center' that is not a trajectory itself, but can be used to compare other trajectories to the given cluster or set.

4.6.6 Implementation in distributed and mobile setups

Mobile computers are a natural platform for application of trajectory signatures, with applications in social mobile networks, autonomous driving, etc. For large computers in automobiles, the differential forms can be pre-loaded into the memory, downloaded incrementally as required. In sensor or other dense network scenarios, the mobile device can obtain local values of ξ from nearby sensors and devices. The signature is computed and stored incrementally.

The knowledge of signatures allows mobile entities to exchange data with other nearby ones and predict which ones are likely to have similar behavior. This is useful, for example, in autonomous vehicles and delay tolerant networks.

The above constructions of differential forms are all naturally implementable in distributed scenarios like sensor networks. For example, consider a Voronoi diagram of sensors where they can detect the direction and identity of the objects crossing the edges of the voronoi graph, as used in (Sarkar and Gao, 2013). The

sensors maintain the weights on the edges giving the differential forms and as an object moves between cells, its signature is handed off (similar to hand-off in cellular network) to the successive sensor. An alternative approach could be for the sensors to record and store the edge crossings of mobile objects, and compute the signature on demand by summing along the handoff path.

4.7 Experiments

In this section, we show experimental evidence that the topological signatures simplify the representation of trajectories and also perform well in clustering, prediction, and other tasks. The main observations are:

- Nearest neighbor of a query trajectory according to Fréchet distance can be found efficiently using fast Locality Sensitive Hashing and pruning on topological signatures.
- Motion prediction of trajectories is accurate and efficient. It achieves similar accuracy as Long Short Term Memory neural networks (henceforth LSTM), but provides much faster training and query time. Prediction results are verified using two real mobility datasets.
- Greedy source selection reduces dimension to get compact signatures, with minimal loss in quality of analytic results.
- Popular paths or paths with the most number of trajectories in a given region can be estimated by kernel density estimation on signatures.
- Topological signature based method is robust to sparse, noisy trajectories; it can predict future direction of mobile objects accurately in trajectories with many missing data points.

4.7.1 Experimental setup

Datasets. We use two publicly available datasets: Rome Taxi dataset (Bracciale et al., 2014) and Porto Dataset[1]. While the former has trajectories of 320 taxis

[1]https://www.kaggle.com/c/pkdd-15-predict-taxi-service-trajectory-i

for a month in Rome, Italy; the latter has trip partitioned trajectories of 442 taxis for one and half years in Porto, Portugal.

Constructing planar graph. The Delaunay triangulation (Edelsbrunner and Harer, 2010) of 20000 random points in the plane make the planar graph G. Each GPS point of a trajectory is mapped to its nearest node in G and connecting them by the shortest path in the graph produces its representation in G.

Identifying obstacles. All faces in G where less than a predefined threshold number of trajectories pass a boundary edge are considered as obstacles. E.g, the portion of Rome dataset in Figure 4.8(a) has 67 such obstacles with threshold 2. In Porto dataset (Figure 4.12(a)), we choose 30 largest regions of low trajectory density as obstacles.

Constructing differential forms. Dual paths along linear rays with random slopes from each obstacle yields the differential forms (Section 4.5.2). E.g, in both Figure 4.8(a) and Figure 4.12(a) 20 dual paths each with weight 0.05 are constructed from each obstacle.

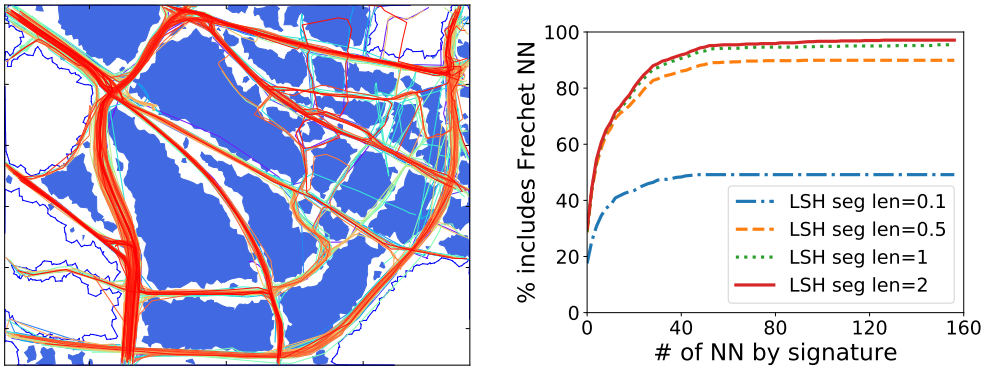

(a) (b)

Figure 4.8: **(a)** A region (latitude$-[41.8708°N, 41.8826°N]$ and longitude$-[12.4919°E, 12.5089°E]$) of size roughly $1km \times 1km$ from Rome taxi dataset with 1189 sub-trajectories. We detect 67 internal holes (shaded) using trajectory density threshold as 2.**(b)** CDF of percentage of times the nearest neighbor is included in the approximate k nearest neighbors (x-axis) found using Locality Sensitive Hashing based on topological signatures. With suitable segment length, Locality Sensitive Hashing can reliably approximate k nearest neighbors to find Fréchet based nearest neighbor.

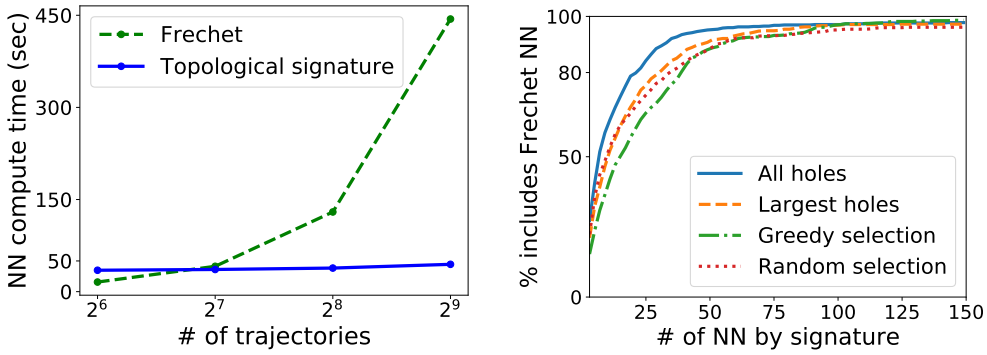

(a) (b)

Figure 4.9: **(a)** Time to run naive Fréchet increases super linearly when increasing the size of the dataset whereas topological signature method consumes very little time in comparison. **(b)** k nearest neighbor query accuracy with 5 obstacles selected using different source selection strategies.

4.7.2 Nearest neighbor search

Fréchet nearest neighbor of a query trajectory is approximated by the pruning based on LSH with trajectory signatures using independently chosen 3 sets of 5 linear projection hash functions. This experiment uses each trajectory in Figure 4.8(a) as a query trajectory in turn.

Figure 4.8(b) confirms that with high probability, Fréchet nearest neighbor is included in the approximate k nearest neighbors found by LSH. Larger bucket size naturally yields better accuracy and offers standard accuracy and efficiency trade-off of LSH.

In efficiency, even including preprocessing time to construct planar graph (15.9 sec), differential forms (20.5 sec), and computing signatures (varies with dataset size), this method greatly outperforms basic Fréchet based method of computing distance to all trajectories (Figure 4.9(a)). The Euclidean distance measure is faster than Fréchet and LSH based pruning makes a query even faster. Fréchet distance is computed using MDA tool (mda, 2017). The experiments are run on a typical desktop machine with 8 GB primary memory and Intel $i5$ processor.

4.7.3 Clustering and estimating density

The signatures are useful to cluster trajectories. Figure 4.10 shows a small example with 66 trajectories. The varied types of trajectories are well separated even

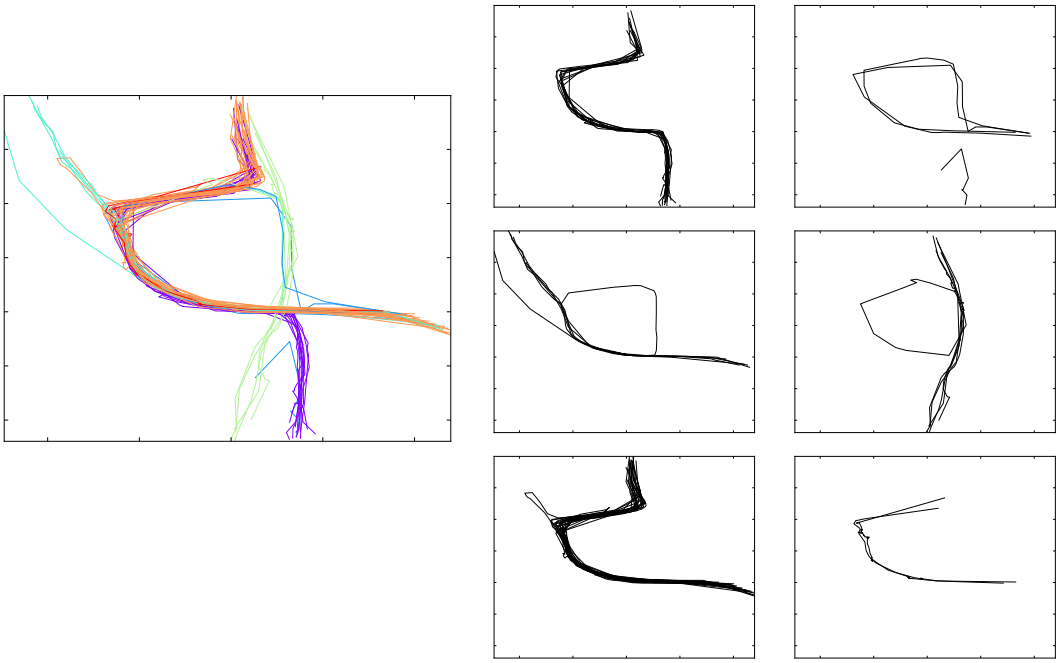

Figure 4.10: Clustering 66 trajectories from Rome taxi dataset using DBSCAN clustering algorithm with neighborhood distance parameter set as 0.25 and minimum samples to form a cluster is set as 2. To construct the triangulation, 20000 random points are used, Sources are placed based on the trajectory density threshold as 2.

if they have large portion of overlapping pattern.

High density regions in the signature space correspond to popular topological types of trajectories. The popular bidirectional traffic flow in Figure 4.11(a) is neatly identifiable in the estimated density using Gaussian Kernel in Figure 4.11(b). Clustering can also be applied to anonymize personal data (Zeng et al., 2017).

4.7.4 Motion prediction

Figure 4.8(a) and Figure 4.12(a) show the datasets from Rome and Porto respectively used in prediction experiments. With randomly chosen 90% trajectories as training, we predict direction ϕ for different scales r on each test trajectory where current location o is randomly chosen from middle 1/3rd of its length. The prediction error is measured as described in Section 4.6.2.

Using topological signatures, next direction is predicted as the mean direction ϕ of k nearest training trajectories that pass within 20 meters of o. The nearest neighbors are computed using kd-tree on the space of signatures with the

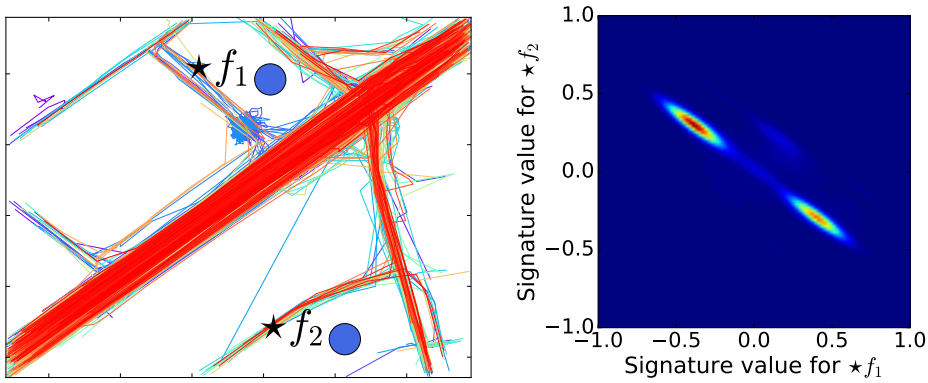

(a) (b)

Figure 4.11: Detecting popular topological types using kernel density estimate of the trajectory signatures. **(a)** Portion of trajectories from (Bracciale et al., 2014) with 1809 trajectories (area $1km \times 1km$). The busiest road in this map is easily visible. Two signature sources are manually placed in the map. **(b)** Two hotspots in the kernel density estimate denotes the two way traffic on the busy road.

training trajectory segments ending near o. In both Porto and Rome datasets, our method attains high accuracy even with small number of nearest neighbors (Figure 4.12(b)) and large prediction radius (Figure 4.13).

As a benchmark we use neural networks with LSTM as regressors (Gers et al., 2000) to predict ϕ, given equi-spaced 20 locations on the trajectory between o and start of the trajectory. Each model has two layers of 20 LSTM cells followed by a fully connected layer with 100 rectified linear units. With a squared error loss function we train these models with a variant of stochastic gradient descent for 50 epochs using a batch size of 32 with the standard optimizer settings (Diederik P. Kingma, 2015). Figure 4.14(a) shows that simple k-NN on topological signatures achieve similar accuracy as LSTM, implying that the topological signatures in fact encode the critical intrinsic features that determine motion.

Figure 4.15 shows that topological signature based prediction is more efficient than LSTM in terms of both preprocessing and query time. Before answering queries, whereas our method requires to setup planar graph, identify obstacles, and create differential forms; LSTM requires data preprocessing and training. Although our method needs to find k nearest neighbors at query time, it offers faster query than LSTM. We use TensorFlow for implementing the LSTM (Abadi et al., 2016). All experiments are run on a typical desktop machine with 8 GB

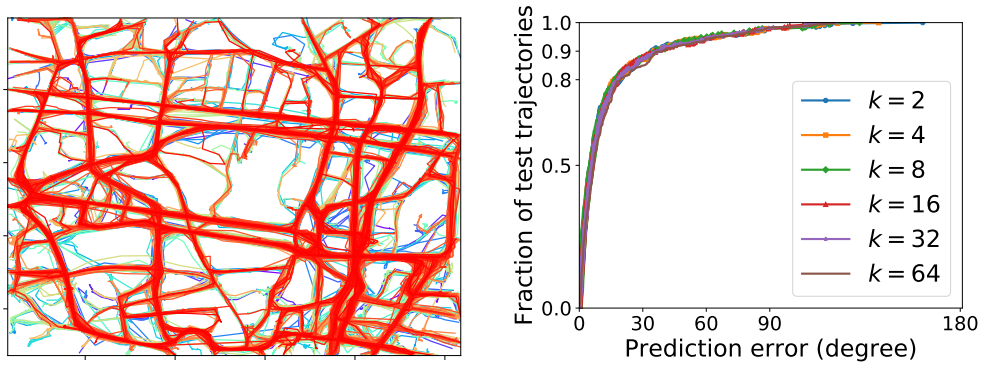

(a) (b)

Figure 4.12: **(a)** A region latitude–$[41.1468°N, 41.1699°N]$ and longitude–$[8.62931°W, 8.60411°W]$ of size $2.5Km \times 2.1Km$ from Porto dataset with 3952 trajectories. Among 101 regions with low trajectory density (threshold 2), we consider largest 30 to be obstacles. **(b)** In Porto dataset, topological signature based method accurately predicts next direction even with small number of nearest neighbors. Here, $r = 100$ meters.

primary memory and Intel $i5$ processor. Note that with increasing dataset size, the number of queries also increase as we randomly choose 10% of the trajectories in the dataset as test data. Figure 4.15(b) shows that with increasing number of queries, the query time for our topological signature based method increases linearly whereas the LSTM based method needs super-linear query time.

Popular regression techniques, Random Forest, Gradient Boosting Trees, and Linear Regression also predict ϕ well given the current location o and topological signature of trajectory segments ending at o. High prediction accuracy of these methods in Figure 4.14(b) suggests that using topological signatures, the plethora of knowledge about these well studied methods can now be leveraged for trajectories and mobility analysis.

4.7.5 Signature source selection

In domains with large number of obstacles, the signatures will have correspondingly large size, losing the benefits of compact representation. We found that in practice, differential forms with respect to a small number of sources suffice to accurately capture the motion.

Figure 4.9(b) compares different signature source selection strategies in Rome

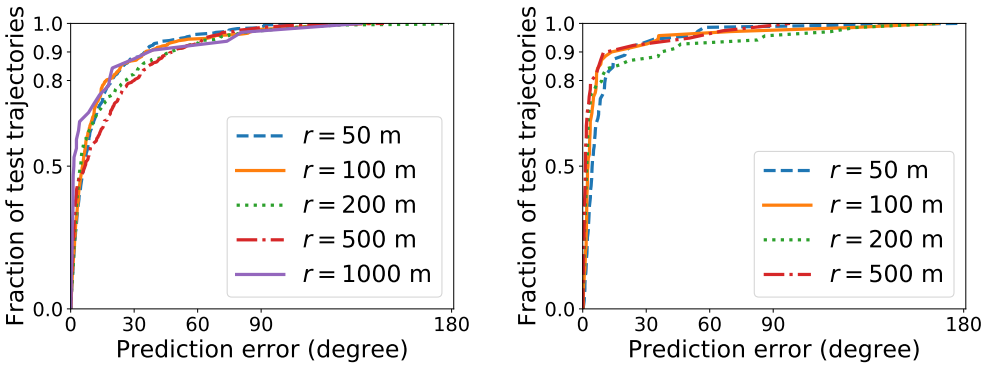

(a) (b)

Figure 4.13: Topological signature based method can accurately predict next direction even for large r in **(a)** Porto dataset and in **(b)** Rome dataset. Here, $k = 4$ neighbors.

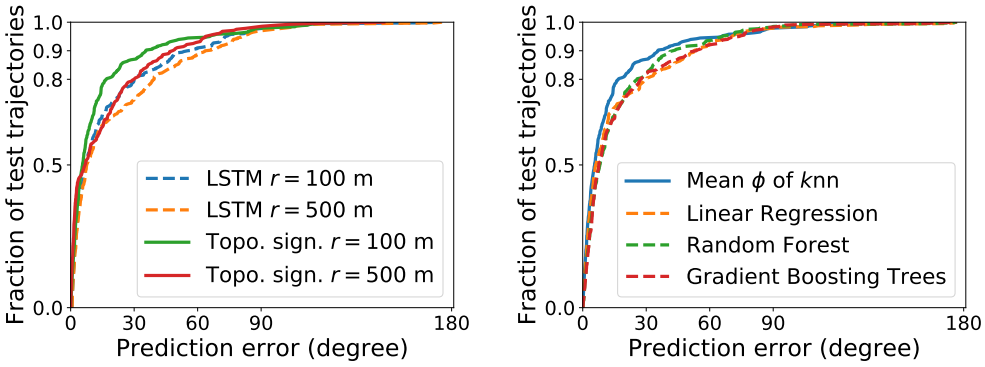

(a) (b)

Figure 4.14: **(a)** Topological signature based method attains similar accuracy as LSTM. **(b)** Popular regression methods using topological signatures achieve similar high accuracy.

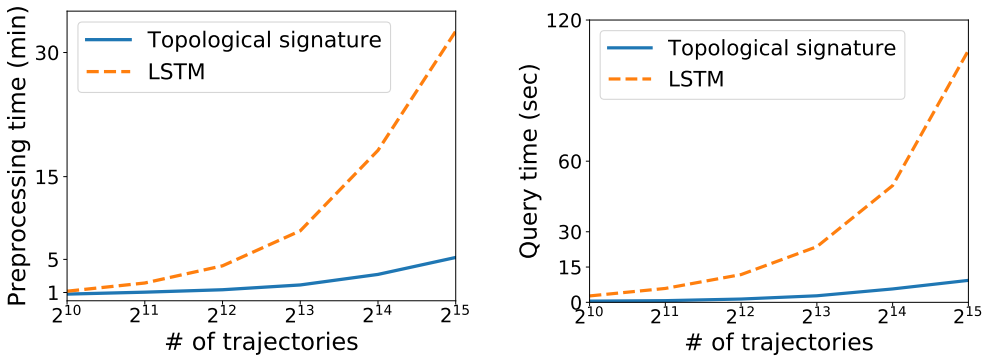

Figure 4.15: **(a)** Preprocessing and **(b)** query time. Both increase slowly for topological signature based method compared to LSTM, with dataset size.

dataset from Figure 4.8(a); different strategies can select small number of signature sources to attain high nearest neighbor query accuracy. Specifically, this experiment compares the following strategies: *i*) all faces in G with low trajectory density (holes) are signature sources, *ii*) k largest holes, *iii*) greedy selection as described in Section 4.6, and *iv*) randomly choose k sources from all faces in G. This result demonstrates that trajectories in a complex domain can be represented by simple low dimensional topological signatures.

In this experiment, we describe an important insight into the strategy to reduce the dimensionality of the signatures and thus the computational cost of our framework and further learning systems. In the Figure 4.9(b) we see that considering all holes naturally gives highest accuracy. Interestingly, the accuracy is almost preserved if only 5 randomly chosen obstacles are kept out of 66 obstacles. This enables an application developer to increase the efficiency of the system by choosing suitable trade-off between accuracy and efficiency.

4.7.6 Robustness to sparsity

Mobility traces differ in sparsity of constituent entities due to varied location sampling frequency. In this experiment, the dense GPS traces are made sparse by randomly retaining location points at fixed rates. The Figure 4.16 shows that our method can accurately predict motion in trajectories with missing locations.

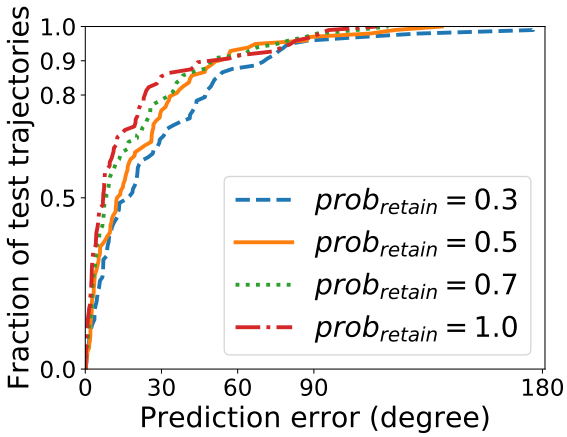

Figure 4.16: Predicting locations with sparse trajectories: Each location point is retained with certain probability in each trajectory. Our method achieves high prediction accuracy even with sparse trajectory.

Chapter 5

Publishing Differentially Private Spatial Data From Distributed Sensors

This chapter focuses on publishing sanitized location stamps of independent events recorded by spatially distributed sensors. We design differential privacy mechanisms for two scenarios, to protect accurate locations of the events and their occurrences. Proposed mechanisms are based on location displacement and inclusion of fake events. They are designed to maintain a balance between privacy and utility for spatial range queries. Our algorithms allow distributed operation and maintains utility for any number of queries.

Previously in Chapter 3 we discussed how to protect event timings in a time series. Here, we do not consider the temporal attributes in the events and describe how to protect privacy for their spatial attributes. All these mechanisms can be augmented with the algorithms in Chapter 3 to attain privacy for spatiotemporal range queries.

5.1 Introduction

Here, we are concerned about the data collected by distributed sensors. Examples of such data include location snapshots of a population, events detected by traffic sensors, occupancy and motion sensing information etc. After the collection, events are delivered to the aggregator services, where they are subject to queries and analysis by users of the service. In the process, implicit sensitive information

can leak or be inferred in spite of best intentions and security. In some cases, users of the service may be malicious and aim to find information not intended to be disclosed. Therefore, in this chapter, we propose mechanisms to protect privacy of spatial attributes, especially we consider statistical guarantees in privacy and utility in publishing such sensor data to an aggregator and performing counting range queries.

We discuss two types of privacy to sanitize spatial attributes. First, we hide the accurate location of an event. Suppose, the adversary has the prior knowledge that an event had occurred and has a rough idea of where the event could have happened. Using spatial attributes of the published events, he will try to localize the event location with more accuracy. Our claim in this setting is that, with the proposed privacy preserving publishing algorithm, the adversary will not be able to localize any event location with vulnerable accuracy. Further, consider a setting where the adversary knows the location where an event could have happened and wants to know if the event had occurred there in the first place. So, we propose sanitization algorithms to hide occurrence of any event in the database.

Most of the current differential privacy mechanisms consider the centralized setting when all data is placed in a secure database which supports interactive queries to the database. Before the query result is returned to the proposer, noise is carefully introduced to protect user privacy. This framework faces challenges in spatial sensing setting. It is unclear if we can always assume a trusted aggregator or a trusted communication channel. It is highly desirable that data is sanitized close to the source, before it reaches an untrusted medium. However, since the answer to a query can be a function of data from multiple sensors, a local mechanism is required in coordinating the privacy mechanism employed by the sensors. Therefore, we develop differential privacy schemes with these models and considerations in mind.

In Subsection 5.4.1, we show a method for achieving differential privacy of localized events by means of collaboration between sensors. In this case, the spatial privacy of events is achieved by sending them on a random walk of W steps for a given constant W, where the final sensor on the walk claims the event as its own. This method is shown to achieve (ε, δ)-differential privacy, if we choose W as a function of ε, δ. See Figure 5.1. This approach makes it difficult for either the aggregator or even a wireless snooping adversary to localize the real event

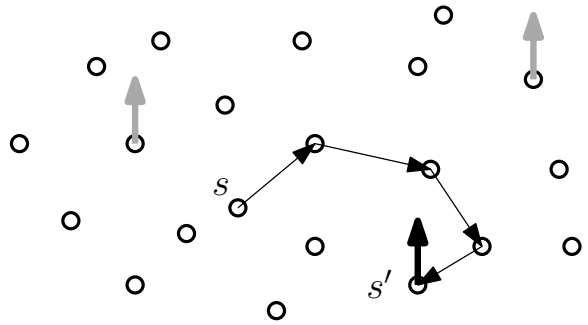

Figure 5.1: To avoid the aggregator/collector knowing the location of the sensor generating the event, the source s uses a random walk to send the message to a node s' who delivers to the aggregator instead. The nodes in the network might also report fake events as shown in gray arrows.

source. From system perspective, this mechanism protects against untrusted aggregator but needs the inter-sensor communication channel to be trusted.

When the inter-sensor communication is also vulnerable then it is difficult to apply the above random walk mechanism. Here, we develop a mechanism involving a stream of spurious, or fake events introduced from a Poisson process with a rate λ dependent on the privacy requirement. This mechanism is an extension of the fake event augmentation mechanism discussed in Chapter 3 in $2D$ spatial dimension. This approach is proved to provide differential privacy of counting range queries for $\lambda = O\left(\frac{1}{\varepsilon^2}\log\frac{1}{\delta}\right)$, while providing accurate results. One nice property is that the intensity magnitude λ of the added noise is only relevant to the privacy guarantee and the absolute error in data utility, and is independent of the real event distribution.

In Section 5.5, we experimentally compare the utility of our algorithms against the local privacy mechanism proposed in (Chan et al., 2011). Although the method was developed for $1D$ temporal sequences, we extend it to $2D$ spatial range queries for our purposes in Subsection 5.4.3. However, this mechanism is not suitable for publishing data. We use a real world dataset of geo-located tweets in and around London. Experiments show that our approaches provide accurate results for range queries in all cases.

In the following, we first discuss the existing research results in Section 5.2, background material and models in Section 5.3 before moving on to the algorithms.

5.2 Related Work

Differential privacy was first proposed in (Dwork et al., 2006), where user data are collected by a trusted aggregator and Laplace noise are added before the aggregator releases the data to achieve differential privacy. After that, there has been a plethora of works on releasing different types of data under differential privacy.

(Andrés et al., 2013) introduced geo-indistinguishability, a generalized version of differential privacy for location information, where using planar Laplace noise, any two locations within a given distance produce observations with similar distributions. Differentially private data aggregation in crowd sensing system is analyzed in (Jin et al., 2016; Yang et al., 2018).

Spatial decomposition under differential privacy. (Cormode et al., 2012) proposed a geometric budget strategy, adding noise with geometric distribution at each level of quad-tree for private spatial range queries. If h is the height of the tree (leaves are on level 0), then $Lap(\varepsilon_i)$ noise is added to the true count of each quad-cell on level i, where $\varepsilon_i = 2^{(h-i)/3}\frac{\sqrt[3]{2}-1}{2^{(h+1)/3}-1}$. The upper bound for the variance of a range query is $2^{h+7}/\varepsilon^2$. (Qardaji et al., 2013) analyzed query errors on uniform grids, which consists of two sources of errors. One is the error is introduced by adding random noise from Laplace distribution, and the other from the assumption that the data points are distributed uniformly in a cell.

If there are N points and the domain is partitioned into a $m \times m$ uniform grid, the error, determined by standard deviation, is $\sqrt{2r}m/\varepsilon + \sqrt{r}N/mc_0$, where r is the ratio of the area of the query over the whole domain, c_0 is constant. To minimize the error, $m = O(\sqrt{N\varepsilon})$ is suggested. They further proposed an adaptive grids methods to adjust the size of the grids considering the density of data. Further works on uniform grids can also be found in (Wang et al., 2018).

Local differential privacy. Most works under differential privacy are in the setting of central model, where a trusted aggregator is present. In the notion of local differential privacy, first proposed by (Kasiviswanathan et al., 2011), data sources sanitize their own data with differential privacy mechanism before sharing with the aggregator. It is widely adopted, for example in (Erlingsson et al., 2014; Bittau et al., 2017). However, the partial sum mechanism does not suit our purpose of data publishing as the amount of noise is decided based on the query.

5.3 Models and problem descriptions

5.3.1 System Model

The typical entities in a distributed sensing scenario are:

- *Sensors*: A sensor detects events generated in the physical environment. This detection could be through wireless connectivity, from visual sensing, or other sensing modalities. We assume that the sensors detecting the events are connected by suitable communication technology.

- *Aggregators*: an aggregator is a service provider who collects data from the sensors and responds to an aggregation query, such as a range counting query – report the number of events that happened within a geographical domain.

- *Query makers*: A user can issue queries to the aggregator to infer knowledge about the event counts and patterns.

In a typical setup, data from sensors are sent to the aggregator. The query maker then queries the aggregator to obtain information. The data that the sensors transmit can be raw data, or aggregated ones. Depending on the trustworthiness of the aggregator or communication channels, the sensors may need to sanitize data before transmission.

5.3.2 Trust Model

Depending on the applications, there could be different levels of trust between the entities:

- *Trusted aggregator.* The most trusted scenario, where the aggregators and all communications upto them are trusted and secure. This is closest to the common differential privacy model, where only the query maker is untrusted, and the aggregator can perform centralized computations on collected data. We do not design algorithms for this setting in this chapter, but we compare with solutions of this setting in the evaluation section.

- *Trusted sensors.* In this model, the sensors trust each other, but not the aggregator or the communication channel to the aggregator. As a result,

query results sent to the aggregator must be sanitized. However, the sensors are allowed to perform in-network computations and apply sanitization to partial results. Section 5.4.1 discusses a privacy mechanism suitable for this setting.

In this setting, we assume that the sensors are aware of other nearby sensors in the system, can send encrypted messages to each other, and a routing mechanism for inter-sensor communication is present.

- *Untrusted sensors.* Where the sensors, or communication between them, are not trusted. Any data going out of a sensor must be sanitized. Section 5.4.2 addresses privacy concerns in this setting.

5.3.3 Distributed Event Model

We consider a bounded domain with a set S of stationary check points or sensors that monitor and collect events. For any event e, we write $L(e)$ for the location of the event. Depending on the setup, the location may be an arbitrary location in the plane (e.g. location of an accident), or they may be location of the sensor s that detected the event, if finer localization is not required. Our algorithm in Section 5.4.2 is designed for the former setup, and the algorithm in Section 5.4.1 considers the later.

The location attributes of the events can be modeled as a point process, a special case of which is when the events are independent, i.e., the Poisson process. More generally, the events may not have a uniform rate at all locations. This is captured by a *non-homogeneous* Poisson process.

We skip the definitions of variety of Poisson processes here as they are discussed in Chapter 3. A sequence of random events at a sensor follows a Poisson distribution with only temporal attribute. The location of events in any subset of the geographical domain follows a Poisson distribution in $2D$, while in the spatiotemporal events will follow a Poisson distribution in $3D$.

5.3.4 Privacy and Utility Models

To elaborate the challenges of this problem, consider existing solutions for protecting data privacy. First, any cryptography based solutions that encrypt the message content cannot help with protecting the location of the events directly.

For example, an adversary can know the location of an event by snooping the vulnerable communication medium. Second, we may consider limiting the location resolution of the reports. However, it is difficult to decide the resolution and shape of discretization and this introduces inaccuracy in the analysis. Therefore, we rigorously define the protection on spatial attributes in terms of differential privacy, which requires revision and adaptation of the differential privacy definitions.

We measure the utility of the data using counting range queries because they are fundamental in many machine learning and data mining algorithms. This chapter considers axis aligned rectangular range queries as defined below.

Definition 5 (Range query $Q(R)$)**.** *Given a rectangular range* $R = [x_1, x_2] \times [y_1, y_2]$*, report the number of events in the range:* $|\{e : L(e) \in R|$.

We have discussed the background of differential privacy in Chapter 3 and therefore skip it here. Both the mechanisms proposed in the following sections publish the event location stamps.

5.4 Algorithms

5.4.1 Location Privacy using Random Walks

Here, we obfuscate the accurate location of an event by attributing the event to a different sensor location than the one that recorded it. We get this spurious location via a random walk on the sensor network.

Let $\mathcal{D}$ be a collection of datasets of events. The spatial data publication process of events is a function, $g : \mathcal{D} \to (\mathbb{R} \times \mathbb{R})^{\mathbb{N}}$, that takes a dataset of events as input and outputs their sanitized locations.

Definition 6 (Spatial neighboring datasets)**.** *Let* $D, D' \in \mathcal{D}$*,* $L = g(D), L' = g(D')$*.* D, D' *are spatial neighboring datasets, if all pairs of locations in* L *and* L' *are the same, except one pair* $\ell \in L$ *and* $\ell' \in L'$*, that* $\ell \neq \ell'$ *and* $||\ell - \ell'||_1 \leq \Delta$ *for a suitable privacy parameter* $\Delta > 0$*.*

We assume that the location of an event is known to the nearby sensor detecting the event. For simplicity, let us consider sensors on a grid. In a real network, such grids can be simulated as a virtual grid, where each virtual node is managed by the sensor whose sensing range covers the location of the virtual node.

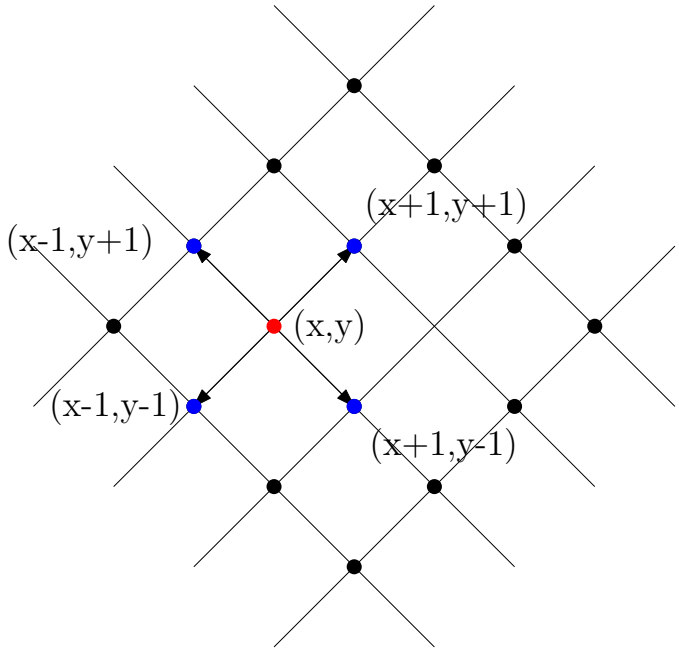

Figure 5.2: A sensor located at (x, y) (red) sends the event to one of its four neighbors (blue).

The algorithm works as follows: When a sensor detects an event, it does not directly report to the aggregator, but randomly sends a message describing the event to one of its neighboring sensors, with a TTL (time-to-live value) set to W. The neighboring sensor decrements the TTL and forwards the message to a random neighbor again. The sensor that receives the message with TTL $= 0$ sends the message to the aggregator with its own location.

Let us take the grid as shown in Figure 5.2. A sensor with coordinate (x, y) has four neighbors located at $(x + 1, y + 1), (x + 1, y - 1), (x - 1, y + 1)$, and $(x - 1, y - 1)$. When a sensor detects an event, it chooses one from the neighbors with equal probability to forward the event. This process can be viewed as making two independent random moves along x and y axes, resulting in two independent random walks on horizontal and vertical coordinates.

Let us consider the walk on the x coordinate. Assume that a random walk starts at x, and let $X_i \in \{-1, +1\}$ denote the movement of step i. After W steps, the position $S_W = \sum_1^W X_i$, S_W follows a binomial distribution, $E(S_W) = 0$, $\mathrm{Var}(S_W) = W$. With Chebyshevs inequality, $\Pr[|S_W - E(S_W)| \geq Q] \leq \frac{\mathrm{Var}(S_W)}{Q^2}$, we have the following lemma.

Lemma 4. $\Pr[|S_W| \geq Q] \leq \frac{W}{Q^2}$.

To establish differential privacy, we consider the probability that walks orig-

inating at two different sensors terminate at the same sensor. Notice that only sensors that are even steps away can come to the same position after W steps. We can make each sensor move W or $W+1$ steps with half chance.

Theorem 8. *The random walk mechanism achieves* (ε, δ)*-differential privacy for* $W \geq \frac{1}{\delta}\left(\frac{\Delta}{\varepsilon}+1\right)^2$.

Proof. We have two spatial neighboring data sets D, D'; $L = g(D), L' = g(D')$. For the only different pair $\ell = (x, y) \in L$ and $\ell' = (x', y') \in L'$, $||\ell - \ell'||_1 \leq \Delta$. Therefore, $||x - x'||_1 \leq \Delta$, $||y - y'||_1 \leq \Delta$. Since the horizontal random walk is independent, now we just focus on the horizontal one.

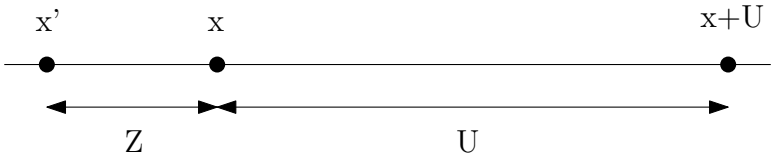

Figure 5.3: Two random walks starting at x, x' with distance Z, after W steps, stop at the same position $x + U$.

Assume $x > x'$, $x - x' = Z$. Now we analyze the probability that the random walks starting from x and x' both arrive at $x+U$ after W steps, shown in Figure 5.3, denoted as $\Pr[x+U \mid x]$ and $\Pr[x+U \mid x']$, where $U = \sqrt{\frac{W}{\delta}} - \Delta$. In Lemma 4, let $Q = U + \Delta$, we have

$$\Pr[|S_W| \geq U + \Delta] \leq \frac{W}{(U+\Delta)^2} = \delta.$$

That is, with probability $1 - \delta$, the horizontal shift of the random walk starting from both x and x' after W steps are within $U+\Delta$. We also have $W \geq \frac{1}{\delta}(\frac{\Delta}{\varepsilon}+1)^2 \geq \frac{1}{\delta}(\frac{2}{\exp(\frac{2\varepsilon}{\Delta})-1}+1)^2$, since $\exp(x) \geq 1 + x$.

$$\begin{aligned}
\frac{\Pr[x+U \mid x]}{\Pr[x+U \mid x']} &= \frac{\binom{W}{\frac{W+U}{2}}(\frac{1}{2})^W}{\binom{W}{\frac{W+U+Z}{2}}(\frac{1}{2})^W} = \frac{\frac{W!}{(\frac{W+U}{2})!(W-\frac{W+U}{2})!}}{\frac{W!}{(\frac{W+U+Z}{2})!(W-\frac{W+U+Z}{2})!}} \\
&= \prod_{i=0}^{\frac{Z}{2}-1} \frac{\frac{W+U+Z}{2}-i}{\frac{W-U}{2}-i} \leq \left(\frac{W+U+Z}{W-U-Z}\right)^{\frac{Z}{2}} \leq \left(\frac{W+U+\Delta}{W-U-\Delta}\right)^{\frac{\Delta}{2}} \\
&= \left(\frac{W+\sqrt{\frac{W}{\delta}}}{W-\sqrt{\frac{W}{\delta}}}\right)^{\frac{\Delta}{2}} \leq \left(\frac{\frac{1}{\delta}(\frac{2}{\exp(\frac{2\varepsilon}{\Delta})-1}+1)^2 + \frac{1}{\delta}(\frac{2}{\exp(\frac{2\varepsilon}{\Delta})-1}+1)}{\frac{1}{\delta}(\frac{2}{\exp(\frac{2\varepsilon}{\Delta})-1}+1)^2 - \frac{1}{\delta}(\frac{2}{\exp(\frac{2\varepsilon}{\Delta})-1}+1)}\right)^{\frac{\Delta}{2}} \\
&= \left(\frac{\frac{2}{\exp(\frac{2\varepsilon}{\Delta})-1}+2}{\frac{2}{\exp(\frac{2\varepsilon}{\Delta})-1}}\right)^{\frac{\Delta}{2}} = \exp(\varepsilon)
\end{aligned}$$

Therefore, the random walk mechanism in one dimension achieves (ε, δ)-differential privacy. Since the random walk on horizontal and vertical directions are independent, we conclude that the random walk on two dimension grids also achieves (ε, δ)-differential privacy.

□

The following lemma shows that the displacement to an event's location due to the random walk is bounded, and therefore, the spatial perturbation process does not significantly change the event distribution.

Lemma 5. *When achieving (ε, δ)-differential privacy, with probability $1-\delta$, after W steps, the Euclidean distance between the sensor reporting to the message and the original sensor detecting the event is at most $\frac{\sqrt{2}}{\delta}\left(\frac{\Delta}{\varepsilon}+1\right)$.*

Proof. In the proof of theorem 8, for the random walk on one dimension, if $W \geq \frac{1}{\delta}\left(\frac{\Delta}{\varepsilon}+1\right)^2$, we have $|S_W|$ satisfies,

$$|S_W| \leq \sqrt{\frac{W}{\delta}} \leq \frac{1}{\delta}\left(\frac{\Delta}{\varepsilon}+1\right).$$

Therefore, the euclidean distance for the random walk in two dimension is at most $\frac{\sqrt{2}}{\delta}\left(\frac{\Delta}{\varepsilon}+1\right)$. □

The random walk mechanism, in addition to perturbing the events to a suitable distribution, has additional privacy properties. In Scenarios where an adversary can sense transmissions from sensors, such random walks generated by many sensors can help to obscure the source of events, particularly when mixed with activities of fake events described in the next section. Such mixing methods are used in the TOR network and known to effectively obscure message sources(Piotrowska et al., 2017).

The results for homogeneous temporal and spatial Poisson processes in this section can be applied to non-homogeneous Poisson processes by changing the sensitivity according to the intensity function, and operating according to the local intensity value.

5.4.2 Poisson Process for Event Privacy

For the setting where the sensors can not trust each other, the above method do not apply. Here, we model the real event sequence by a non-homogeneous

Poisson process with spatial intensity function $\lambda(\Sigma)$, where Σ are the parameters for space. This model closely relate to the privacy preserving method presented in Section 3.5.2. Events there follow a non-homogeneous Poisson process with a one dimensional intensity function.

To protect the occurrence of a single event using differential privacy, the following algorithm, $\mathcal{A}_D(R)$, is designed. Here, D is the input dataset and $R \subseteq \mathbb{R}^2$ denotes the domain range. Augment D with N' fake events uniformly distributed over the domain where N' follows a Poisson distribution with intensity function $\lambda(\Sigma)$. Then given a range R, the algorithm $A_D(R)$ outputs the total number of events (real and fake) inside the range, R.

We first prove that the above algorithm satisfies differential privacy.

Theorem 9. *$\mathcal{A}_D(R)$ is (ε, δ)-differentially private, when $\Lambda = O\left(\frac{1}{\varepsilon^2}\log\frac{1}{\delta}\right)$, where Λ denotes the integrated intensity over the range, R, i.e., $\Lambda = \int_R \lambda(s)ds$.*

Proof. For simplicity of the proof, let's consider one dimensional data along real line $\mathbb{R}$. Note that the below argument hold for two dimensional space as the Poisson process is trivially extended to two dimension considering a two dimensional intensity function.

Consider two neighboring datasets D and D' (one dimensional data). Without loss of generality, assume that D has one additional event at τ. Now, any query range not containing τ have the same probability for all the outputs given the input datasets D and D'.

Now, consider a query interval, I, containing τ. To have the same outputs given input D and D', $A_{D'}$ need to introduce one more fake event than A_D. Therefore,

$$\frac{\Pr[\mathcal{A}_D(I) = N]}{\Pr[\mathcal{A}_{D'}(I) = N]} = \frac{\exp\left(-\Lambda\frac{(\Lambda)^{N'}}{N'!}\right)}{\exp\left(-\Lambda\frac{(\Lambda)^{N'+1}}{(N'+1)!}\right)} = \frac{\Lambda}{N'+1},$$

where N' is the number of fake events introduced by A_D.

Let's partition the range of the values of N', into two parts N_1 and N_2. Let, $N_1 = \{x \in \mathbb{N} | \, |\Lambda - x| \leq \Lambda(1 - e^{-\varepsilon}) + 1\}$ and $N_2 = \{x \in \mathbb{N} | \, |\Lambda - x| > \Lambda(1 - e^{-\varepsilon}) + 1\}$.

Let $\alpha = \Lambda(1 - e^{-\varepsilon}) + 1$. For $N' \in N_2$, using Lemma 1 we have,

$$\Pr[|N' - \Lambda| \geq \alpha] \leq 2\exp\left(-\frac{\alpha^2}{2(\Lambda+\alpha)}\right)$$
$$= 2\exp\left(-\frac{(\Lambda(1-e^{-\varepsilon})+1)^2}{2(\Lambda(2-e^{-\varepsilon})+1)}\right) \leq 2\exp\left(-\frac{\Lambda(1-e^{-\varepsilon})^2}{2(2-e^{-\varepsilon})}\right) \leq \delta,$$

where $\Lambda = \frac{2(2-e^{-\varepsilon})\log\frac{2}{\delta}}{(1-e^{-\varepsilon})^2}$, which is $O(\frac{1}{\varepsilon^2}\log\frac{1}{\delta})$ when ε is small.

For $N' \in N_1$, we have

$$\frac{\Pr[\mathcal{A}_D(I) = N]}{\Pr[\mathcal{A}'_D(I) = N]} = \frac{\Lambda}{N'+1} \leq \frac{\Lambda}{\Lambda e^{-\varepsilon} - 1 + 1} = e^{\varepsilon}.$$

Therefore, combining above equations we have,

$$\Pr[\mathcal{A}_D(I) = N] = \Pr[N' \in R_1] + \Pr[N' \in R_2]$$
$$\leq e^{\varepsilon}\Pr[\mathcal{A}_{D'}(I) = N] + \delta$$

□

Publishing data. The above sanitization algorithm $A_D(R)$ can be considered for publishing data; If one considers query for all possible intervals it is equivalent to publishing the events. Practically, each sensor can publish the union of the real and fake events and the published data would preserve differential privacy as argued above.

Answering Range Queries. Now, we design an algorithm, $\mathcal{Q}(\mathcal{A}_D(R))$, to accurately answer range queries based on the results published by $\mathcal{A}_D(R)$. As in the most security and privacy settings where the algorithms and their parameters are all public except the specific random choices the algorithms make, consider ε, δ, and the event intensity λ are known.

Counting query on a spatial range $R = [x_1, x_2] \times [y_1, y_2]$ is estimated as $\mathcal{A}_D(R) - \Lambda$, where $\Lambda = \int_{x_1}^{x_2}\int_{y_1}^{y_2}\lambda(s)ds$. Let's denote $\mathcal{A}_D(R)$ as n for simplicity.

Let's denote the count of real events inside the range R in the dataset D as n^*. Now, $n^* - n$ gives an unbiased estimator for n^*, by the well known superposition theorem. We present the main statement below.

Theorem 10. ***Superposition Theorem (Kingman, 1992; Grimmett and Stirzaker, 2001).*** *The superposition of independent Poisson point processes $N_1, N_2, \cdots, N_m$ with mean rates $\Lambda_1, \Lambda_2, \cdots, \Lambda_m$ respectively is a Poisson point process with mean rate of $\Lambda = \sum_{i=1}^{m}\Lambda_i$.*

Now we analyze the utility of our algorithm.

Lemma 6. *The algorithm $\mathcal{Q}_S$, for a probability $0 \leq \beta \leq 1$, gives the following range query error*

$$\Pr\left[|\mathcal{Q}_S(\mathcal{A}(R)) - n^*| \leq \log\frac{2}{\beta} + \sqrt{\log^2\frac{2}{\beta} + 2\Lambda\log\frac{2}{\beta}}\right] \geq 1 - \beta.$$

Proof. Notice that $\mathcal{Q}_S(\mathcal{A}(R))$ is $n - \Lambda$. The count of fake events, $n - n^*$, follows the Poisson distribution with mean Λ. Therefore, applying $\alpha \geq \log\frac{2}{\beta} + \sqrt{\log^2\frac{2}{\beta} + 2\Lambda\log\frac{2}{\beta}}$ in Lemma 1, we have $2\exp\left(-\frac{\alpha^2}{2(\Lambda+\alpha)}\right) \leq \beta$. Therefore,

$$\Pr\left[|n - \Lambda - n^*| \geq \log\frac{2}{\beta} + \sqrt{\log^2\frac{2}{\beta} + 2\Lambda\log\frac{2}{\beta}}\right] \leq \beta.$$

Rearranging we get the lemma. □

Theorem 11. *If $\Lambda = O\left(\frac{1}{\varepsilon^2}\log\frac{1}{\delta}\right)$, $\mathcal{Q}_D(\mathcal{A}(R))$ estimates the counts of real events with error $O\left(\sqrt{\frac{1}{\varepsilon^2}\log\frac{1}{\delta}\log\frac{1}{\beta}}\right)$, with probability $1 - \beta$.*

Replacing the value of Λ in the above Lemma gives the theorem.

Extension to spatiotemporal data. Poisson process is trivially extended to spatiotemporal dimension by using suitable intensity function in three dimensions. The spatiotemporal sanitization mechanism can generate fake events to obfuscate both the accurate location and timing. This method is suitable for realtime data analysis.

5.4.3 Extending Psum Method to Spatial Dimension

Here, we extend the results from (Chan et al., 2011) designed for temporal queries to spatial dimension and we compare its accuracy with our algorithms in the experiments.

Let's assume that the sensors are positioned on a $\sqrt{m} \times \sqrt{m}$ unit square grid. An event occurring at location (x, y) is recorded by the sensor nearest to (x, y); for multiple nearest sensors we choose one arbitrarily. Suppose, $S(x, y) \in \mathbb{N}$ denotes the number of events recorded by the sensor at grid location (x, y).

To protect the presence of a single event in the dataset, differential privacy considers neighboring dataset S and S' that have event count differing by 1 at one sensor.

Similar to the binary mechanism in (Chan et al., 2011), a quadtree (Samet, 1988) can be constructed over S and any range query can be answered by adding the canonical ranges of the query range; Let's call these sums as partial sums. Thus, a change in a cell $S(x, y)$ affects at most $\lceil \log_2 m \rceil$ queries.

The randomized mechanism $\mathcal{A}$ adds Laplace noise with $b = \log m/\varepsilon$ to each partial sum. We now analyze the privacy and utility of this mechanism.

Theorem 12 (Differential privacy)**.** *The above mechanism preserves ε-differential privacy.*

Proof. It is easy to see that for a single query, the above mechanism preserves $\frac{\varepsilon}{\log m}$-differential privacy. As there can be at most $\lceil \log m \rceil$ queries affected by this change, sequential composition of the differential privacy gives the theorem. □

Before analyzing the utility of the method, we need the following lemma

Theorem 13 (Utility)**.** *For a spatiotemporal range query, the error of the above mechanism is $O\left(\frac{\log_2^{1.5} m}{\varepsilon} \log \frac{1}{\beta}\right)$ with probability $1 - \beta$.*

Proof. Corresponding to noises at partial sums, a query accumulates total noise from $\lceil \log_2 m \rceil$ Laplace distributions each with $b_i = \log m/\varepsilon$. This gives the theorem. □

5.5 Experiments

This section describes experiments showing that the privacy preserving mechanisms for the proposed algorithms. Highlights of the results are

- Proposed methods are more accurate for range queries than existing continual release methods for same privacy guarantees.
- Privacy preserving mechanisms work in real datasets of geo-located tweets.

5.5.1 Experimental Setup

Dataset. We use a publicly available dataset of $9,267$ Geo-located tweets from London, UK[1].

Evaluating utility using range queries. Range queries are fundamental to mining and learning methods and thus used here as the measure of utility of the

[1] http://followthehashtag.com/datasets/170000-uk-geolocated-tweets-free-twitter-dataset/

sanitized data. Each experiment uses 5000 uniformly chosen query ranges and the experiments are repeated 10 times to capture confidence in the result. If the count of events in a query range with n events is estimated as $\tilde{n}$, then the error in estimation is $\xi = \frac{|n-\tilde{n}|}{\tilde{n}}$. The relative error is symmetric with respect to addition, i.e., estimating $n + \Delta$ and $n - \Delta$ incur same error.

5.5.2 Evaluating Random walk based algorithm

This subsection evaluates the mechanisms proposed in Section 5.4.1 for publishing spatial events.

Accuracy for spatial range queries. Figure 5.4(a), (b), and (c) show how relative error changes for spatial range queries on the spatial data publish model. The range queries are accurate for reasonable privacy, i.e., with large Δ and small ε and δ values.

5.5.3 Evaluating Poisson Process based algorithm

This section describes experiments corresponding to methods proposed in Section 5.4.2.

In this setting, the the space is divided into cubic grid cells indexed by (x, y) with spatial resolution as 50 meters. Each event is mapped to its nearest grid point and the intensity of the fake events at each cell is determined using Theorem 9. The events are sanitized using the mechanism described in Section 5.4.2. Relative error, ξ increases with increasing privacy as shown in Figure 5.5(a) and (b) by varying ε and δ.

Spatial privacy for synchronous model. This section evaluates range queries in synchronous setting described in 5.4.3. The space-time is divided into a gird, with the spatial resolution being 50 meters. A quadtree is built on this grid and a query is answered by aggregating counts of the partial canonical ranges.

Compare utility of methods. In Figure 5.6, we notice that the spatial partial sum method achieves lowest error for range queries compared to privacy preserving mechanism with Poisson process method and naive Laplace perturbation. The naive Laplace perturbation algorithm first computes the accurate answer to the range query and then adds $Lap(m)/\varepsilon$ noise in a domain with $\sqrt{m} \times \sqrt{m}$ grid. Also note that neither the naive Laplace mechanism nor the partial sum method

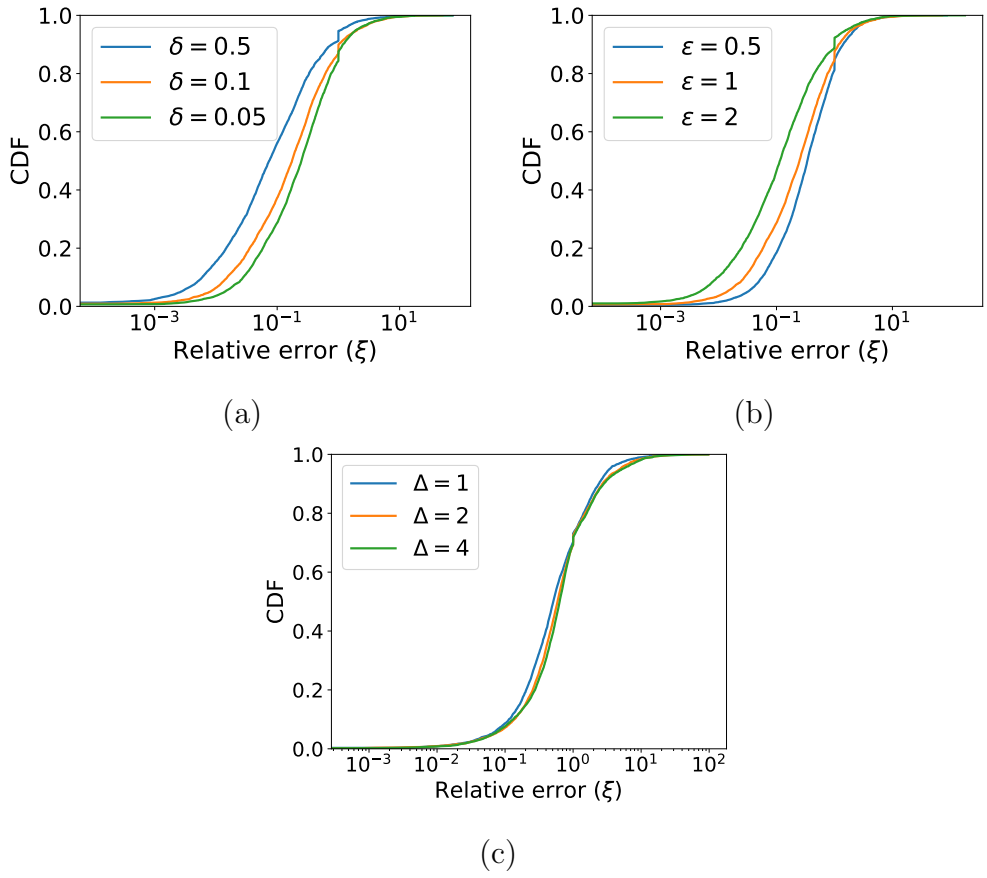

Figure 5.4: **(a,b,c)** Accuracy of spatial range queries for random walk based sanitization. **(a)** CDF of the relative error for varying δ with $\varepsilon = 1$ and $\Delta = 1$. **(b)** varying ε with $\delta = 0.05$ and $\Delta = 1$. **(c)** varying Δ with $\varepsilon = 1$ and $\delta = 0.05$. All of these figures show natural privacy-utility trade-off and utility is well-preserved for reasonable privacy.

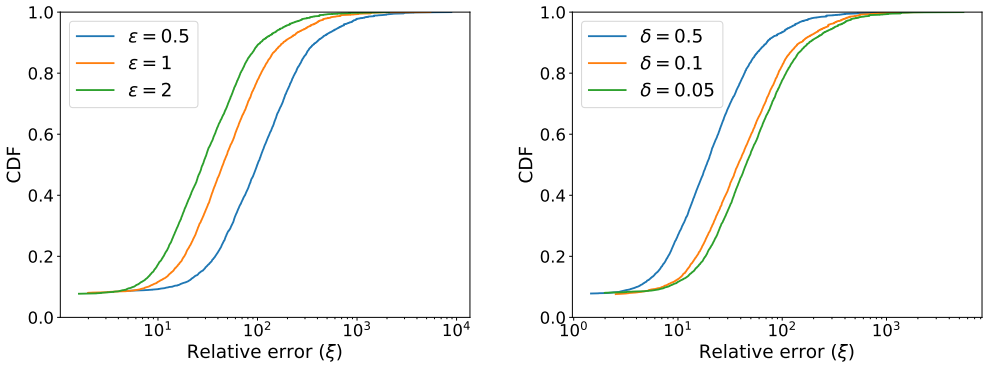

(a) (b)

Figure 5.5: CDF of the relative errors for range queries (a) using the mechanism for adding Poisson noise events. **(a)** Error decreases with increasing ε. Here, $\delta = 0.05$ **(b)** Error decreases with increasing δ. Here, $\varepsilon = 1$. These shows natural trade-off between privacy parameters and utility.

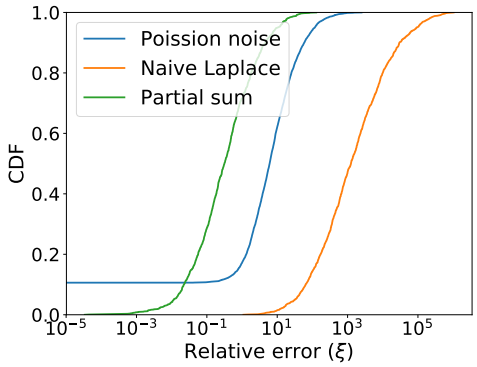

Figure 5.6: The spatial partial sum method achieves lowest error for range queries compared to Poisson process based method and naive Laplace mechanism. All methods have $\varepsilon = 1$ and Poisson noise method has $\delta = 0.05$. All comparing methods discretize space-time using spatial resolution of $50m$. However, note that except our Poisson process based method, the rest are not suitable for publishing data.

can support data publication as both these methods need to add noise to the true answer.

Chapter 6

Conclusion and Future Directions

Sensing using IoT devices and mobile phones have proliferated in pervasive areas of modern day living (Gubbi et al., 2013). Fundamental learning techniques such as the ones proposed in this dissertation will be of interest for years to come.

In this dissertation, we present multiple learning algorithms for spatiotemporal sensing data. The algorithms are efficient with online and distributed computation. They preserve individual privacy and learn aggregate knowledge from the data. This chapter presents the concluding remarks and brief ideas on related open research areas.

Learning periodicity from noisy streams. We have demonstrated the use of a sequential Monte Carlo method to detect and track the periodicity in discrete event streams. Unlike other methods, this technique does not rely on the underlying process sticking to a constant phase. As a result, it adapts to noise and changes in the period very quickly. Experiments show this method to be more accurate and efficient than existing methods for detecting periodicity in noisy event streams.

Our basic approach is quite general and can be adapted to detect and characterize more complex temporal patterns. Doing so will require a more flexible class of event-generating functions, which we expect will be a fruitful area for future research.

Many applications require inference from an aggregate signal contributed by multiple periodic signals. Examples include forecasting demand for an item (e.g., shampoo) at a super market. Many users buy shampoos at regular intervals, although their phases and intervals are dynamic. It is interesting and as well as challenging to analyze the interweaving pattern in the data. Frequency analysis

techniques are not applicable due to dynamic phases and periodicity in each signal; Markov models become complicated for high dimensional data. It is possible to treat the signal as a univariate signal of demands and apply regression techniques, but that misses the structure provided by the periodicity in individual user's buying patterns.

Chapter 2 empirically shows that the algorithm works in real and artificial data, but a rigorous mathematical analysis would be required to characterize the algorithm, for example, lower bound of the number of events required for convergence, the number of particles needed for robust operation, etc.

Private Sensing of Asynchronous Event Sequences. In Chapter 3, we proposed multiple privacy preserving mechanisms for protecting individual event timings and hiding the occurrence of an event. The proposed framework uses contemporary Pufferfish definition of privacy – a generalization of differential privacy – and supports asynchronous event timings. The mechanisms add considerably less noise than the existing algorithms to achieve the same privacy guarantee. We also proposed a system design to implement the framework in mobile phones. Multivariate event streams that carry interrelations are harder to sanitize as they may contain a complex relation between attributes, and this remains to be investigated in future works.

Topological Signatures For Fast Mobility Analysis. In Chapter 4, We presented a topological framework to represent a trajectory as a point in a Euclidean space, enabling natural applications of well established machine learning and mining techniques. The topological construct preserves relevant qualitative features in trajectories while ignoring the extraneous details and noise. The framework can be set up using fast distributed algorithms and used in an online manner by mobile entities. The framework is quite general and flexible, and it allows application specific choice of obstacles and domains.

The proposed framework uses the obstacles and designs a method to infer obstacles from trajectory data (no or less mobility correspond to obstacles), however, further study is needed to characterize the obstacles in a domain. This would provide insight to causality behind mobility (Cobb et al., 2017).

Many applications like driver-less cars need to consider dynamic obstacles (other vehicles and pedestrians on road). Our framework does not trivially extend to dynamic obstacles and needs further work.

Time is an essential attribute in mobility traces for many applications. However, it is nontrivial to extend our framework to the temporal dimension because of the uni-direction property of time (Ghrist and Krishnan, 2017). Therefore, it needs further study to analyze spatiotemporal trajectories using topology.

Publishing Differentially Private Spatial Data From Distributed Sensors. In Chapter 5, we proposed a differentially private sensing framework for spatial data publication. The proposed framework supports distributed operation and has good privacy and utility guarantees for independent events. However, in many applications, spatial events are correlated, for example, occupancy relates to mobility and locations in a trajectory, etc. Due to the correlation in the data, traditional differential privacy frameworks do not apply and therefore, need further investigation.

Moreover, the algorithms in this chapter apply to axis aligned rectangular queries where sensors are arranged on a grid. Further study is required to support more realistic general graph topology and general shaped ranges.

Bibliography

(2017). Mdanalysis 0.16.2. `http://www.mdanalysis.org/`.

Abadi, M., Barham, P., Chen, J., Chen, Z., Davis, A., Dean, J., Devin, M., Ghemawat, S., Irving, G., Isard, M., et al. (2016). Tensorflow: A system for large-scale machine learning. In *OSDI*, volume 16, pages 265–283.

Ahmadi, H., Pham, N. T., Ganti, R. K., Abdelzaher, T. F., Nath, S., and Han, J. (2010). Privacy-aware regression modeling of participatory sensing data. In *SenSys*.

Alt, H. and Godau, M. (1995). Computing the fréchet distance between two polygonal curves. *International Journal of Computational Geometry & Applications*, 5(01n02):75–91.

Andrés, M. E., Bordenabe, N. E., Chatzikokolakis, K., and Palamidessi, C. (2013). Geo-indistinguishability: Differential privacy for location-based systems. In *Proceedings of the 2013 ACM SIGSAC Conference on Computer & Communications Security*, CCS '13, pages 901–914. ACM.

Astefanoaei, M., Cesaretti, P., Katsikouli, P., Goswami, M., and Sarkar, R. (2018). Multi-resolution sketches and locality sensitive hashing for fast trajectory processing. In *26th ACM SIGSPATIAL International Conference on Advances in Geographic Information Systems (ACM SIGSPATIAL)*.

Bachem, O., Lucic, M., and Krause, A. (2017). Scalable and distributed clustering via lightweight coresets. *arXiv preprint arXiv:1702.08248*.

Bao, L. and Intille, S. S. (2004). Activity recognition from user-annotated acceleration data. In *International conference on pervasive computing*, pages 1–17. Springer.

Barbosa, H., Barthelemy, M., Ghoshal, G., James, C. R., Lenormand, M., Louail, T., Menezes, R., Ramasco, J. J., Simini, F., and Tomasini, M. (2018). Human mobility: Models and applications. *Physics Reports*, 734:1–74.

Barth, J., Klucken, J., Kugler, P., Kammerer, T., Steidl, R., Winkler, J., Hornegger, J., and Eskofier, B. (2011). Biometric and mobile gait analysis for early diagnosis and therapy monitoring in parkinson's disease. In *Engineering in Medicine and Biology Society, EMBC, 2011 Annual International Conference of the IEEE*, pages 868–871. IEEE.

Baryshnikov, Y. and Ghrist, R. (2009). Target enumeration via euler characteristic integrals. *SIAM Journal on Applied Mathematics*, 70(3):825–844.

Benson, T., Akella, A., and Maltz, D. A. (2010). Network traffic characteristics of data centers in the wild. In *Proceedings of the 10th ACM SIGCOMM conference on Internet measurement*, pages 267–280. ACM.

Bindschaedler, V. and Shokri, R. (2016). Synthesizing plausible privacy-preserving location traces. In *2016 IEEE Symposium on Security and Privacy (SP)*, pages 546–563. IEEE.

Bittau, A., Erlingsson, U., Maniatis, P., Mironov, I., Raghunathan, A., Lie, D., Rudominer, M., Kode, U., Tinnes, J., and Seefeld, B. (2017). Prochlo: Strong privacy for analytics in the crowd. In *Proceedings of the 26th Symposium on Operating Systems Principles*, pages 441–459. ACM.

Bracciale, L., Bonola, M., Loreti, P., Bianchi, G., Amici, R., and Rabuffi, A. (2014). Crawdad data set roma/taxi (v. 2014-07-17). *July*.

Buchin, K., Buchin, M., Gudmundsson, J., Löffler, M., and Luo, J. (2011). Detecting commuting patterns by clustering subtrajectories. *International Journal of Computational Geometry & Applications*, 21(03):253–282.

Buchin, K., Buchin, M., Van Kreveld, M., Löffler, M., Silveira, R. I., Wenk, C., and Wiratma, L. (2013). Median trajectories. *Algorithmica*, 66(3):595–614.

Candes, E. (2006). Compressive sampling.

Canini, K. R., Shi, L., and Griffiths, T. L. (2009). Online inference of topics with latent dirichlet allocation. In *International conference on artificial intelligence and statistics*, pages 65–72.

Cao, L. and Krumm, J. (2009). From gps traces to a routable road map. In *Proceedings of the 17th ACM SIGSPATIAL international conference on advances in geographic information systems*, pages 3–12. ACM.

Cao, Y., Yoshikawa, M., Xiao, Y., and Xiong, L. (2018). Quantifying differential privacy in continuous data release under temporal correlations. *IEEE Transactions on Knowledge and Data Engineering*.

Chambers, E. W., De Verdiere, E. C., Erickson, J., Lazard, S., Lazarus, F., and Thite, S. (2010). Homotopic fréchet distance between curves or, walking your dog in the woods in polynomial time. *Computational Geometry*, 43(3):295–311.

Chambers, E. W. and Wang, Y. (2013). Measuring similarity between curves on 2-manifolds via homotopy area. In *Proceedings of the twenty-ninth annual symposium on Computational geometry*, pages 425–434. ACM.

Chan, T.-H. H., Shi, E., and Song, D. (2011). Private and continual release of statistics. *ACM Trans. Inf. Syst. Secur.*, 14(3):26:1–26:24.

Chen, Y., Machanavajjhala, A., Hay, M., and Miklau, G. (2017). Pegasus: Data-adaptive differentially private stream processing. In *Proceedings of the 2017 ACM SIGSAC Conference on Computer and Communications Security*, pages 1375–1388. ACM.

Cheng, C.-M., Kung, H., and Tan, K.-S. (2002). Use of spectral analysis in defense against dos attacks. In *Global Telecommunications Conference, 2002. GLOBECOM'02. IEEE*, volume 3, pages 2143–2148. IEEE.

Cobb, A. D., Markham, A., and Roberts, S. J. (2017). Learning from lions: inferring the utility of agents from their trajectories. *arXiv preprint arXiv:1709.02357*.

Cormode, G., Procopiuc, C., Srivastava, D., Shen, E., and Yu, T. (2012). Differentially private spatial decompositions. In *Data engineering (ICDE), 2012 IEEE 28th international conference on*, pages 20–31. IEEE.

Datar, M., Immorlica, N., Indyk, P., and Mirrokni, V. S. (2004). Locality-sensitive hashing scheme based on p-stable distributions. In *Proceedings of the twentieth annual symposium on Computational geometry*, pages 253–262. ACM.

De Montjoye, Y.-A., Hidalgo, C. A., Verleysen, M., and Blondel, V. D. (2013). Unique in the crowd: The privacy bounds of human mobility. *Scientific reports*, 3:1376.

Desbrun, M., Kanso, E., and Tong, Y. (2008). Discrete differential forms for computational modeling. In *Discrete differential geometry*, pages 287–324. Springer.

Diederik P. Kingma, J. B. (2015). Adam: A method for stochastic optimization. In *Proceedings of the 3rd International Conference on Learning Representations (ICLR)*, ICLR '15.

Ding, J., Gao, J., and Xiong, H. (2015). Understanding and modelling information dissemination patterns in vehicle-to-vehicle networks. In *Proceedings of the 23rd SIGSPATIAL International Conference on Advances in Geographic Information Systems*, page 41. ACM.

Ding, J., Ghosh, A., Sarkar, R., and Gao, J. (2019). Private sensing of asynchronous event sequences. In *Under Review at Sensys 2019*.

Doucet, A., Freitas, N. d., and Gordon, N., editors (2001). *Sequential Monte Carlo Methods in Practice*. Springer, New York.

Driemel, A. and Silvestri, F. (2017). Locality-Sensitive Hashing of Curves. In *33rd International Symposium on Computational Geometry (SoCG 2017)*, volume 77, pages 37:1–37:16.

Dwork, C. (2006). Differential privacy. In *Proceedings of the 33rd International Conference on Automata, Languages and Programming - Volume Part II*, ICALP'06, pages 1–12. Springer-Verlag.

Dwork, C., McSherry, F., Nissim, K., and Smith, A. (2006). Calibrating noise to sensitivity in private data analysis. In *Theory of cryptography conference*, pages 265–284. Springer.

Dwork, C., Naor, M., Pitassi, T., and Rothblum, G. N. (2010). Differential privacy under continual observation. In *Proceedings of the forty-second ACM symposium on Theory of computing*, pages 715–724. ACM.

Dwork, C., Naor, M., Reingold, O., and Rothblum, G. N. (2015). Pure differential privacy for rectangle queries via private partitions. In *International Conference*

on the Theory and Application of Cryptology and Information Security, pages 735–751. Springer.

Dwork, C., Naor, M., Reingold, O., Rothblum, G. N., and Vadhan, S. (2009). On the complexity of differentially private data release: Efficient algorithms and hardness results. In *Proceedings of the Forty-first Annual ACM Symposium on Theory of Computing*, STOC '09, pages 381–390, New York, NY, USA. ACM.

Dwork, C. and Roth, A. (2014). The algorithmic foundations of differential privacy. *Found. Trends Theor. Comput. Sci.*, 9(3–4):211–407.

Easley, D. and Kleinberg, J. (2010). *Networks, crowds, and markets: Reasoning about a highly connected world*. Cambridge University Press.

Edelsbrunner, H. and Harer, J. (2010). *Computational topology: an introduction*. American Mathematical Soc.

Elmokashfi, A., Zhou, D., and Baltrünas, D. (2017). Adding the next nine: An investigation of mobile broadband networks availability. In *Proceedings of the 23rd Annual International Conference on Mobile Computing and Networking*, pages 88–100. ACM.

Erlingsson, Ú., Pihur, V., and Korolova, A. (2014). Rappor: Randomized aggregatable privacy-preserving ordinal response. In *Proceedings of the 2014 ACM SIGSAC conference on computer and communications security*, pages 1054–1067. ACM.

Fan, L., Xiong, L., and Sunderam, V. (2013). Differentially private multi-dimensional time series release for traffic monitoring. In *IFIP Annual Conference on Data and Applications Security and Privacy*, pages 33–48. Springer.

Frahling, G. and Sohler, C. (2008). A fast k-means implementation using coresets. *International Journal of Computational Geometry & Applications*, 18(06):605–625.

Funke, S. and Milosavljevic, N. (2007). Network sketching or: How much geometry hides in connectivity?–part ii. In *Proceedings of the eighteenth annual ACM-SIAM symposium on Discrete algorithms*, pages 958–967. Society for Industrial and Applied Mathematics.

Ganti, R. K., Pham, N., Tsai, Y.-E., and Abdelzaher, T. F. (2008). Poolview: stream privacy for grassroots participatory sensing. In *Proceedings of the 6th ACM conference on Embedded network sensor systems*, pages 281–294. acm.

Gers, F. A., Schmidhuber, J., and Cummins, F. A. (2000). Learning to forget: Continual prediction with lstm. *Neural Computation*, 12:2451–2471.

Ghassemi, N. H. and Diesenroth, M. (2014). Analytic long term forecasting with periodic gaussian processes. In *AISTATS*, pages 303–311.

Ghosh, A., Ding, J., Sarkar, R., and Gao, J. (2019). Differentially private sensing of distributed spatial data. In *Working for submission.*

Ghosh, A., Lucas, C., and Sarkar, R. (2017). Finding periodic discrete events in noisy streams. In *Proceedings of the 2017 ACM on Conference on Information and Knowledge Management*, pages 627–636. ACM.

Ghosh, A., Rozemberczki, B., Ramamoorthy, S., and Sarkar, R. (2018). Topological signatures for fast mobility analysis. In *Proceedings of the 26th ACM SIGSPATIAL International Conference on Advances in Geographic Information Systems*, pages 159–168. ACM.

Ghrist, R. and Krishnan, S. (2017). Positive alexander duality for pursuit and evasion.

Goldberg, Y. (2017). Neural network methods for natural language processing. *Synthesis Lectures on Human Language Technologies*, 10(1):1–309.

Goldreich, O. (2017). *Introduction to property testing.* Cambridge University Press.

González, M. C., Hidalgo, C. A., and Barabási, A.-L. (2009). Understanding individual human mobility patterns. *Nature*, 458(7235):238–238.

Gramaglia, M. and Fiore, M. (2015). Hiding mobile traffic fingerprints with glove. In *Proceedings of the 11th ACM Conference on Emerging Networking Experiments and Technologies*, page 26. ACM.

Gramaglia, M., Fiore, M., Tarable, A., and Banchs, A. (2017). Preserving mobile subscriber privacy in open datasets of spatiotemporal trajectories. In *IEEE*

INFOCOM 2017-IEEE Conference on Computer Communications, pages 1–9. IEEE.

Grimmett, G. and Stirzaker, D. (2001). *Probability and random processes*. Oxford university press.

Gubbi, J., Buyya, R., Marusic, S., and Palaniswami, M. (2013). Internet of things (iot): A vision, architectural elements, and future directions. *Future Generation Comp. Syst.*, 29:1645–1660.

HajiGhassemi, N. and Deisenroth, M. (2014). Analytic long-term forecasting with periodic gaussian processes. In *Artificial Intelligence and Statistics*, pages 303–311.

Hallac, D., Vare, S., Boyd, S., and Leskovec, J. (2017). Toeplitz inverse covariance-based clustering of multivariate time series data. In *Proceedings of the 23rd ACM SIGKDD International Conference on Knowledge Discovery and Data Mining*, pages 215–223. ACM.

Han, J., Dong, G., and Yin, Y. (1999). Efficient mining of partial periodic patterns in time series database. In *Data Engineering, 1999. Proceedings., 15th International Conference on*, pages 106–115. IEEE.

He, X., Machanavajjhala, A., and Ding, B. (2014). Blowfish privacy: tuning privacy-utility trade-offs using policies. In *SIGMOD Conference*.

Hershberger, J. and Snoeyink, J. (1994a). Computing minimum length paths of a given homotopy class. *Computational geometry*, 4(2):63–97.

Hershberger, J. and Snoeyink, J. (1994b). An o(n log n) implementation of the douglas-peucker algorithm for line simplification. In *Symposium on Computational Geometry*.

Hirani, A. N. (2003). *Discrete exterior calculus*. PhD thesis, California Institute of Technology.

Indyk, P. (2002). Approximate nearest neighbor algorithms for fréchet distance via product metrics. In *Proceedings of the eighteenth annual symposium on Computational geometry*, pages 102–106. ACM.

Indyk, P., Koudas, N., and Muthukrishnan, S. (2000). Identifying representative trends in massive time series data sets using sketches. In *VLDB*, pages 363–372.

Jain, M. and Dovrolis, C. (2002). *End-to-end available bandwidth: Measurement methodology, dynamics, and relation with TCP throughput*, volume 32. ACM.

Jia, X., Khandelwal, A., Nayak, G., Gerber, J., Carlson, K., West, P., and Kumar, V. (2017). Incremental dual-memory lstm in land cover prediction. In *Proceedings of the 23rd ACM SIGKDD International Conference on Knowledge Discovery and Data Mining*, pages 867–876. ACM.

Jin, H., Su, L., Xiao, H., and Nahrstedt, K. (2016). Inception: Incentivizing privacy-preserving data aggregation for mobile crowd sensing systems. In *Proceedings of the 17th ACM International Symposium on Mobile Ad Hoc Networking and Computing*, pages 341–350. ACM.

Jindal, T., Giridhar, P., Tang, L.-A., Li, J., and Han, J. (2013). Spatiotemporal periodical pattern mining in traffic data. In *Proceedings of the 2nd ACM SIGKDD International Workshop on Urban Computing*, page 11. ACM.

Junier, I., Hérisson, J., and Képès, F. (2010). Periodic pattern detection in sparse boolean sequences. *Algorithms for Molecular Biology*, 5(1):1.

Jurafsky, D. and Martin, J. H. (2014). *Speech and language processing*, volume 3. Pearson London.

Kasiviswanathan, S. P., Lee, H. K., Nissim, K., Raskhodnikova, S., and Smith, A. (2011). What can we learn privately? *SIAM Journal on Computing*, 40(3):793–826.

Katsikouli, P., Astefanoaei, M., and Sarkar, R. (2018). Distributed mining of popular paths in road networks. In *DCOSS 2018-International Conference on Distributed Computing in Sensor Systems*, pages 1–8. IEEE.

Katsikouli, P., Sarkar, R., and Gao, J. (2014). Persistence based online signal and trajectory simplification for mobile devices. In *Proceedings of the 22nd ACM SIGSPATIAL International Conference on Advances in Geographic Information Systems*, pages 371–380. ACM.

Kellaris, G., Papadopoulos, S., Xiao, X., and Papadias, D. (2014). Differentially private event sequences over infinite streams. *Proceedings of the VLDB Endowment*, 7(12):1155–1166.

Kifer, D. and Machanavajjhala, A. (2014a). Pufferfish: A framework for mathematical privacy definitions. *ACM Transactions on Database Systems (TODS)*, 39(1):3.

Kifer, D. and Machanavajjhala, A. (2014b). Pufferfish: A framework for mathematical privacy definitions. *ACM Trans. Database Syst.*, 39(1):3:1–3:36.

Kingman, J. F. C. (1992). *Poisson processes*, volume 3. Clarendon Press.

Kinsey, L. C. (2012). *Topology of surfaces*. Springer Science & Business Media.

Király, F. J. and Oberhauser, H. (2019). Kernels for sequentially ordered data. *Journal of Machine Learning Research*.

Kleindessner, M., Awasthi, P., and Morgenstern, J. (2019). Fair k-center clustering for data summarization. *arXiv preprint arXiv:1901.08628*.

Klucken, J., Barth, J., Kugler, P., Schlachetzki, J., Henze, T., Marxreiter, F., Kohl, Z., Steidl, R., Hornegger, J., Eskofier, B., et al. (2013). Unbiased and mobile gait analysis detects motor impairment in parkinson's disease. *PloS one*, 8(2):e56956.

Kolyaie, S. and Yaghooti, M. (2011). Evaluation of geostatistical analysis capability in wireless signal propagation modeling. In *Proc. 11th International Conference on GeoComputation*.

Krause, A., Singh, A., and Guestrin, C. (2008). Near-optimal sensor placements in gaussian processes: Theory, efficient algorithms and empirical studies. *Journal of Machine Learning Research*, 9(Feb):235–284.

Krishnamurthy, B., Malandrino, D., and Wills, C. E. (2007). Measuring privacy loss and the impact of privacy protection in web browsing. In *Proceedings of the 3rd symposium on Usable privacy and security*, pages 52–63. ACM.

Leskovec, J., Rajaraman, A., and Ullman, J. D. (2014). *Mining of massive datasets*. Cambridge university press.

Levine, B. N., Reiter, M. K., Wang, C., and Wright, M. (2004). Timing attacks in low-latency mix systems. In *International Conference on Financial Cryptography*, pages 251–265. Springer.

Li, H., Xiong, L., Jiang, X., and Liu, J. (2015a). Differentially private histogram publication for dynamic datasets: an adaptive sampling approach. *Proceedings of the ACM International Conference on Information and Knowledge Management.*, 2015:1001–1010.

Li, Z., Wang, J., and Han, J. (2012). Mining event periodicity from incomplete observations. In *Proceedings of the 18th ACM SIGKDD international conference on Knowledge discovery and data mining*, pages 444–452. ACM.

Li, Z., Wang, J., and Han, J. (2015b). eperiodicity: Mining event periodicity from incomplete observations. *IEEE Transactions on Knowledge and Data Engineering*, 27(5):1219–1232.

Liu, C., Hoi, S. C., Zhao, P., and Sun, J. (2016). Online arima algorithms for time series prediction. In *Thirtieth AAAI conference on artificial intelligence.*

Liu, T., Bahl, P., and Chlamtac, I. (1998). Mobility modeling, location tracking, and trajectory prediction in wireless atm networks. *IEEE Journal on selected areas in communications*, 16(6):922–936.

Lv, J., Li, Q., Sun, Q., and Wang, X. (2018). T-conv: A convolutional neural network for multi-scale taxi trajectory prediction. In *Big Data and Smart Computing (BigComp), 2018 IEEE International Conference on*, pages 82–89. IEEE.

Miao, C., Jiang, W., Su, L., Li, Y., Guo, S., Qin, Z., Xiao, H., Gao, J., and Ren, K. (2015). Cloud-enabled privacy-preserving truth discovery in crowd sensing systems. In *SenSys.*

Mirzasoleiman, B., Karbasi, A., Sarkar, R., and Krause, A. (2016). Distributed submodular maximization. *The Journal of Machine Learning Research*, 17(1):8330–8373.

Mitrovic, M., Kazemi, E., Zadimoghaddam, M., and Karbasi, A. (2018). Data summarization at scale: A two-stage submodular approach. *arXiv preprint arXiv:1806.02815.*

Murphy, K. P. (2012). *Machine learning: a probabilistic perspective*. MIT press.

Nath, B. and Niculescu, D. (2003). Routing on a curve. *ACM SIGCOMM Computer Communication Review*, 33(1):155–160.

Niu, C., Zheng, Z., Tang, S., Gao, X., and Wu, F. (2019). Making big money from small sensors: Trading time-series data under pufferfish privacy. In *IEEE INFOCOM 2019-IEEE Conference on Computer Communications*, pages 568–576. IEEE.

Nummiaro, K., Koller-Meier, E., and Van Gool, L. (2003). An adaptive color-based particle filter. *Image and vision computing*, 21(1):99–110.

Osborne, M. A., Roberts, S. J., Rogers, A., Ramchurn, S. D., and Jennings, N. R. (2008). Towards real-time information processing of sensor network data using computationally efficient multi-output gaussian processes. In *Proceedings of the 7th international conference on Information processing in sensor networks*, pages 109–120. IEEE Computer Society.

Pan, W., Ghoshal, G., Krumme, C., Cebrian, M., and Pentland, A. (2013). Urban characteristics attributable to density-driven tie formation. *Nature communications*, 4:1961.

Papadopoulos, E. P., Diamantaris, M., Papadopoulos, P., Petsas, T., Ioannidis, S., and Markatos, E. P. (2017). The long-standing privacy debate: Mobile websites vs mobile apps. In *Proceedings of the 26th International Conference on World Wide Web*, pages 153–162. International World Wide Web Conferences Steering Committee.

Parmar, K., Bushi, S., Bhattacharya, S., and Kumar, S. (2017). Forecasting ad-impressions on online retail websites using non-homogeneous hawkes processes. In *Proceedings of the 2017 ACM on Conference on Information and Knowledge Management*, pages 1089–1098. ACM.

Piotrowska, A. M., Hayes, J., Elahi, T., Meiser, S., and Danezis, G. (2017). The loopix anonymity system. In *26th USENIX Security Symposium, USENIX Security*, pages 16–18.

Pokorny, F. T., Goldberg, K., and Kragic, D. (2016). Topological trajectory clustering with relative persistent homology. In *Robotics and Automation (ICRA), 2016 IEEE International Conference on*, pages 16–23. IEEE.

Qardaji, W., Yang, W., and Li, N. (2013). Differentially private grids for geospatial data. In *Data Engineering (ICDE), 2013 IEEE 29th International Conference on*, pages 757–768. IEEE.

Rabiner, L. R. and Juang, B.-H. (1986). An introduction to hidden markov models. *IEEE ASSP Magazine*, 3:4–16.

Rastogi, V. and Nath, S. (2010). Differentially private aggregation of distributed time-series with transformation and encryption. In *Proceedings of the 2010 ACM SIGMOD International Conference on Management of data*, pages 735–746. ACM.

Rezaei, A., Gao, J., Phillips, J. M., and Tóth, C. D. (2018). Improved bounds on information dissemination by manhattan random waypoint model. In *Proceedings of the 26th ACM SIGSPATIAL International Conference on Advances in Geographic Information Systems*, pages 139–148. ACM.

Sakoe, H. and Chiba, S. (1978). Dynamic programming algorithm optimization for spoken word recognition. *Acoustics, Speech and Signal Processing, IEEE Transactions on*, 26(1):43–49.

Saleheen, N., Chakraborty, S., Ali, N., Rahman, M. M., Hossain, S. M., Bari, R., Buder, E. H., Srivastava, M. B., and Kumar, S. (2016). msieve: differential behavioral privacy in time series of mobile sensor data. *Proceedings of the ACM International Conference on Ubiquitous Computing (UbiComp)*, 2016:706–717.

Samet, H. (1988). An overview of quadtrees, octrees, and related hierarchical data structures. In *Theoretical Foundations of Computer Graphics and CAD*, pages 51–68. Springer.

Sarkar, R. and Gao, J. (2013). Differential forms for target tracking and aggregate queries in distributed networks. *IEEE/ACM Transactions on Networking (TON)*, 21(4):1159–1172.

Sarkar, R., Yin, X., Gao, J., Luo, F., and Gu, X. D. (2009). Greedy routing with guaranteed delivery using ricci flows. In *Information Processing in Sensor Networks, 2009. IPSN 2009. International Conference on*, pages 121–132. IEEE.

Schilit, B. N., Adams, N., Want, R., et al. (1994). *Context-aware computing applications*. Xerox Corporation, Palo Alto Research Center.

Shepard, C., Rahmati, A., Tossell, C., Zhong, L., and Kortum, P. (2011). Livelab: measuring wireless networks and smartphone users in the field. *ACM SIGMETRICS Performance Evaluation Review*, 38(3):15–20.

Song, C., Qu, Z., Blumm, N., and Barabási, A.-L. (2010). Limits of predictability in human mobility. *Science*, 327(5968):1018–1021.

Song, S., Wang, Y., and Chaudhuri, K. (2017). Pufferfish privacy mechanisms for correlated data. In *Proceedings of the 2017 ACM International Conference on Management of Data*, pages 1291–1306. ACM.

Srivatsa, M., Ganti, R., Wang, J., and Kolar, V. (2013). Map matching: Facts and myths. In *Proceedings of the 21st ACM SIGSPATIAL International Conference on Advances in Geographic Information Systems*, pages 484–487. ACM.

Stewart, L. and McCarty, P. (1992). Use of bayesian belief networks to fuse continuous and discrete information for target recognition, tracking, and situation assessment. In *Signal Processing, Sensor Fusion, and Target Recognition*, volume 1699, pages 177–186. International Society for Optics and Photonics.

Sweeney, L. (2002). k-anonymity: A model for protecting privacy. *International Journal of Uncertainty, Fuzziness and Knowledge-Based Systems*, 10:557–570.

Tang, J., Korolova, A., Bai, X., Wang, X., and Wang, X. (2017). Privacy loss in apple's implementation of differential privacy on macos 10.12. *arXiv preprint arXiv:1709.02753*.

Thrun, S., Burgard, W., and Fox, D. (2005). *Probabilistic robotics*. MIT press.

Venkataramani, R. and Bresler, Y. (2001). Optimal sub-nyquist nonuniform sampling and reconstruction for multiband signals. *IEEE Trans. Signal Processing*, 49:2301–2313.

Vlachos, M., Philip, S. Y., and Castelli, V. (2005). On periodicity detection and structural periodic similarity. In *SDM*, volume 5, pages 449–460. SIAM.

Wang, J., Zhu, R., Liu, S., and Cai, Z. (2018). Node location privacy protection based on differentially private grids in industrial wireless sensor networks. *Sensors*, 18(2):410.

Wang, Y., Gao, J., and Mitchell, J. S. (2006). Boundary recognition in sensor networks by topological methods. In *Proceedings of the 12th annual international conference on Mobile computing and networking*, pages 122–133. ACm.

Wong, R. C.-W., Fu, A. W.-C., Wang, K., and Pei, J. (2009). Anonymization-based attacks in privacy-preserving data publishing. *ACM Transactions on Database Systems (TODS)*, 34(2):8.

Wu, H., Chen, Z., Sun, W., Zheng, B., and Wang, W. (2017). Modeling trajectories with recurrent neural networks. IJCAI.

Xiao, H., Gao, J., Vu, L., and Turaga, D. S. (2017). Learning temporal state of diabetes patients via combining behavioral and demographic data. In *Proceedings of the 23rd ACM SIGKDD International Conference on Knowledge Discovery and Data Mining*, pages 2081–2089. ACM.

Xiao, X., Wang, G., and Gehrke, J. (2011). Differential privacy via wavelet transforms. *IEEE Transactions on knowledge and data engineering*, 23(8):1200–1214.

Xu, F., Tu, Z., Li, Y., Zhang, P., Fu, X., and Jin, D. (2017). Trajectory recovery from ash: User privacy is not preserved in aggregated mobility data. In *Proceedings of the 26th International Conference on World Wide Web*, pages 1241–1250. International World Wide Web Conferences Steering Committee.

Xue, A. Y., Zhang, R., Zheng, Y., Xie, X., Huang, J., and Xu, Z. (2013). Destination prediction by sub-trajectory synthesis and privacy protection against such prediction. In *Data Engineering (ICDE), 2013 IEEE 29th International Conference on*, pages 254–265. IEEE.

Yan, S., Wu, C., Dai, W. P., Ghanem, M., and Guo, Y. (2012a). Environmental monitoring via compressive sensing. In *SensorKDD '12*.

Yan, T., Chu, D., Ganesan, D., Kansal, A., and Liu, J. (2012b). Fast app launching for mobile devices using predictive user context. In *Proceedings of the 10th international conference on Mobile systems, applications, and services*, pages 113–126. ACM.

Yang, J., Wang, W., and Yu, P. S. (2003). Mining asynchronous periodic patterns in time series data. *IEEE Transactions on Knowledge and Data Engineering*, 15(3):613–628.

Yang, L., Zhang, M., He, S., Li, M., and Zhang, J. (2018). Crowd-empowered privacy-preserving data aggregation for mobile crowdsensing. In *Proceedings of the Eighteenth ACM International Symposium on Mobile Ad Hoc Networking and Computing*, pages 151–160. ACM.

Yin, X., Ni, C.-C., Ding, J., Han, W., Zhou, D., Gao, J., and Gu, X. D. (2015). Decentralized human trajectories tracking using hodge decomposition in sensor networks. In *Proceedings of the 23rd SIGSPATIAL International Conference on Advances in Geographic Information Systems*, page 54. ACM.

Zeng, J., Telang, G., Johnson, M. P., Sarkar, R., Gao, J., Arkin, E. M., and Mitchell, J. S. (2017). Mobile r-gather: Distributed and geographic clustering for location anonymity. In *Proceedings of the 18th ACM International Symposium on Mobile Ad Hoc Networking and Computing*. ACM.

Zhang, Z.-K., Cho, M. C. Y., Wang, C.-W., Hsu, C.-W., Chen, C.-K., and Shieh, S. (2014). Iot security: ongoing challenges and research opportunities. In *2014 IEEE 7th international conference on service-oriented computing and applications*, pages 230–234. IEEE.

Zhao, H., Garcia-Palacios, E., Wei, J., and Xi, Y. (2009). Accurate available bandwidth estimation in ieee 802.11-based ad hoc networks. *Computer Communications*, 32(6):1050–1057.

Zheng, Y. (2015). Trajectory data mining: an overview. *ACM Transactions on Intelligent Systems and Technology (TIST)*, 6(3):29.

Zhu, Y., Li, Z., Zhu, H., Li, M., and Zhang, Q. (2013). A compressive sensing approach to urban traffic estimation with probe vehicles. *IEEE Transactions on Mobile Computing*, 12(11):2289–2302.

Ziebart, B. D., Maas, A. L., Bagnell, J. A., and Dey, A. K. (2008). Maximum entropy inverse reinforcement learning. In *AAAI*, volume 8, pages 1433–1438. Chicago, IL, USA.